AD-A065 929 COLORADO STATE UNIV FORT COLLINS DEPT OF CIVIL ENGI--ETC F/G 4/2
WIND CHARACTERISTICS OVER SUBIC BAY, PHILIPPINE ISLANDS, DURING--ETC(U)
OCT 78 H B WOO, J E CERMAK, J J LOU N00228-77-C-3086
UNCLASSIFIED CSU-CER77-78HW-JEC-JJL-43 NEPRF-CR-78-02 NL

1 OF 2
AD
A065829

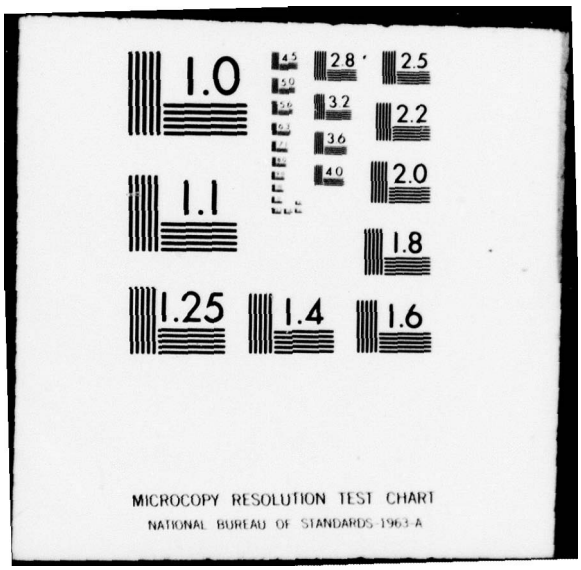
1.0
1.1
1.25
1.4
1.6
1.8
2.0
2.2
2.5
2.8
3.2
3.6
4.0
MICROCOPY RESOLUTION TEST CHART
NATIONAL BUREAU OF STANDARDS 1963-A

UNCLASSIFIED

SECURITY CLASSIFICATION OF THIS PAGE (When Data Entered)

REPORT DOCUMENTATION PAGE

READ INSTRUCTIONS BEFORE COMPLETING FORM

1. REPORT NUMBER: NAVENVPREDRSCHFAC CR78-02
2. GOVT ACCESSION NO.:
3. RECIPIENT'S CATALOG NUMBER:

4. TITLE (and Subtitle): Wind Characteristics over Subic Bay, Philippine Islands, during Typhoon Passage -- Determination by Physical Modeling in a Meteorological Wind Tunnel.

5. TYPE OF REPORT & PERIOD COVERED: Final Report.

6. PERFORMING ORG. REPORT NUMBER: CSU-CER77-78HGW-JEC-JJL-43

7. AUTHOR(s): H.G.C. Woo*, J.E. Cermak**, J.J. Lou*

8. CONTRACT OR GRANT NUMBER(s): N00228-77-C-3086

9. PERFORMING ORGANIZATION NAME AND ADDRESS: Fluid Dynamics and Diffusion Laboratory, College of Engineering, Colorado State University, Fort Collins, Colorado 80523

10. PROGRAM ELEMENT, PROJECT, TASK AREA & WORK UNIT NUMBERS: NEPRF WU 6.2-14

11. CONTROLLING OFFICE NAME AND ADDRESS: Naval Air Systems Command, Department of the Navy, Washington, DC 20361

12. REPORT DATE: October 1978

13. NUMBER OF PAGES: 102

14. MONITORING AGENCY NAME & ADDRESS (if different from Controlling Office): Naval Environmental Prediction Research Facility, Monterey, California 93940 (12) 102p.

15. SECURITY CLASS. (of this report): UNCLASSIFIED

15a. DECLASSIFICATION/DOWNGRADING SCHEDULE:

16. DISTRIBUTION STATEMENT (of this Report)

Approved for public release; distribution unlimited

(18) NEPRF (19) CR-78-02

17. DISTRIBUTION STATEMENT (of the abstract entered in Block 20, if different from Report)

18. SUPPLEMENTARY NOTES

*Research assistants, Fluid Mechanics and Wind Engineering Program, Department of Civil Engineering, Colorado State University

**Director, Fluid Dynamics and Diffusion Laboratory, Colorado State University

Original manuscript received in May 1978.

19. KEY WORDS (Continue on reverse side if necessary and identify by block number)

Typhoon winds
Wind tunnel experiments
Subic Bay, Philippines
Tropical cyclone winds

(180 deg T) (270 deg T) 15 deg.

20. ABSTRACT (Continue on reverse side if necessary and identify by block number)

A simulated atmospheric boundary-layer flow over a 1:15,000 scale model of the Subic Bay Basin, Philippines, was studied in the environmental wind tunnel of the Fluid Dynamics and Diffusion Laboratory, Colorado State University. Surface flow patterns were obtained by visualization with smoke and surface oil films. Mean wind speed isotachs and turbulence intensity contour lines were obtained at four elevations of 70, 150, 195 and 275 ft (21.3, 45.7, 59.5 and 83.7 m) for wind from the south (180°T) through west (270°T) at increments of 15°. Data obtained also include slides and motion pictures of the flow patterns.

DD FORM 1 JAN 73 1473 EDITION OF 1 NOV 65 IS OBSOLETE S/N 0102-014-6601

UNCLASSIFIED

SECURITY CLASSIFICATION OF THIS PAGE (When Data Entered)

400 826 LB

TABLE OF CONTENTS

Chapter		Page
	LIST OF TABLES	ii
	LIST OF FIGURES	iii
	LIST OF SYMBOLS	viii
	ACKNOWLEDGMENTS	ix
1.	INTRODUCTION	1
2.	THE PHYSICAL MODEL	3
	2.1 Similarity of Wind Tunnel Boundary-Layer Flow and Natural Wind	3
	2.2 Wind Tunnel Facility	6
	2.3 Topographical Model	7
3.	INSTRUMENTATION AND DATA ACQUISITION	8
	3.1 Flow Visualization	8
	3.2 Velocity Measurements	9
4.	RESULTS AND DISCUSSION	11
	4.1 Flow Visualization	11
	4.2 Wind Velocity	12
5.	CONCLUSIONS	15
	REFERENCES	16
	FIGURES	17
	TABLES	92

LIST OF TABLES

Table No.		Page
I.	Motion-Picture Scenes	93

LIST OF FIGURES

Figure		Page
1	Environmental Wind Tunnel, Fluid Dynamics and Diffusion Laboratory, Colorado State University	18
2	Topographical Model in Wind Tunnel 180°T Viewing Downstream	19
3	Topographical Model in Wind Tunnel 180°T Viewing Upstream	20
4	Oil Flow Pattern for the Subic Bay Basin at 225°T	21
5	Oil Flow Pattern for the Subic Bay Basin at 270°T	22
6	Mean Velocity and Turbulence Intensity Profiles of the Approach Flows	23
7	Locations of Velocity Measurement Station (elevation contours are in feet)	24
8	Surface Streamlines for the Subic Bay Basin at 180°T	25
9	Surface Streamlines for the Subic Bay Basin at 195°T	26
10	Surface Streamlines for the Subic Bay Basin at 210°T	27
11	Surface Streamlines for the Subic Bay Basin at 225°T	28
12	Surface Streamlines for the Subic Bay Basin at 240°T	29
13	Surface Streamlines for the Subic Bay Basin at 255°T	30
14	Surface Streamlines for the Subic Bay Basin at 270°T	31
15-1-a	Mean Wind Speed Isotachs for the Subic Bay Basin at 180°T, z = 70 ft (21.3 m)	32
15-1-b	Turbulence Intensity Contour Lines for the Subic Bay Basin at 180°T, z = 70 ft (21.3 m)	33

Figure		Page
15-2-a	Mean Wind Speed Isotachs for the Subic Bay Basin at 180°T, z = 150 ft (45.7 m)	34
15-2-b	Turbulence Intensity Contour Lines for the Subic Bay Basin at 180°T, z = 150 ft (45.7 m)	35
15-3-a	Mean Wind Speed Isotachs for the Subic Bay Basin at 180°T, z = 195 ft (59.5 m)	36
15-3-b	Turbulence Intensity Contour Lines for the Subic Bay Basin at 180°T, z = 195 ft (59.5 m)	37
15-4-a	Mean Wind Speed Isotachs for the Subic Bay Basin at 180°T, z = 275 ft (83.9 m)	38
15-4-b	Turbulence Intensity Contour Lines for the Subic Bay Basin at 180°T, z = 275 ft (83.9 m)	39
16-1-a	Mean Wind Speed Isotachs for the Subic Bay Basin at 195°T, z = 70 ft (21.3 m)	40
16-1-b	Turbulence Intensity Contour Lines for the Subic Bay Basin at 195°T, z = 70 ft (21.3 m)	41
16-2-a	Mean Wind Speed Isotachs for the Subic Bay Basin at 195°T, z = 150 ft (45.7 m)	42
16-2-b	Turbulence Intensity Contour Lines for the Subic Bay Basin at 195°T, z = 150 ft (45.7 m)	43
16-3-a	Mean Wind Speed Isotachs for the Subic Bay Basin at 195°T, z = 195 ft (59.5 m)	44
16-3-b	Turbulence Intensity Contour Lines for the Subic Bay Basin at 195°T, z = 195 ft (59.5 m)	45
16-4-a	Mean Wind Speed Isotachs for the Subic Bay Basin at 195°T, z = 275 ft (83.9 m)	46
16-4-b	Turbulence Intensity Contour Lines for the Subic Bay Basin at 195°T, z = 275 ft (83.9 m)	47
17-1-a	Mean Wind Speed Isotachs for the Subic Bay Basin at 210°T, z = 70 ft (21.3 m)	48
17-1-b	Turbulence Intensity Contour Lines for the Subic Bay Basin at 210°T, z = 70 ft (21.3 m)	49
17-2-a	Mean Wind Speed Isotachs for the Subic Bay Basin at 210°T, z = 150 ft (45.7 m)	50

Figure		Page
17-2-b	Turbulence Intensity Contour Lines for the Subic Bay Basin at 210°T, z = 150 ft (45.7 m)	51
17-3-a	Mean Wind Speed Isotachs for the Subic Bay Basin at 210°T, z = 195 ft (59.5 m)	52
17-3-b	Turbulence Intensity Contour Lines for the Subic Bay Basin at 210°T, z = 195 ft (59.5 m)	53
17-4-a	Mean Wind Speed Isotachs for the Subic Bay Basin at 210°T, z = 275 ft (83.9 m)	54
17-4-b	Turbulence Intensity Contour Lines for the Subic Bay Basin at 210°T, z = 275 ft (83.9 m)	55
18-1-a	Mean Wind Speed Isotachs for the Subic Bay Basin at 225°T, z = 70 ft (21.3 m)	56
18-1-b	Turbulence Intensity Contour Lines for the Subic Bay Basin at 225°T, z = 70 ft (21.3 m)	57
18-2-a	Mean Wind Speed Isotachs for the Subic Bay Basin at 225°T, z = 150 ft (45.7 m)	58
18-2-b	Turbulence Intensity Contour Lines for the Subic Bay Basin at 225°T, z = 150 ft (45.7 m)	59
18-3-a	Mean Wind Speed Isotachs for the Subic Bay Basin at 225°T, z = 195 ft (59.5 m)	60
18-3-b	Turbulence Intensity Contour Lines for the Subic Bay Basin at 225°T, z = 195 ft (59.5 m)	61
18-4-a	Mean Wind Speed Isotachs for the Subic Bay Basin at 225°T, z = 275 ft (83.9 m)	62
18-4-b	Turbulence Intensity Contour Lines for the Subic Bay Basin at 225°T, z = 275 ft (83.9 m)	63
19-1-a	Mean Wind Speed Isotachs for the Subic Bay Basin at 240°T, z = 70 ft (21.3 m)	64
19-1-b	Turbulence Intensity Contour Lines for the Subic Bay Basin at 240°T, z = 70 ft (21.3 m)	65
19-2-a	Mean Wind Speed Isotachs for the Subic Bay Basin at 240°T, z = 150 ft (45.7 m)	66
19-2-b	Turbulence Intensity Contour Lines for the Subic Bay Basin at 240°T, z = 150 ft (45.7 m)	67

Figure		Page
19-3-a	Mean Wind Speed Isotachs for the Subic Bay Basin at 240°T, z = 195 ft (59.5 m)	68
19-3-b	Turbulence Intensity Contour Lines for the Subic Bay Basin at 240°T, z = 195 ft (59.5 m)	69
19-4-a	Mean Wind Speed Isotachs for the Subic Bay Basin at 240°T, z = 275 ft (83.9 m)	70
19-4-b	Turbulence Intensity Contour Lines for the Subic Bay Basin at 240°T, z = 275 ft (83.9 m)	71
20-1-a	Mean Wind Speed Isotachs for the Subic Bay Basin at 255°T, z = 70 ft (21.3 m)	72
20-1-b	Turbulence Intensity Contour Lines for the Subic Bay Basin at 255°T, z = 70 ft (21.3 m)	73
20-2-a	Mean Wind Speed Isotachs for the Subic Bay Basin at 255°T, z = 150 ft (45.7 m)	74
20-2-b	Turbulence Intensity Contour Lines for the Subic Bay Basin at 255°T, z = 150 ft (45.7 m)	75
20-3-a	Mean Wind Speed Isotachs for the Subic Bay Basin at 255°T, z = 195 ft (59.5 m)	76
20-3-b	Turbulence Intensity Contour Lines for the Subic Bay Basin at 225°T, z = 195 ft (59.5 m)	77
20-4-a	Mean Wind Speed Isotachs for the Subic Bay Basin at 255°T, z = 275 ft (83.9 m)	78
20-4-b	Turbulence Intensity Contour Lines for the Subic Bay Basin at 225°T, z = 275 ft (83.9 m)	79
21-1-a	Mean Wind Speed Isotachs for the Subic Bay Basin at 270°T, z = 70 ft (21.3 m)	80
21-1-b	Turbulence Intensity Contour Lines for the Subic Bay Basin at 270°T, z = 70 ft (21.3 m)	81
21-2-a	Mean Wind Speed Isotachs for the Subic Bay Basin at 270°T, z = 150 ft (45.7 m)	82
21-2-b	Turbulence Intensity Contour Lines for the Subic Bay Basin at 270°T, z = 150 ft (45.7 m)	83
21-3-a	Mean Wind Speed Isotachs for the Subic Bay Basin at 270°T, z = 195 ft (59.5 m)	84

Figure		Page
21-3-b	Turbulence Intensity Contour Lines for the Subic Bay Basin at 270°T, z = 195 ft (59.5 m)	85
21-4-a	Mean Wind Speed Isotachs for the Subic Bay Basin at 270°T, z = 275 ft (83.9 m)	86
21-4-b	Turbulence Intensity Contour Lines for the Subic Bay Basin at 270°T, z = 275 ft (83.9 m)	87
22-a	Mean Velocity and Turbulence Profiles at Cubi Point Meteorological Station at 15 Degree Intervals . . .	88
22-b	Mean Velocity and Turbulence Profiles at Cubi Point Meteorological Station at 15 Degree Intervals . . .	89
23	Mean Velocity at Cubi Point Meteorological Station . . .	90
24	Turbulence Intensity at Cubi Point Meteorological Station	91

LIST OF SYMBOLS

Symbol	Definition
A,B,n	Hot-wire anemometer calibration constants
E	Mean anemometer bridge voltage
E_{rms}	Root-mean-square anemometer bridge voltage
k	Diameter of equivalent sand roughness
L	Characteristic length
R	Reynolds number
U	Local mean velocity
U_{rms}	Root-mean-square of velocity fluctuation
z	Elevation above mean sea level
Z_o	Aerodynamic roughness height

Subscripts

M	Model
P	Prototype
∞	Value of quantity above the boundary layer

Greek Symbols

δ	Boundary-layer thickness
δ_L	Thickness of viscous wall zone
ρ	Mass density of air
ν	Kinematic viscosity

ACKNOWLEDGMENTS

This study was performed under contract N00228-77-C-3086 for the Naval Environmental Prediction Research Facility through the Naval Supply Center, Oakland, California. Their support and the assistance of Mr. Samson Brand of NEPRF are gratefully acknowledged. Model construction was supervised by Mr. Christopher D. Caron. Mr. Jeffrey R. Hurd took photographs and motion pictures of the flow visualization.

Chapter 1

INTRODUCTION

As in other regions of the Western Pacific, tropical cyclones create a severe natural hazard in the Philippine Islands area (1). In some cases, the tropical cyclones cause severe damage to ships in harbor (2). Therefore, it is very important to know what effects local topography has upon mean wind velocity and gust intensity in the location of ship anchorages, new piers and in the vicinity of aircraft facilities in order to take advantage of any sheltering effects.

The purpose of this wind tunnel study program is to determine wind characteristics such as mean wind speed, turbulence level and wind direction inside the Subic Bay Basin for a range of wind directions corresponding to those most probable for typhoons.

A 1:15,000 scale model that included the mountain and valley system affecting wind inside the Bay was constructed. The model was studied in the environmental wind tunnel of the Fluid Dynamics and Diffusion Laboratory at Colorado State University. In this facility, flow simulating an atmospheric boundary layer with neutral thermal stratification was developed over the model.

The study included flow visualization using oil films and smoke and hot-wire anemometer velocity measurements. The studies were conducted in sufficient detail so that the wind at piers, anchorages, airfield, mouth of the Bay, and far south to the entrance of the Bay may be compared with the wind direction and speed observed by the meteorological station at Cubi Point.

Surface flow patterns, mean wind speed isotachs and turbulence intensity contour lines were developed for the entire Bay area. The gradient wind direction ranged from 180°T to 270°T with increments of 15°.

This report is supplemented by a 750-foot color motion picture and a set of 95 color slides which show the flow structure inside the Bay and the surrounding area.

Chapter 2

THE PHYSICAL MODEL

2.1 Similarity of Wind Tunnel Boundary-Layer Flow and Natural Wind

The requirements to obtain good simulation of natural winds by wind tunnels have been discussed by Cermak and Arya (3) and Cermak (4,5). Generally speaking, the criteria for similarity of atmospheric boundary layers are the following: (1) undistorted scaling of boundary geometry (geometric similarity), (2) bulk Richardson number equality, (3) Rossby number equality, (4) kinematic similarity of approach flow (distribution of mean wind speed and turbulence characteristics), and (5) Reynolds number equality.

For this study, geometrical similarity was achieved by an undistorted model having a scale of 1:15,000 for both horizontal and vertical directions. This scale was chosen to facilitate ease of measurements as well as to permit inclusion of significant topography surrounding Subic Bay.

For the strong winds (typhoons) considered in this study, the thermal stability is essentially neutral. Thus, thermal similarity was achieved by using isothermal flow in the wind tunnel.

With existing wind-tunnel facilities, Rossby number equality cannot be achieved. However, when fluid particle transit times from the location of a major boundary-layer disturbance across the prototype area of concern is a small fraction of one day, the Coriolis acceleration will have minor effect on the flow. In this case distances from surrounding mountains across the Bay are about 10 mi (16 km) and wind speeds may be about 70 knots (130 km/hr). Therefore, transit times are small relative to one day and Coriolis effects would be negligible.

Wind tunnel studies of atmospheric motions near the Earth's surface at meso-scales--from 5 to 50 mi (8 to 80 km) in extent--require use of models of the order of 10^4 smaller than the prototype topographical features [Cermak (5)]. In this case, if the Reynolds number for both the prototype and scale model is based on the ambient flow velocity U, the characteristic length L, and the kinematic viscosity ν, and if the same fluid and approximately the same flow speed are used then the ratio of the Reynolds number for prototype and scale model will be of the same order as the length scale ratio; i.e.,

$$R_p/R_M = \left(\frac{U_p L_p}{\nu_p}\right) / \left(\frac{U_M L_M}{\nu_M}\right) \sim L_p/L_M$$

In other words, the Reynolds number difference is so large that similarity in the ordinary sense does not exist.

In this study, an approximate similarity method suggested by Cermak and Peterka (7) was used. Basically, the concept is that when both the prototype and model flows are in the turbulent state over essentially flat surfaces, the model may be roughened to produce flow characteristics corresponding to those found at Reynolds number larger than the actual value. This approach depends upon producing flows in which the flow characteristics become independent of Reynolds number if a lower limit of the Reynolds number is exceeded. For example, the resistance coefficient for flow in a sufficiently rough pipe as shown in Schlichting (8, p. 578) is constant for a Reynolds number larger than 2×10^4. This implies that the basic flow quantity of surface shear stress is directly proportional to the fluid density times the mean flow speed squared. In turn, this condition is the necessary condition for mean turbulence

statistics such as root-mean-square values and correlation coefficients of the turbulence velocity components to be equal for the model and the prototype flow.

All the studies contained in this report were conducted with the upstream edge of the model set at less than 2 ft (0.6 m) from the entrance of the wind-tunnel test section. In this approach region, the floor of the wind tunnel was covered with a layer of sandpaper to provide roughness (0.06 in.) equivalent to a typhoon roughened sea surface. With this experimental arrangement, a boundary layer of 2.5 in. (0.06 m) depth with a mean velocity power-law exponent of 0.22 was obtained at the test site. The vertical distributions of longitudinal mean velocity and turbulence intensity are shown in Fig. 6. The measurement techniques for mean velocity and turbulence are discussed in Section 3.2.

The boundary-layer thickness versus model height above the sea surface (about 2 in. (5.08 cm)) ratio in this case is of the order one. Although the model surface was smoothed by using clay (described in Section 2.3), the surface was still quite rough--some of the ridges presented rather sharp edges. The model surface apparently produced an aerodynamically fully rough flow. A Reynolds number based on the height of the model terrain above sea level and a free-stream velocity of 35.5 ft/s (21 knots) was 3.9×10^4. Therefore, with this wind speed, the flow characteristics within the bay basin is considered as Reynolds number independent. Thus, acceptable flow similarity was achieved without precise Reynolds number equality. It should be noted that all the velocity measurements were conducted at only one free-stream velocity of 35.5 ft/s (21 knots) in the tunnel.

The average roughness height of the sandpaper particles was about 0.06 in. (0.15 cm) which corresponds to a prototype wave of 75 ft (22.9 m). Selection of the sandpaper roughness was made based on the following considerations: (1) the viscous wall-layer thickness δ_L was determined to be approximately 0.1 in. (0.25 cm) over a smooth surface at the test site for a wind speed of 35.5 ft/s (21 knots), (2) the aerodynamic roughness Z_o corresponding to a 0.1 in. (0.25 cm) thick viscous layer is 0.001 in. (0.0025 cm) ($\delta_L/100$) which for a sand roughened surface requires a particle size k of 0.03 in. (0.08 cm) ($30Z_o$), (3) wave-height data for a wind speed of about 70 knots indicate wave heights at the harbor mouth of about 32 ft (9.8 m) or 0.026 in. (0.07 cm) for the model and (4) the water surface of the model bay area was made of smooth plexiglass. In order to ensure that the flow characteristics inside the bay area was Reynolds number independent (corresponding to an aerodynamic rough surface), especially with wind from 180°T to 210°T, a sand particle size of Z_o for the smooth surface plus the wave height, i.e., 0.03 in. (0.08 cm) plus 0.026 in. (0.07 cm) or 0.06 in. (0.15 cm) was selected.

2.2 Wind-Tunnel Facility

The physical modeling was conducted in the environmental wind tunnel located in the Fluid Dynamics and Diffusion Laboratory at Colorado State University. A plan view of this wind tunnel is shown in Fig. 1. This wind tunnel may be described generally as a low-speed open-circuit facility. The variable speed fan is driven by a 50 H.P. DC motor. The test section is nominally 12 ft (3.66 m) wide, 8 ft (2.44 m) high and 57 ft (17.4 m) long. Honey-comb straighteners and two screens are provided at the intake to calm the flow and eliminate large-scale

disturbances from entering the test section. The roof is adjustable to maintain a zero pressure gradient along the test section. The mean free-stream velocity can be adjusted continuously from 1 to about 40 ft/s (0.6 to 23.7 knots).

2.3 Topographical Model

The terrain model was constructed at an undistorted scale of 1:15,000. Excepting for the base plate which was made of 0.125 in. (0.32 cm) plywood, the terrain model was made from styrofoam sheets cut to match contour lines of a topographic map provided by the Navy. The model terrain was then smoothed with clay and coated with a layer of green paint.

In order to use the oil-film technique (described in Section 3.1) to study the flow pattern near the water surface inside the bay area, the water surface of the bay area was made of a 0.125 in. (0.32 cm) thick plexiglass base plate. A 4x4 in. (10.16x10.16 cm) square grid was painted on the plate to enable accurate location of measurement stations. The topographical model inside the wind tunnel for a wind direction of 180°T is shown in Figs. 2 and 3.

Chapter 3

INSTRUMENTATION AND DATA ACQUISITION

3.1 Flow Visualization

Flow visualization over the Bay and surrounding areas is necessary to define the overall flow pattern and its characteristics. Both the smoke and the oil-film techniques were used. The smoke technique shows both the unsteady and average character of the flow at any position in space by proper positioning of the smoke source. The oil-film technique reveals long-time average features of the flow pattern very near the surface.

Titanium tetrachloride was used for the smoke study. The smoke either was released from a tube which could be held at any position in space or was released from a syringe to form a line source on the surface of the model. Motion pictures were taken to record the flow patterns.

The oil-film technique was used to observe flow patterns near the sea surface within the bay area. The oil-film technique uses a mixture of zinc-oxide powder, "Crisco" and light mineral oil. The mixture ratio proportion by volumes are about 10 percent zinc-oxide powder and 90 percent oil. The surface of the plexiglass base plate was coated uniformly with a layer of the oil mixture. After running the wind tunnel for a period of time, the oil film formed a steady pattern for a particular wind direction.

It has been argued that very close to the surface in a turbulent flow the mean streamlines are parallel to the mean shear stress lines but are different from mean particle paths. These differences may be quite marked in the highly turbulent flow near some obstacles--Hunt et al. (9) and Lighthill (10). Since motion of the oil-film is affected

strongly by viscosity of the oil the suspended particles in the oil film do not follow random motions of the air particles but depicts the mean streamline or mean shear stress line. Typical oil film patterns are shown in Figs. 4 and 5.

Conclusions obtained from the flow-visualization studies are discussed in Section 4.1.

3.2 Velocity Measurements

Velocity measurements were made at four elevations (70, 150, 195, and 275 ft) for 60 locations shown in Fig. 7. The vertical distribution of mean velocity and turbulence intensity was made at the location shown in Fig. 7 to define characteristics of the approach flow boundary layer. These measurements were made with a probe consisting of a pair of tungsten hot-wire sensing elements. The wires are 0.0002 in. in diameter and 0.063 in. long and are mounted parallel to each other horizontally, one above the other, with a separation distance of 1/16 in. Based on information obtained from the flow-visualization, the hot-wire probe was properly set with its axis perpendicular to the mean flow at each measurement location.

Two Thermo-Systems constant-temperature hot-wire anemometers (Model 1050) were used. Mean voltage outputs were read from two digital voltmeters. The rms voltages were obtained from two DISA RMS meters (Model 55D35) and were read from two digital voltmeters. The anemometer units were operated without filtering or linearization.

The probe was calibrated prior to each wind-tunnel measurement by using a Thermo-Systems, Inc., Model 1125 calibrator and a MKS Baratron pressure meter. Calibration data were fitted to a variable exponent form of King's Law

$$E^2 = A + BU^n$$

using a least-squares curve fitting program. In this relationship E is the hot-wire output voltage, U the approach velocity and A, B and n are coefficients determined to fit the calibration data. The above relationship was used to recover the mean velocity at measurement points from the measured mean voltage. From this equation it follows, to a first order approximation, that the fluctuating velocity in the form U_{rms} (root-mean-square velocity) can be given by

$$U_{rms} = \frac{2\ E\ E_{rms}}{B\ n\ U^{n-1}}$$

where E_{rms} is the root-mean-square voltage output from the anemometer. All rms values of turbulent velocity U_{rms} were divided by the local mean velocity U to obtain local turbulence intensity U_{rms}/U.

During the measurements air temperature in the wind tunnel was also recorded. A method suggested by Bearman (12) was used to correct for the error due to air temperature differences during calibration and while making the measurements. There are two restrictions for Bearman's correction method to be valid: (1) the temperature difference must be small (less than 20°F) and (2) the wind speed must be greater than 3 to 5 ft/s (0.9 to 1.5 m/s). Both of these restrictions were met for all the measurements performed.

For each new probe used or during a prolonged usage of the same probe, calibration was performed both before and after the day's measurements. This procedure was used to check the calibration and also to assure system accuracy and repeatability.

Chapter 4

RESULTS AND DISCUSSION

4.1 Flow Visualization

A 750-ft film showing the characteristics of flow in the Bay basin and the surrounding area by smoke visualization supplements this report. This color motion picture has been arranged into titled sequences that are specified in Table 1.

Ninety-five color slides taken during the wind-tunnel test period also supplement this report. The slides are numbered according to the test sequence. The slides show the general model arrangement in the wind tunnel, the overall and detailed oil-film pattern for each wind direction. Figures 4 and 5 show typical examples of these oil-flow patterns.

For wind directions near 180°T the flow is generally quite straight and directly into the Bay through the Bay entrance excepting at the southwest part of the Bay where the flow curves slightly along the coastline. For wind directions near 270°T, the motion pictures reveal a highly complex flow with interesting secondary flows produced by the ridge and valley system on the west side of the Bay. The surface flow tends to follow the direction of the valley and therefore forms several mean streams with fairly large-scale motions moving onto the Bay. Once the flow moves over the water surface of the Bay, the flow pattern becomes less complex and streamlines tend to become parallel.

Based on the oil-film patterns supplemented with visual observations of the smoke pattern, the surface flow patterns for each wind direction were developed. They are shown in Figs. 8 through 14.

This wind study was conducted primarily to obtain overall information about the wind field over the Bay. Therefore, details of wind characteristics in the wake of small islands and other local topographical features and structures were not measured.

4.2 Wind Velocity

Mean velocity and turbulence profiles of the approach flow were taken at locations upstream of the Bay entrance or of the model (at locations free from the effect of topography) and therefore are characteristic of the boundary layer approaching the model. Several sets of the approach flow data were taken during this study as a precautionary measure and they were found to be identical. The mean velocity and turbulence profiles of the approach flow are shown in Fig. 6. The boundary-layer thickness δ was 2.5 in. (6.35 cm) corresponding to a prototype value of 3125 ft (953 m). This seems to be a reasonable value as compared with the field data of Fort Wayne, Indiana--Chaudhry and Cermak (11). In the form $\frac{U}{U_\infty} = \left(\frac{z}{\delta}\right)^n$, the velocity profile has an exponent n of 0.22 for the approach flow and is considered as reasonable as compared to observed n values for tropical cyclone profiles (range from 0.14 to 0.30).* The longitudinal turbulence intensity is defined as the root-mean-square of the longitudinal velocity fluctuations divided by the local mean velocity. The turbulence intensity at the sea level is about 25%.

Measurements of mean velocity and turbulence intensity were also made at four different heights--70, 150, 195, and 275 ft (21.3, 45.7, 59.5 and 83.7 m)--above the sea level at approximately 60 locations

*For a more detailed discussion, refer to Bates (13).

within the Bay area for each wind direction. Seven wind directions were studied--180°T, 195°T, 210°T, 225°T, 240°T, 255°T, and 270°T.

The mean wind speed isotachs ($U(z)/U_\infty$) and turbulence intensity (in percent of local mean velocity) contours inside the Bay for each wind direction at each of the four elevations are shown in Figs. 15-1-a through 21-4-b. The contour lines are based on the data measured at 60 locations shown in Fig. 7 with 85 additional intermediate points generated by a parabolic curve fitting method. The local mean wind speed was normalized by the free-stream wind speed in all the plots. The normalized wind speed and local turbulence level at Alava Pier, Rivera Pier, NSD(Supply) Pier, Fuel Pier, Leyte Pier, Bonton Pier, Camayan Pier, Nabassan Pier, and Cubi Point meteorological station are also shown in these figures.

The flow characteristics are rather uniform inside the Bay for wind directions near 180°T, excepting for the lee sides of ridges where lower mean wind speed with higher turbulence levels occur. In interpreting the turbulence data, one should note that large values of gustiness must be interpreted in terms of the magnitude of mean velocity since a low local wind velocity can lead to large values as effectively as large root-mean-square velocities.

The wind characteristics become more and more complicated as the wind direction approaches 270°T. This is caused by mountains on the west side of the Bay. As described in the previous section, the flow tends to follow the course of the valley when it passes over the mountain region. This results in high wind shear (a high velocity gradient) and therefore causes high turbulence levels. This effect can easily be seen in many of the figures such as Figs. 19-4-a and 19-4-b. Generally

speaking, the mountains provide good shielding effect for the region along the west coast of the bay when the wind approaches from behind the mountains, but no such effect is observed on the east part of the bay. In some cases even higher wind speeds are observed. This is apparently due to the effect of secondary flows.

The mean velocity and turbulence profiles at the Cubi Point meteorological station are compared with those of the approach flow in Figs. 22-a and 22-b. Figures 23 and 24 are mean velocity and turbulence intensity at various elevations at Cubi Point plotted as a function of wind direction.

Chapter 5

CONCLUSIONS

A simulated atmospheric boundary-layer flow over a model of the Subic Bay Basin in the Philippine Islands was established.

Results of the flow visualization study show that for wind directions near 180°T, the wind is generally uniform over the Bay and blows quite straight and direct into the Bay through the mouth of the Bay. For wind directions near 270°T, due to the effects of the mountains on the west side of the Bay, the flow is more complex with large scale secondary flow occurring. The westerly wind tends to follow the course of the valley into the Bay. Once over water the wind moves directly across the Bay with increasing speed. High wind shear is observed for westerly winds on the west part of the Bay due to effects of the ridges and valleys. Although turbulence intensities are high along the west side of the Bay for westerly winds the local mean wind speeds are low. Therefore, the mountains to the west provide significant sheltering from strong westerly winds.

REFERENCES

1. Proceeding Report of Tropical Cyclone Conference, Environmental Group Pacific Command, 7-10 February 1977, Kadena Air Base, Japan.

2. Brand, S., and Blelloch, J. W., "Cost Effectiveness of Typhoon Forecast Improvements," American Meteorological Society, Vol. 56, No. 3, March 1975, pp. 352-361.

3. Cermak, J. E., and Arya, S. P. S., "Problems of Atmospheric Shear Flows and Their Laboratory Simulation," AGARD Conference Proceedings, No. 48, 1970, pp. 12.1-12.16.

4. Cermak, J. E., "Applications of Fluid Mechanics to Wind Engineering," 1974 Freeman Scholar Lecture, ASME Journal of Fluid Engineering, Vol. 97, Ser. 1, No. 1, March 1975.

5. Cermak, J. E., "Laboratory Simulation of the Atmospheric Boundary Layer," AIAA Journal, Vol. 9, No. 9, September 1971, pp. 1746-1754.

6. Cermak, J. E., Sandborn, V. A., Plate, E. J., Binder, G. H., Chuang, H., Meroney, R. N., and Ito, S., "Simulation of Atmospheric Motion by Wind Tunnel Flows," Fluid Dynamics and Diffusion Laboratory Report CER66-17, Colorado State University, 1966.

7. Cermak, J. E., and Peterka, J. A., "Simulation of Wind Fields Over Point Arguello, California, by Wind-Tunnel Flow Over a Topographical Model," Fluid Dynamics and Diffusion Laboratory Report CER65JEC-JAP64, Colorado State University, 1965.

8. Schlichting, H., Boundary Layer Theory, McGraw-Hill, New York, 1968.

9. Hunt, J. C. R., Abell, C. J., Peterka, J. A., and Woo, H., "Kinematical Studies of the Flows Around Free or Surface Mounted Obstacles: Applying Topology to Flow Visualization," J. Fluid Mech. (1978), Vol. 86, Part 1, pp. 179-200.

10. Lighthill, M. J., [Article in Laminar Boundary Layer (edited by L. Rosenhead)], Oxford Press, 1963, pp. 48-88.

11. Chaudhry, F. H., and Cermak, J. E., "Wind-Tunnel Modeling of Flow and Diffusion Over an Urban Complex," Fluid Dynamics and Diffusion Laboratory Report CER70-71FHC-JEC24, Colorado State University, 1971.

12. Bearman, P. W., "Corrections for the Effect of Ambient Temperature Drift on Hot-Wire Measurements in Incompressible Flow," DISA Information Bulletin No. 11, 1970.

13. Bates, J., "Vertical Shear of the Horizontal Wind Speed in Tropical Cyclones," NOAA Technical Memorandum ERL-WMPO-39, 1977.

Figures

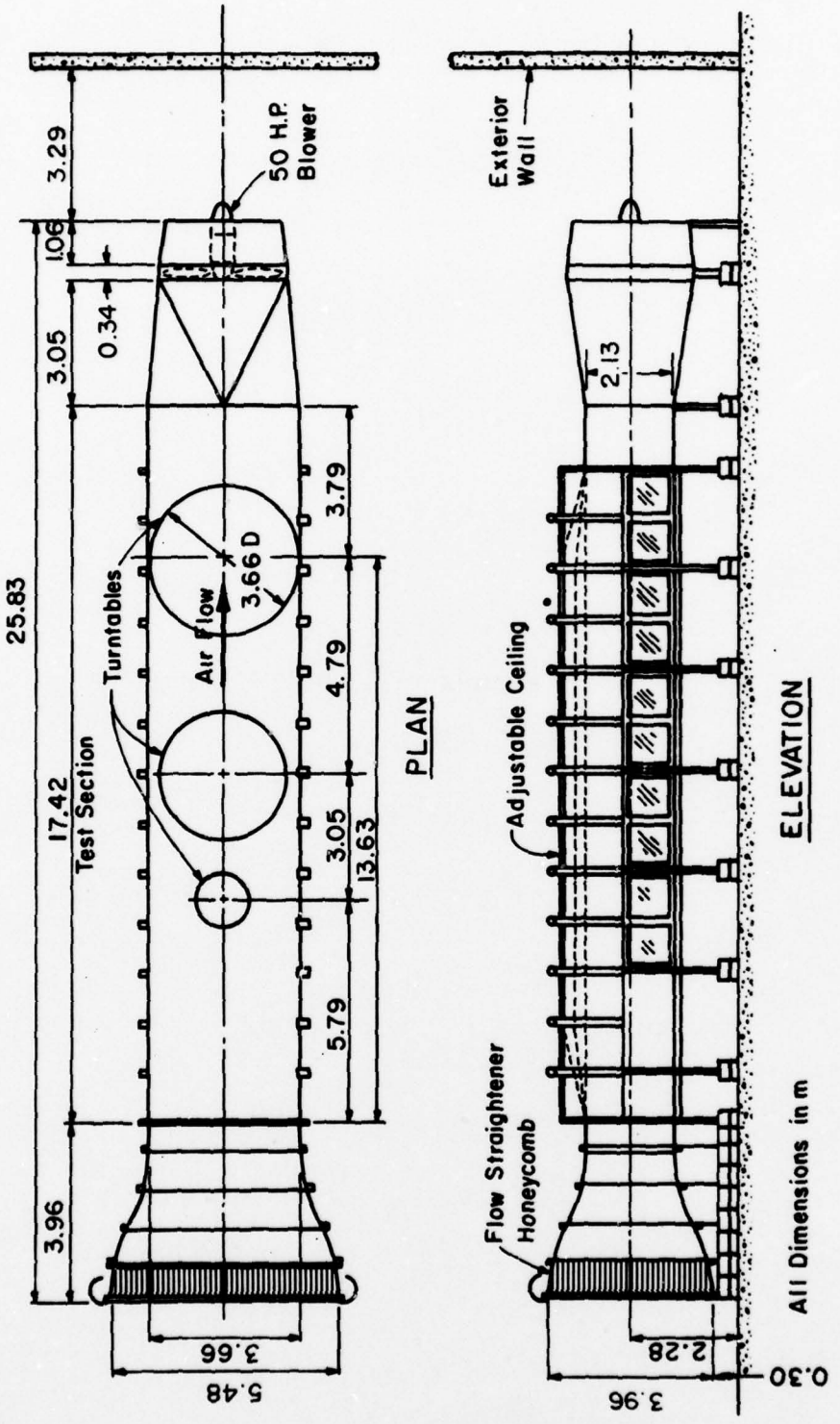

Fig. 1. ENVIRONMENTAL WIND TUNNEL
FLUID DYNAMICS & DIFFUSION LABORATORY
COLORADO STATE UNIVERSITY

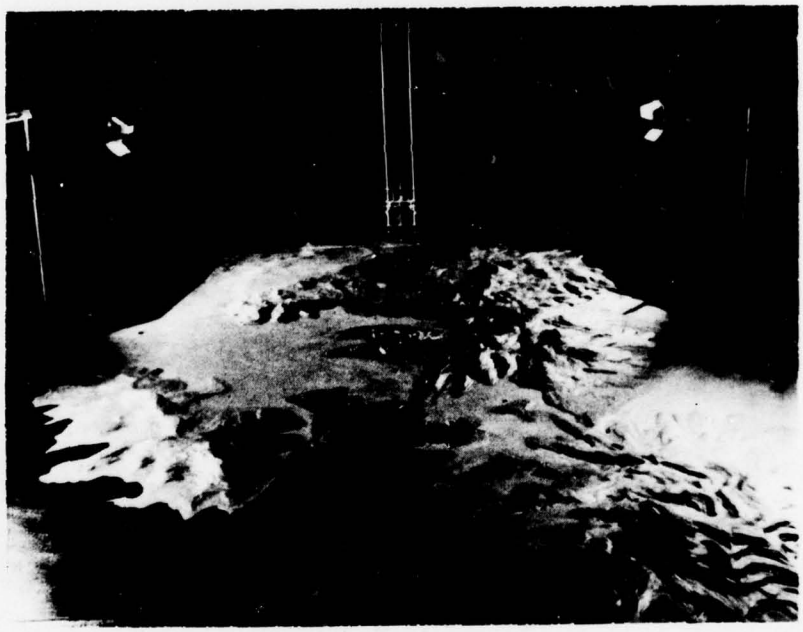

Fig. 2. Topographical Model in Wind Tunnel
180° Viewing Downstream

Fig. 3. Topographical Model in Wind Tunnel
180° Viewing Upstream

Fig. 4. Oil Flow Pattern for the Subic Bay Basin at 225°T

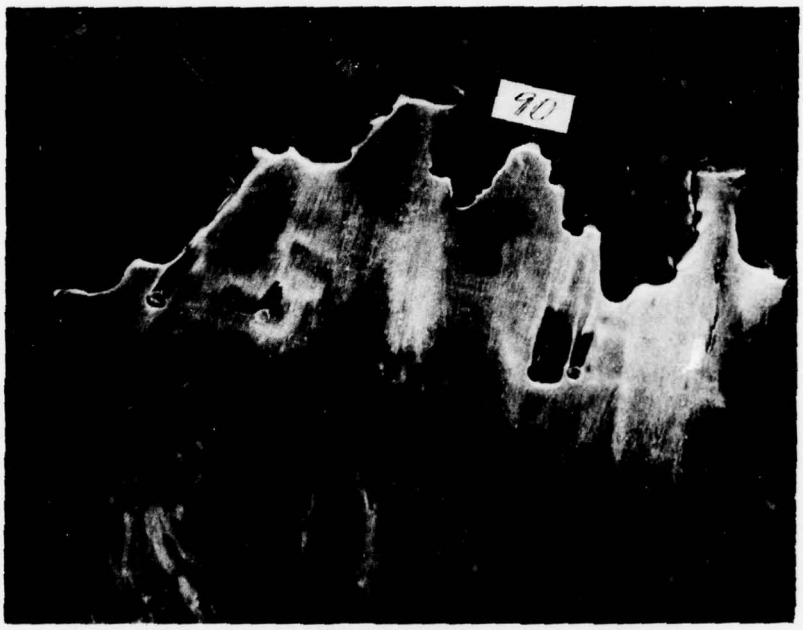

Fig. 5. Oil Flow Pattern for the Subic Bay Basin at 270°T

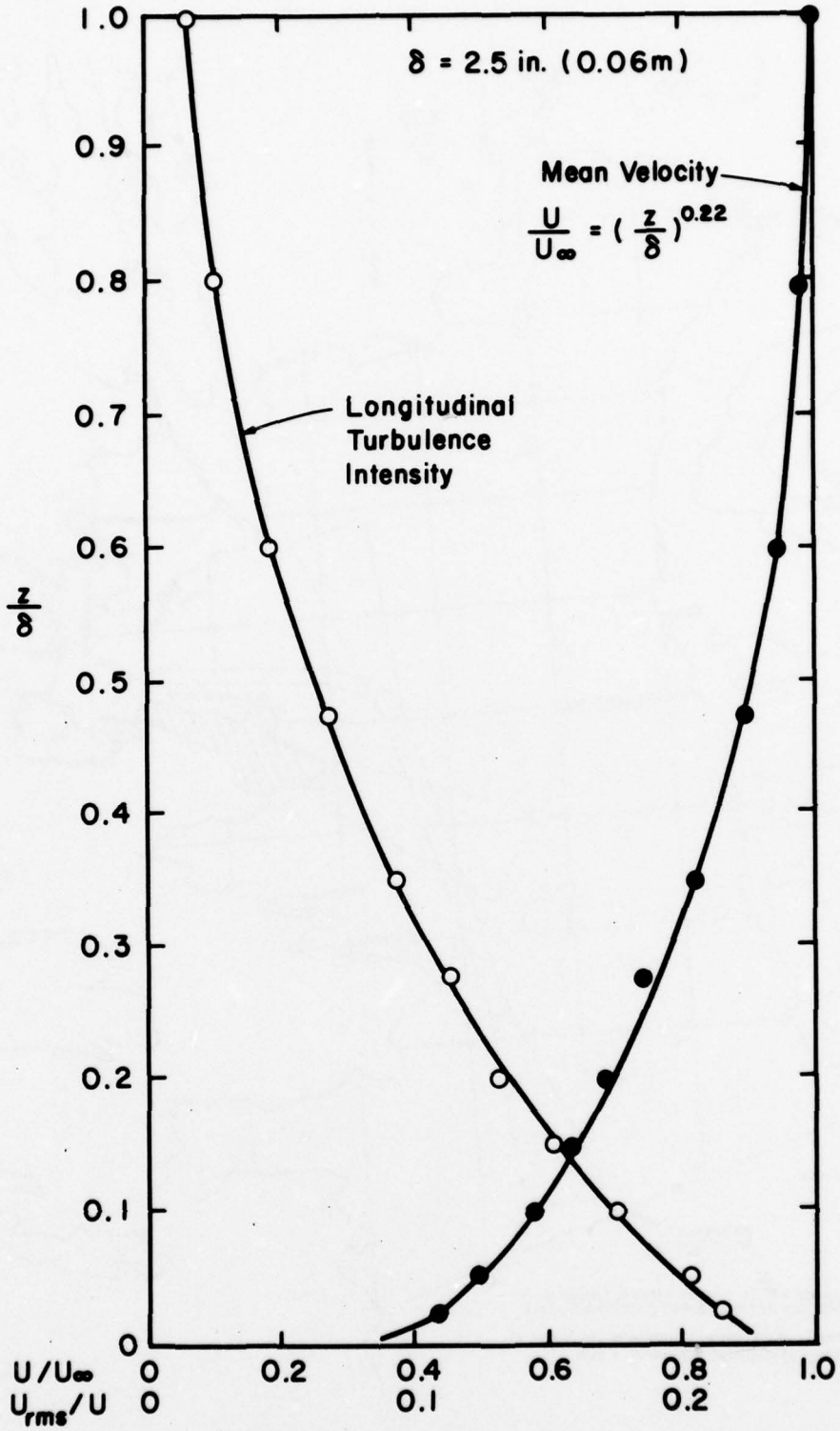

Fig. 6. Mean Velocity and Turbulence Intensity Profiles of the Approach Flows.

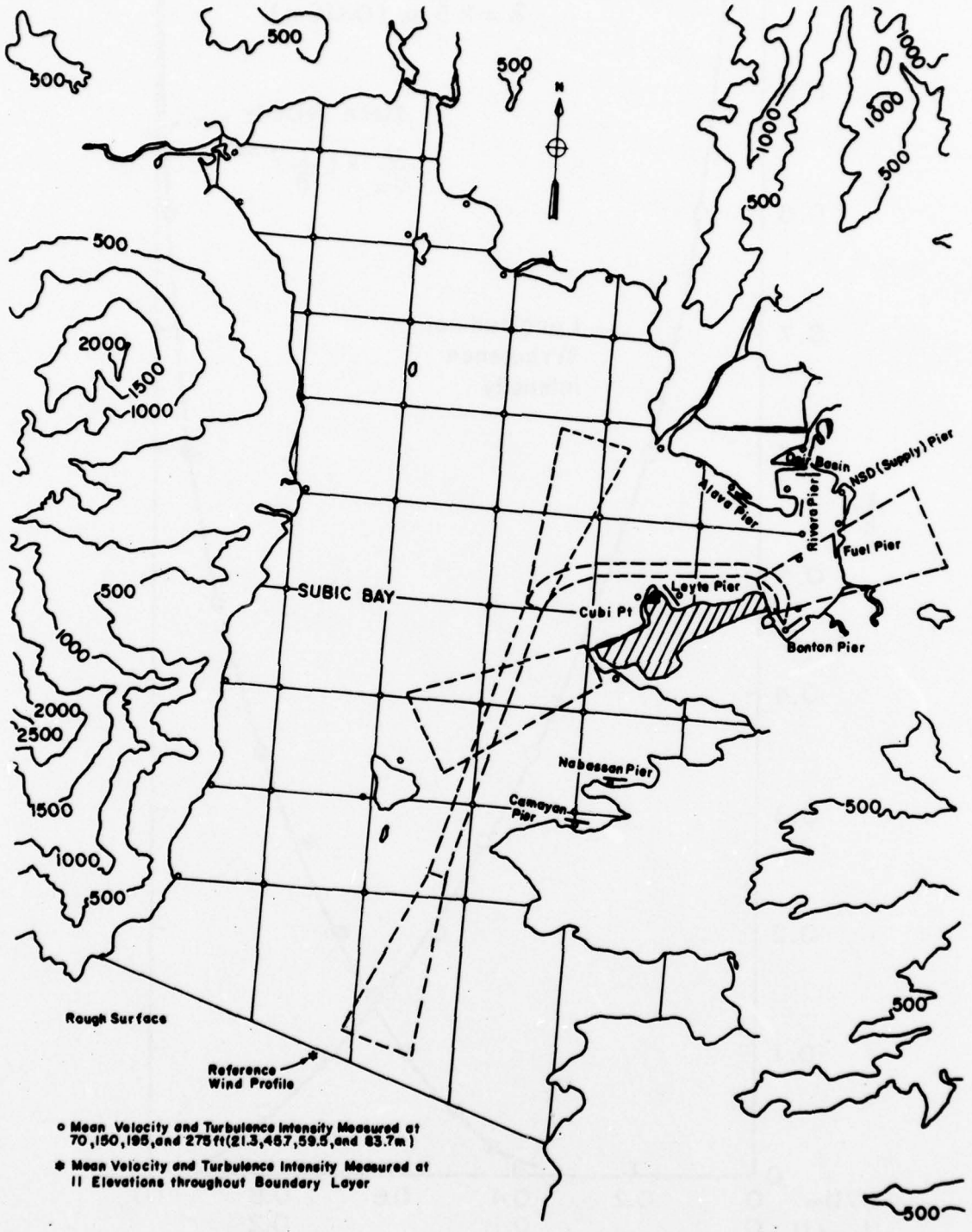

Fig. 7. Locations of Velocity Measurement Station (elevation contours are in feet).

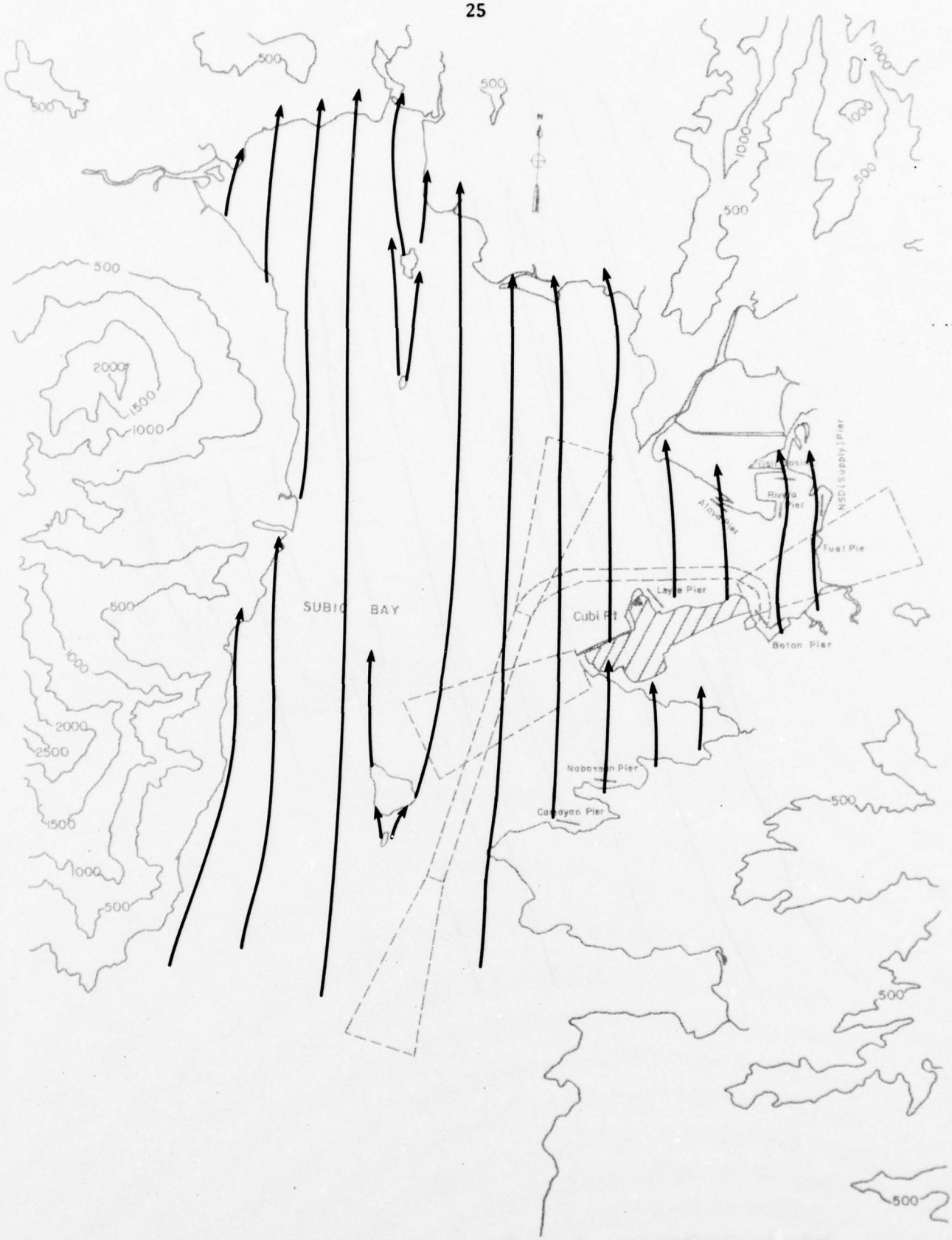

Fig. 8. Surface Streamlines for the Subic Bay Basin at 180°T

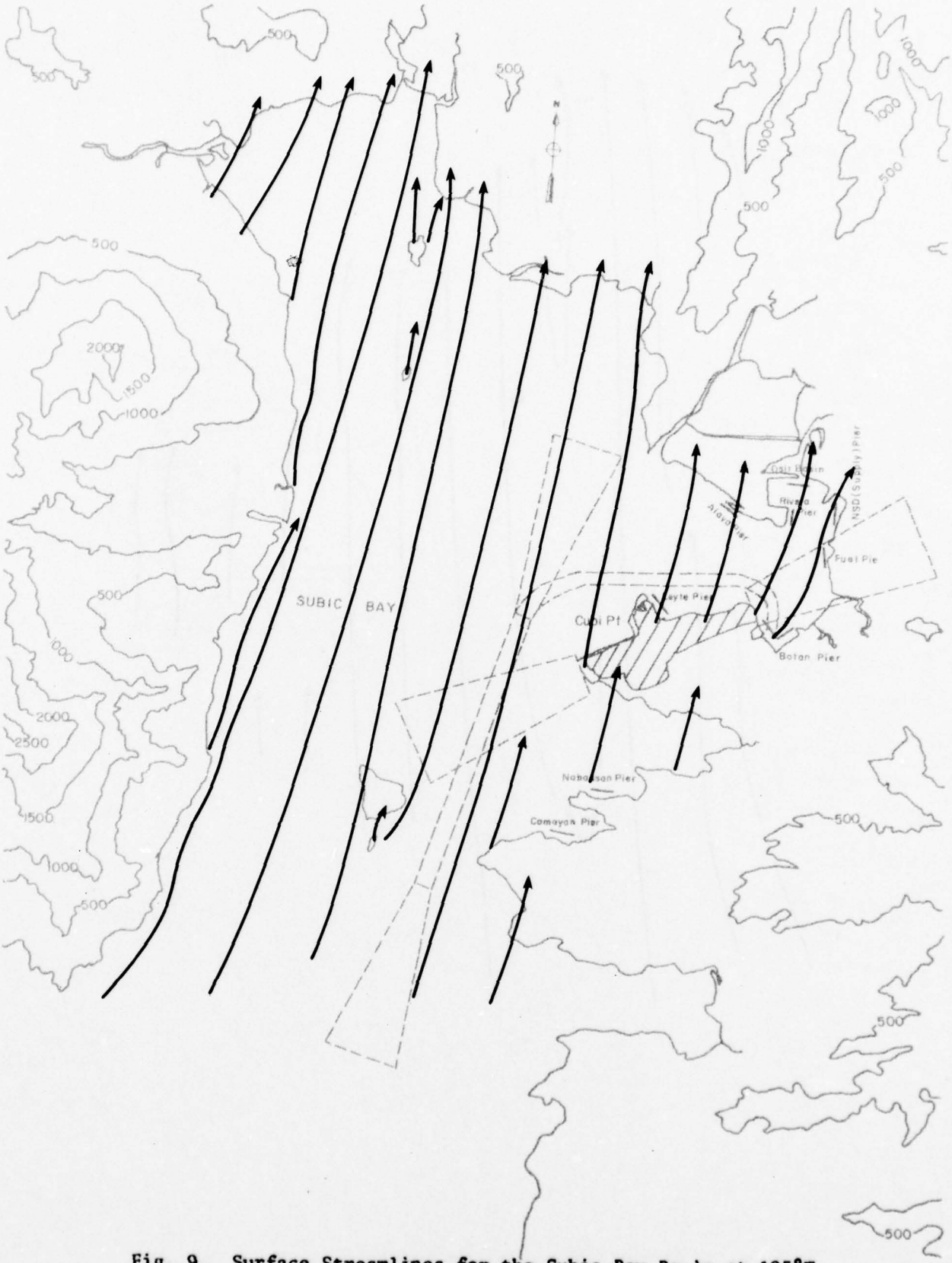

Fig. 9. Surface Streamlines for the Subic Bay Basin at 195°T

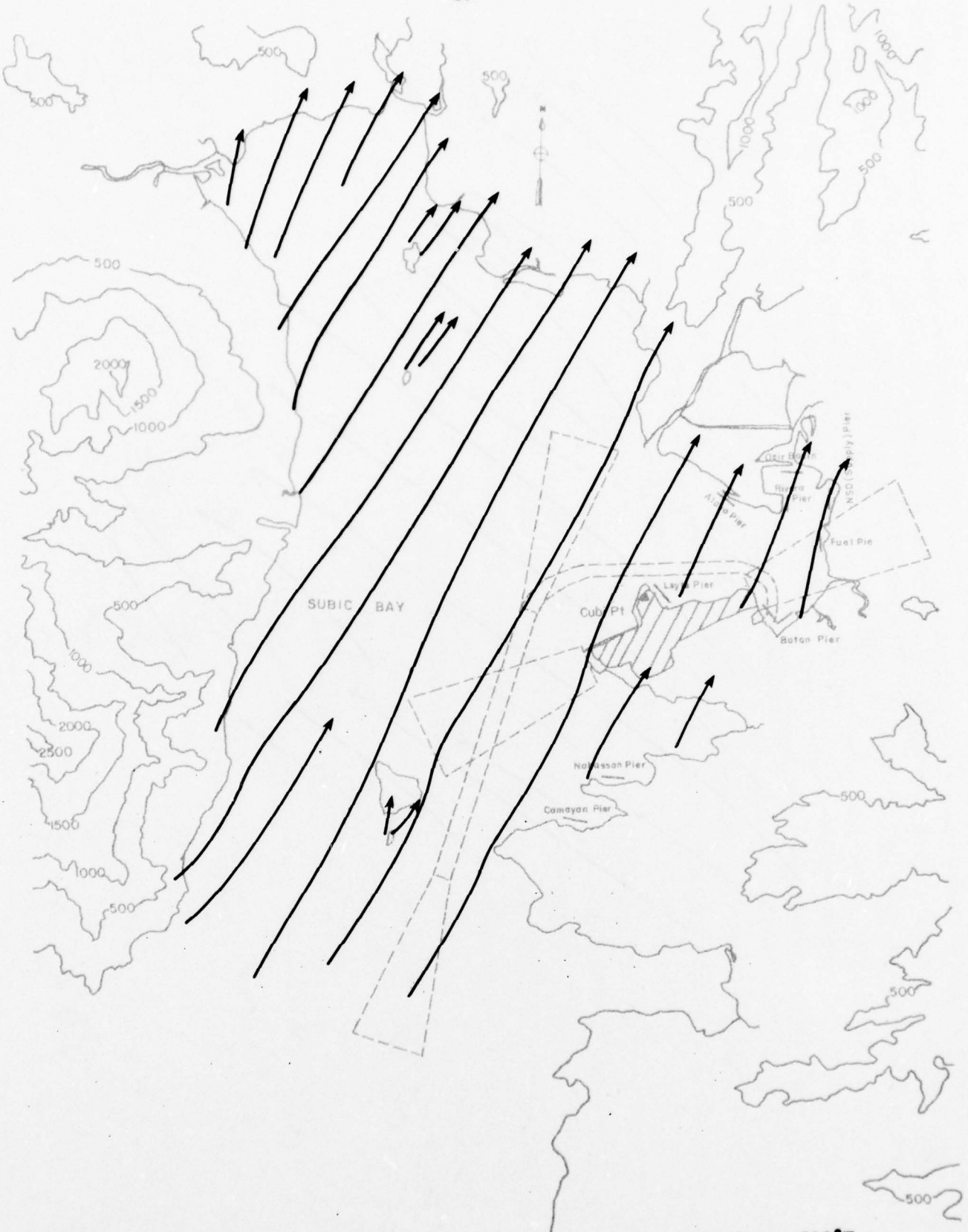

Fig. 10. Surface Streamlines for the Subic Bay Basin at 210°T

Fig. 11. Surface Streamlines for the Subic Bay Basin at 225°T

Fig. 12. Surface Streamlines for the Subic Bay Basin at 240°T

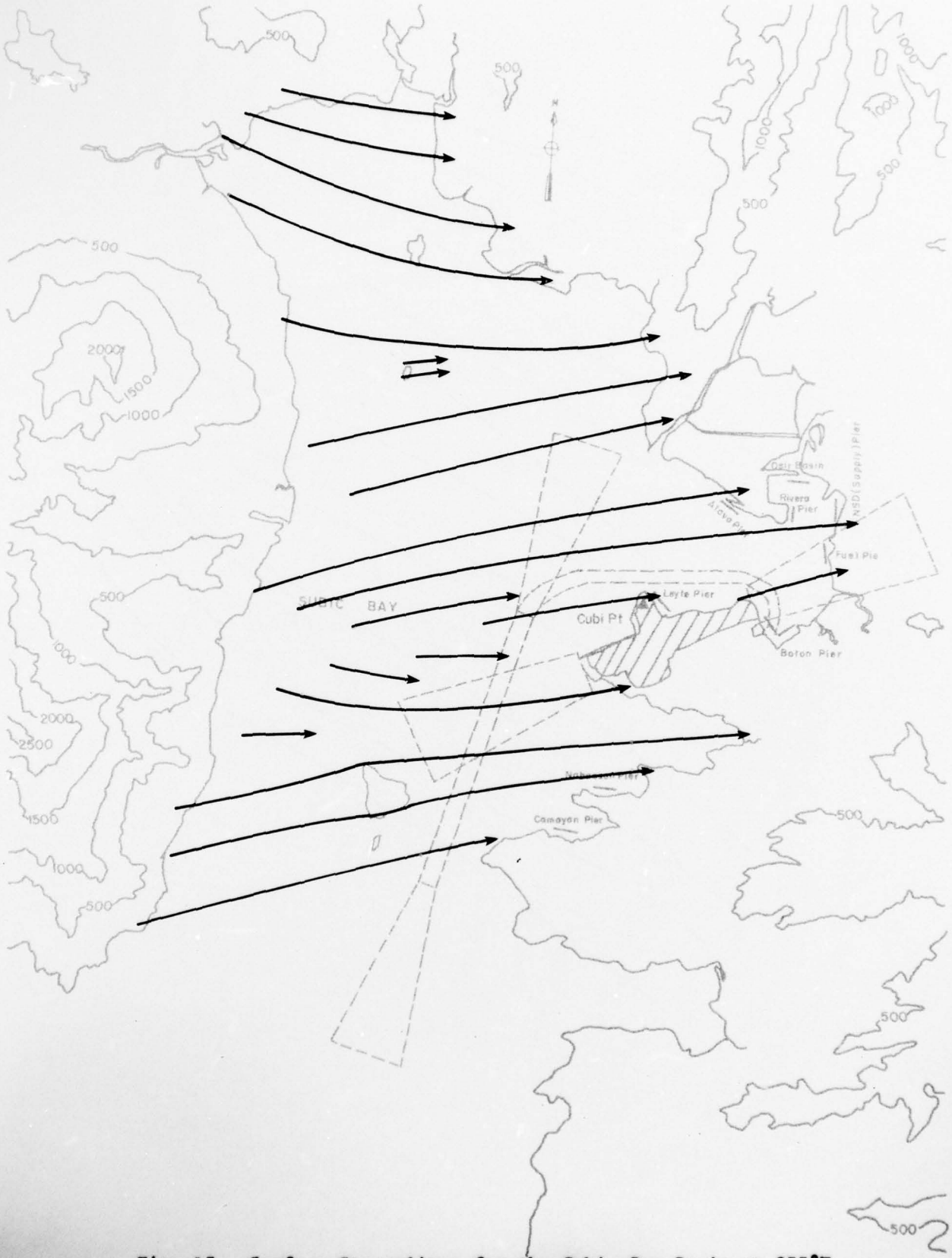

Fig. 13. Surface Streamlines for the Subic Bay Basin at 255°T

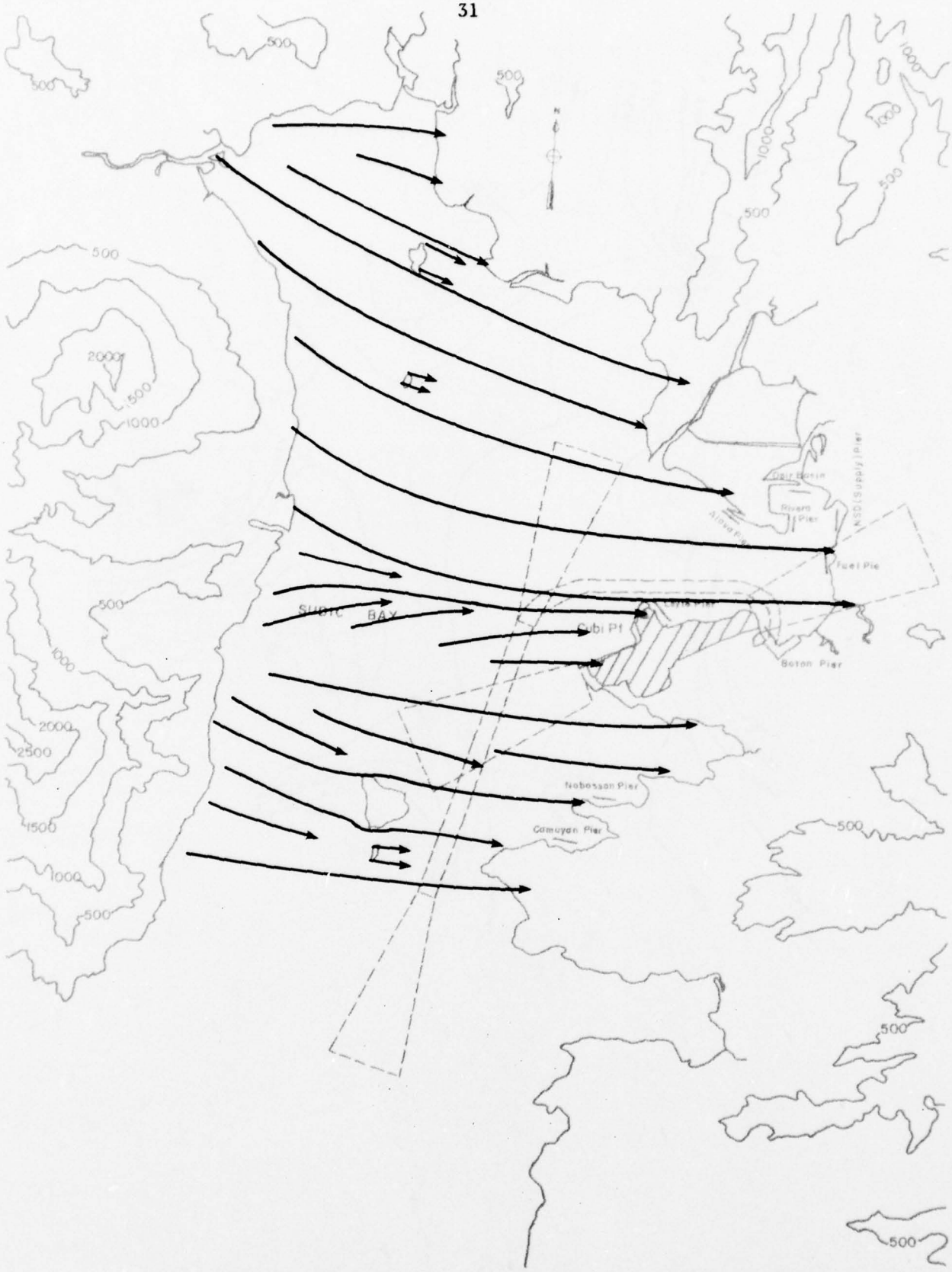

Fig. 14. Surface Streamlines for the Subic Bay Basin at 270°T

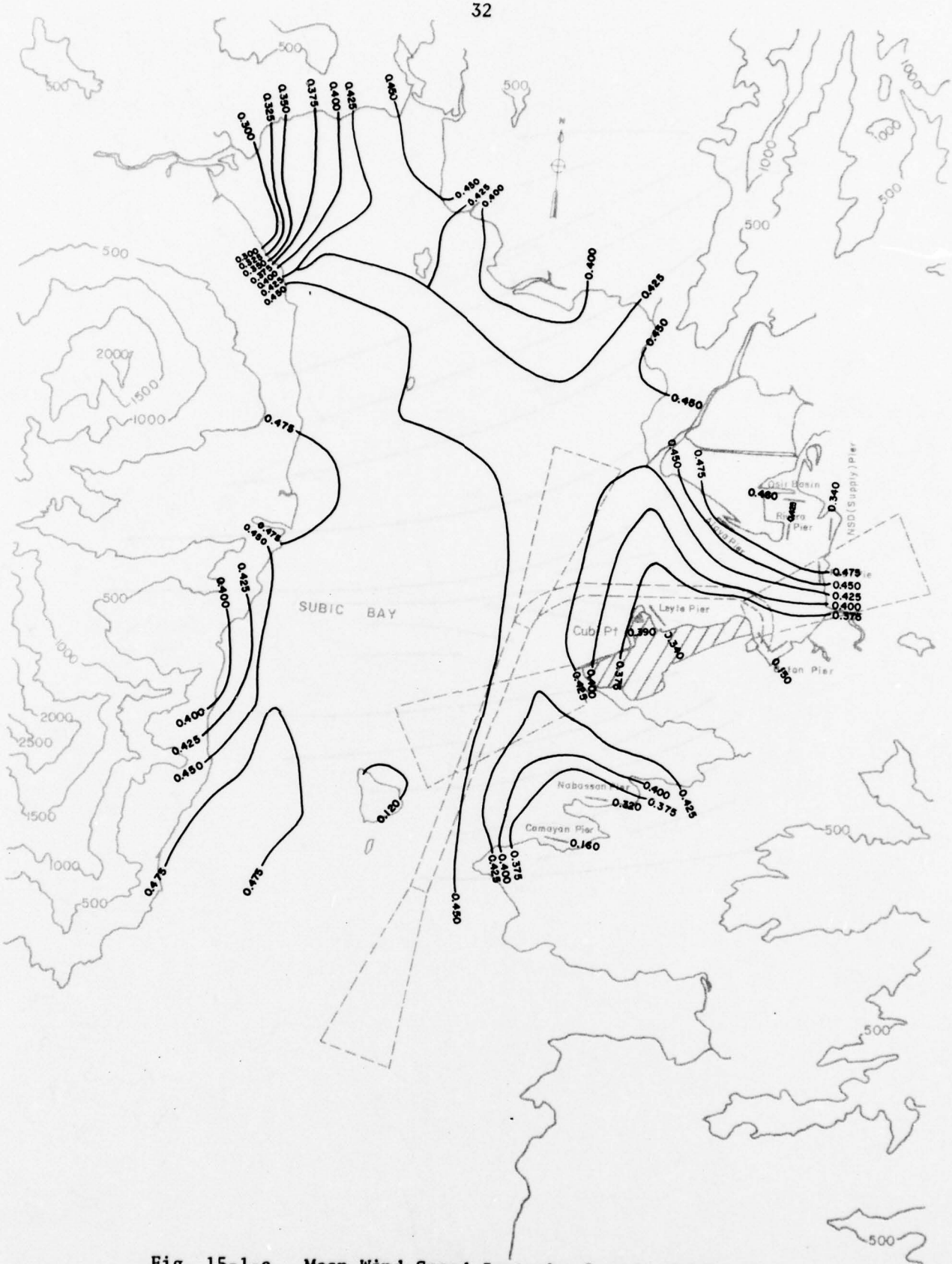

Fig. 15-1-a. Mean Wind Speed Isotachs for the Subic Bay Basin at 180°T, z = 70 ft (21.3 m)

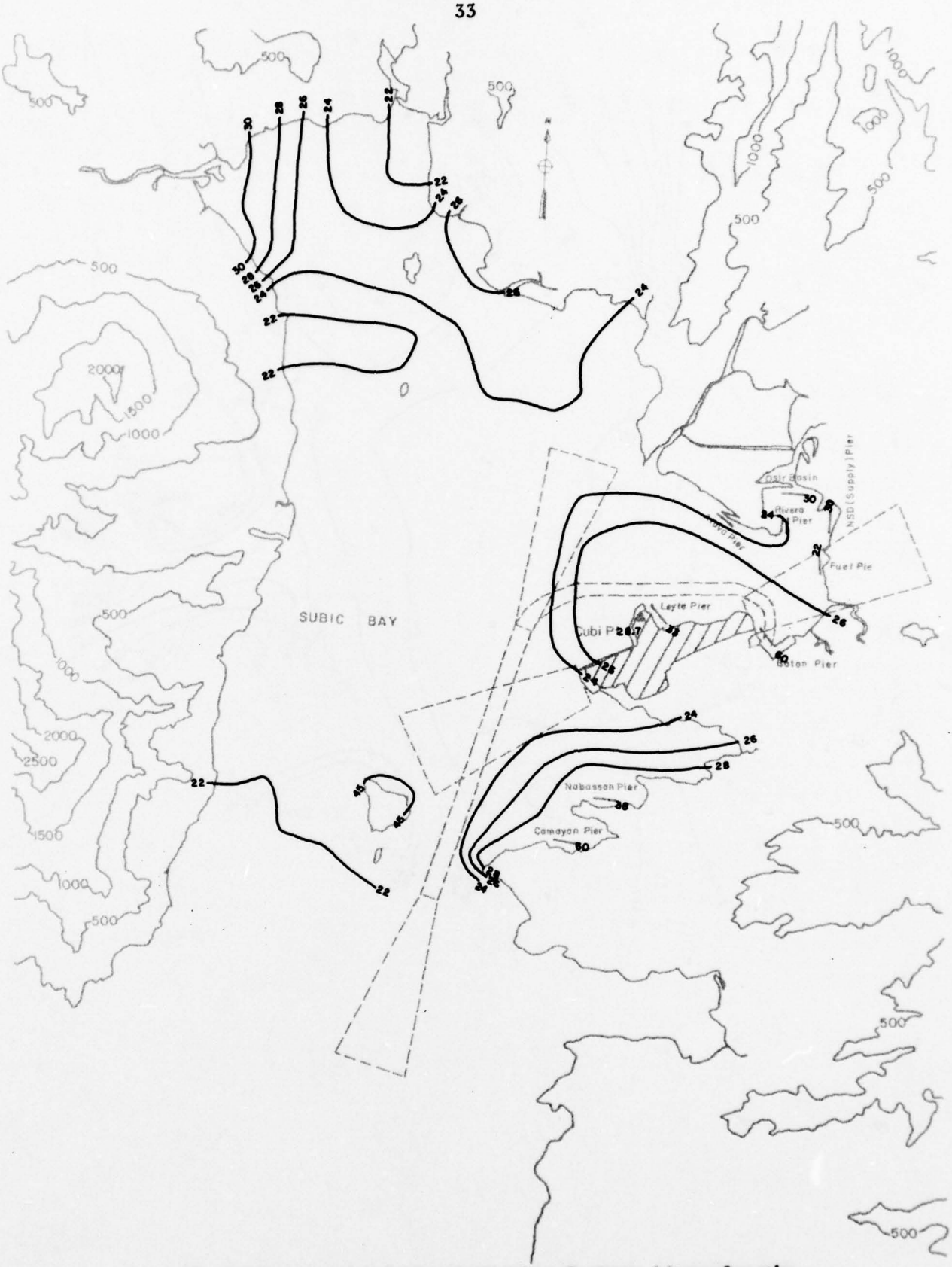

Fig. 15-1-b. Turbulence Intensity Contour Lines for the Subic Bay Basin at 180°T, z = 70 ft (21.3 m)

Fig. 15-2-a. Mean Wind Speed Isotachs for the Subic Bay Basin at 180°T, z = 150 ft (45.7 m)

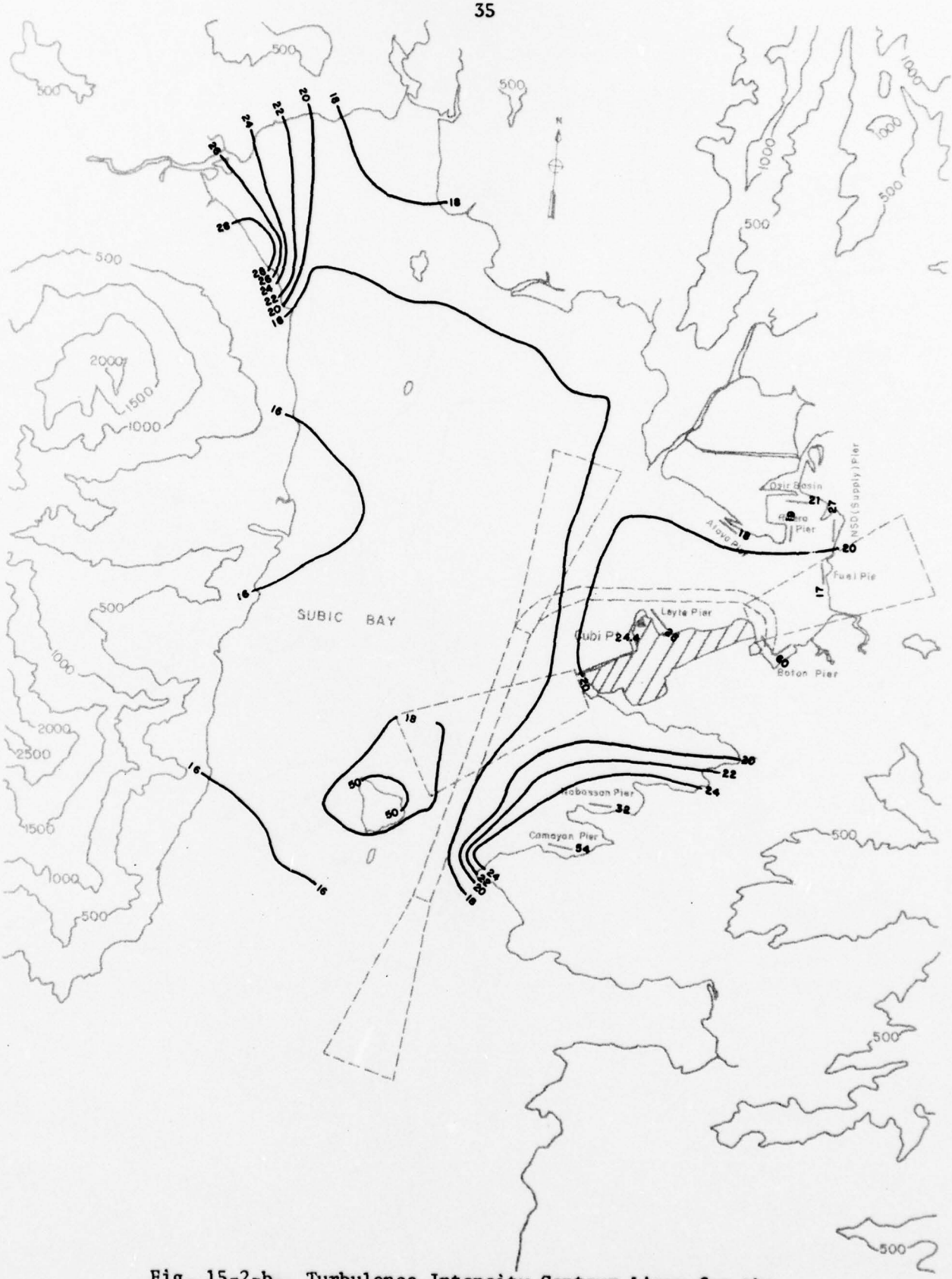

Fig. 15-2-b. Turbulence Intensity Contour Lines for the Subic Bay Basin at 180°T, z = 150 ft (45.7 m)

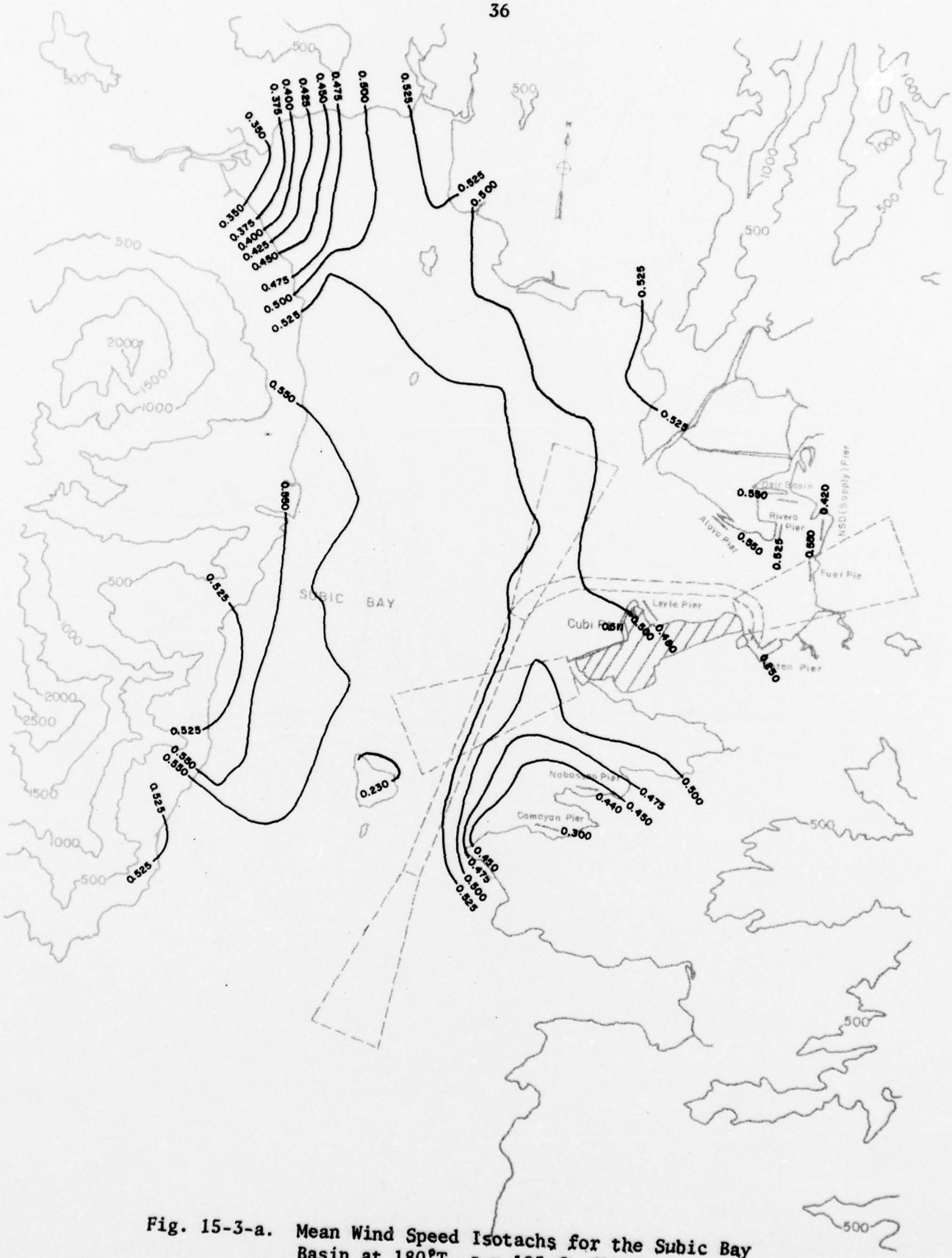

Fig. 15-3-a. Mean Wind Speed Isotachs for the Subic Bay Basin at 180°T, z = 195 ft (59.5 m)

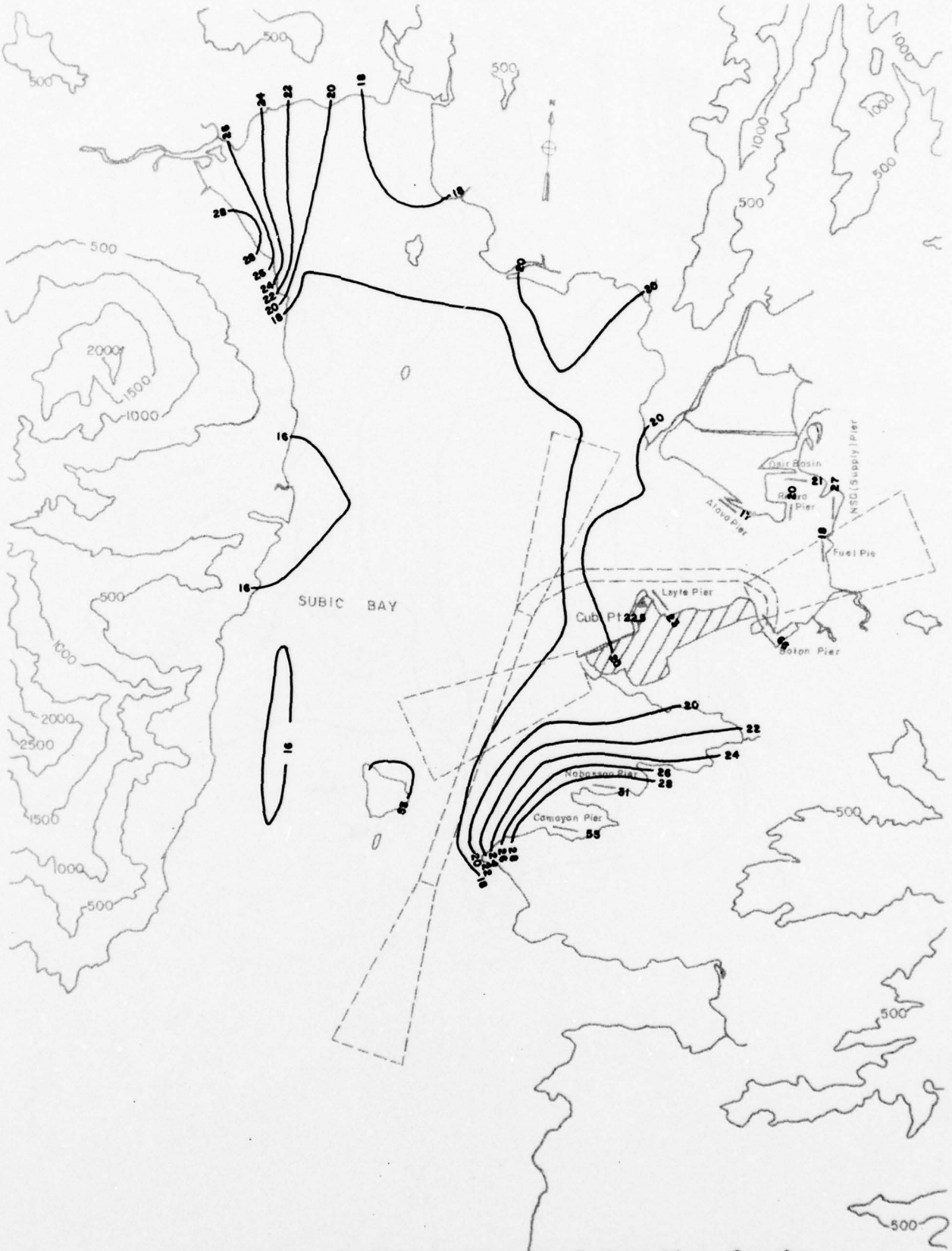

Fig. 15-3-b. Turbulence Intensity Contour Lines for the Subic Bay Basin at 180°T, z = 195 ft (59.5 m)

Fig. 15-4-a. Mean Wind Speed Isotachs for the Subic Bay Basin at 180°T, z = 275 ft (83.9 m)

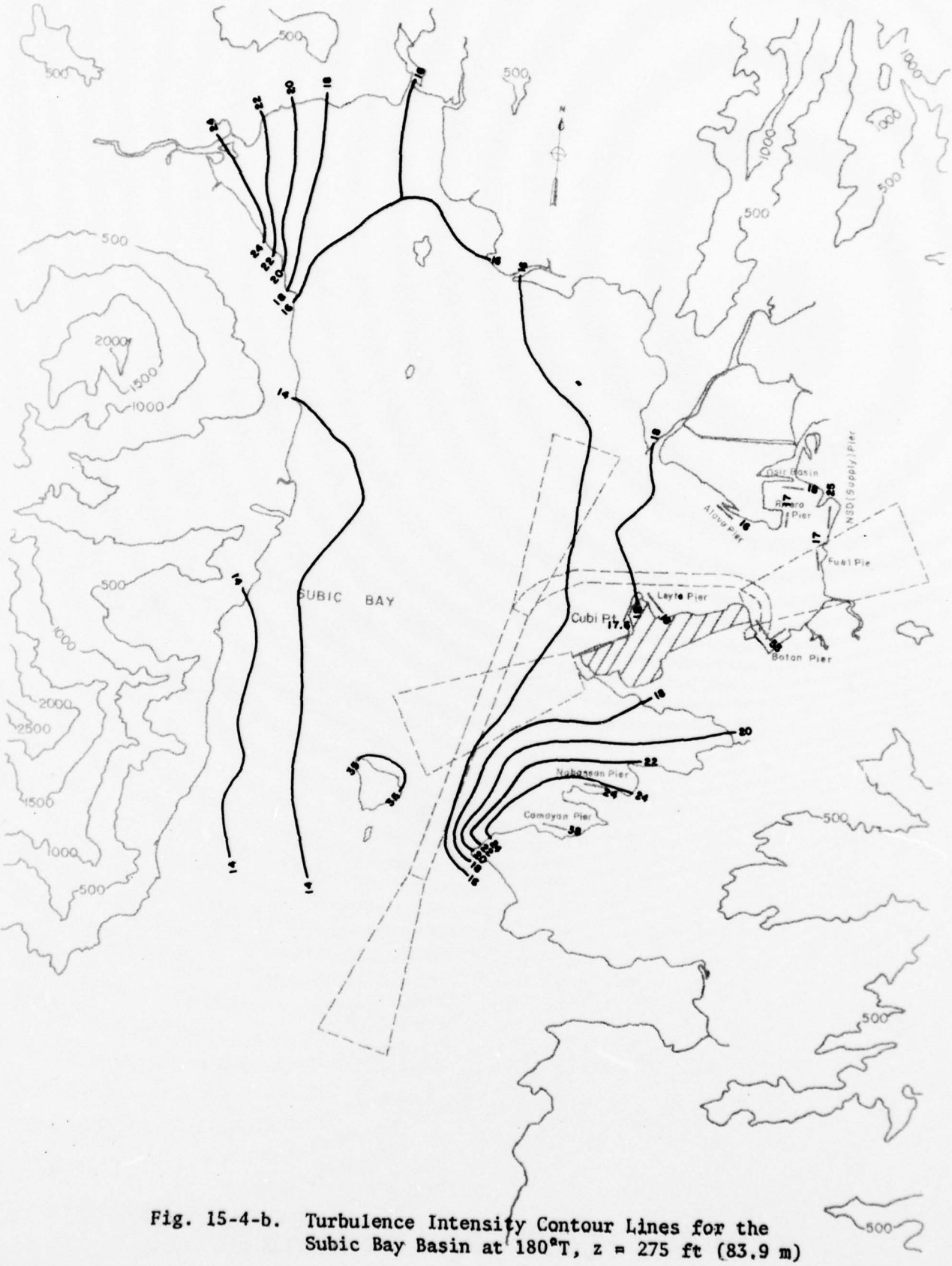

Fig. 15-4-b. Turbulence Intensity Contour Lines for the Subic Bay Basin at 180°T, z = 275 ft (83.9 m)

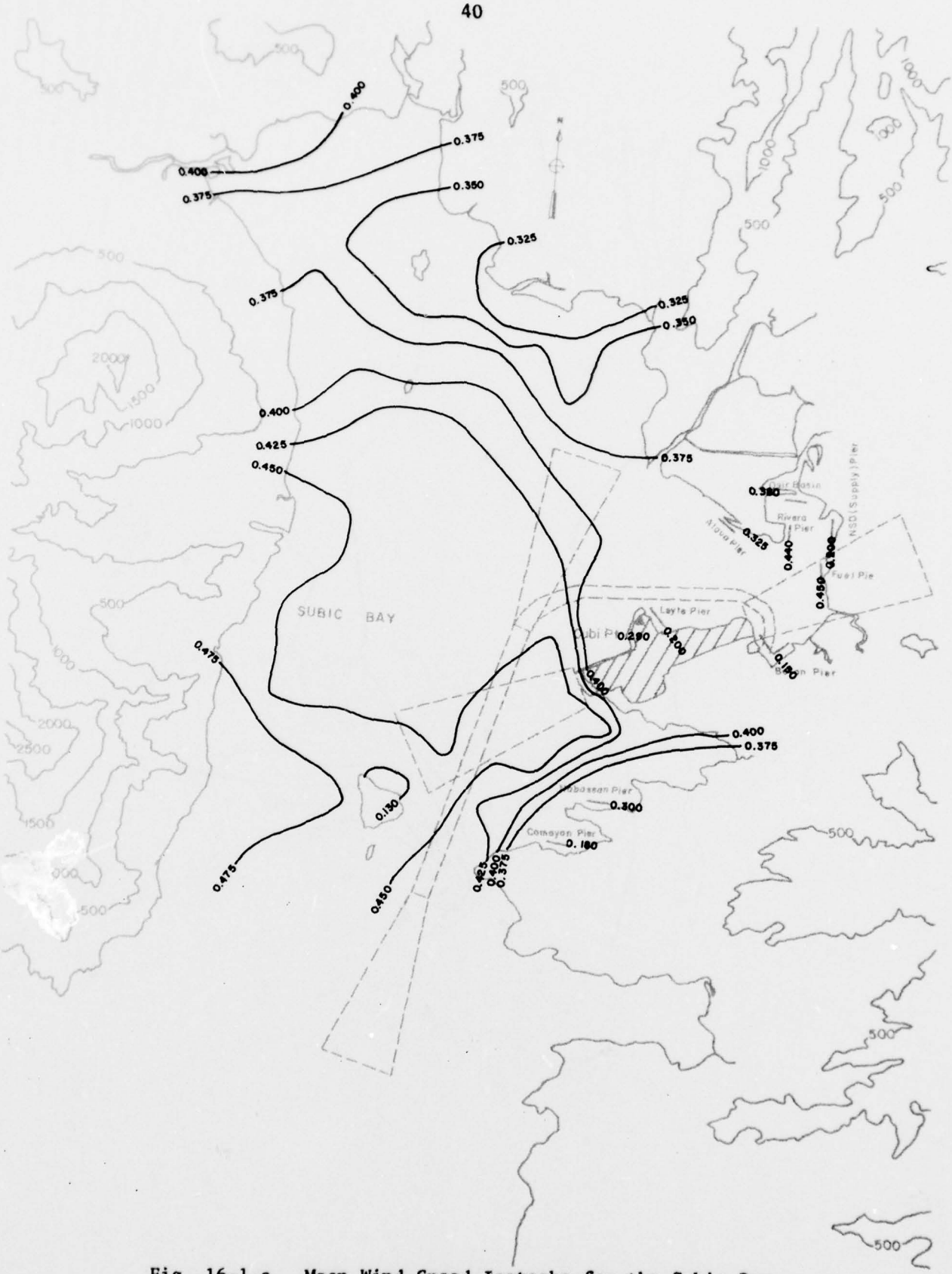

Fig. 16-1-a. Mean Wind Speed Isotachs for the Subic Bay Basin at 195°T, z = 70 ft (21.3 m)

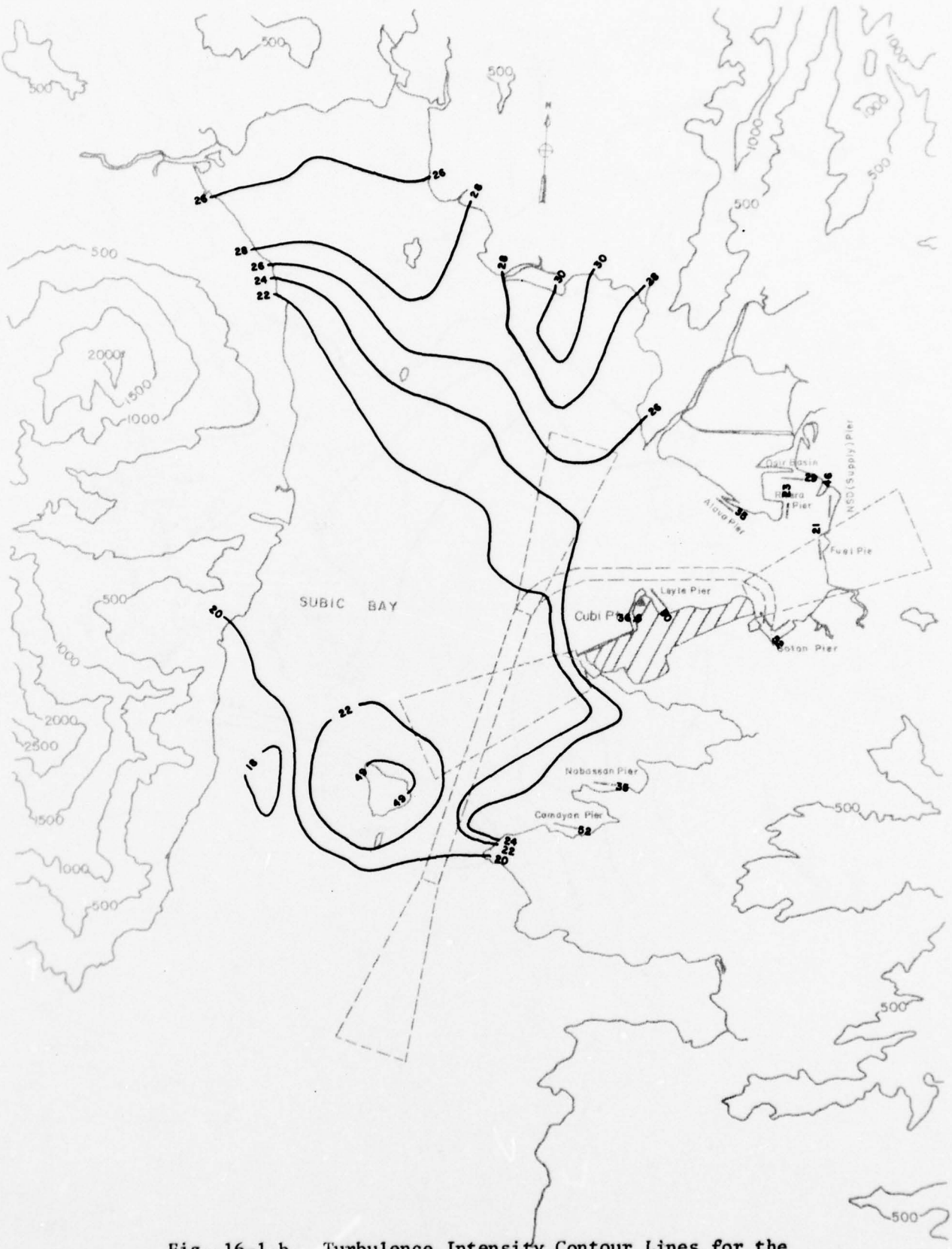

Fig. 16-1-b. Turbulence Intensity Contour Lines for the Subic Bay Basin at 1950°T, z = 70 ft (21.3 m)

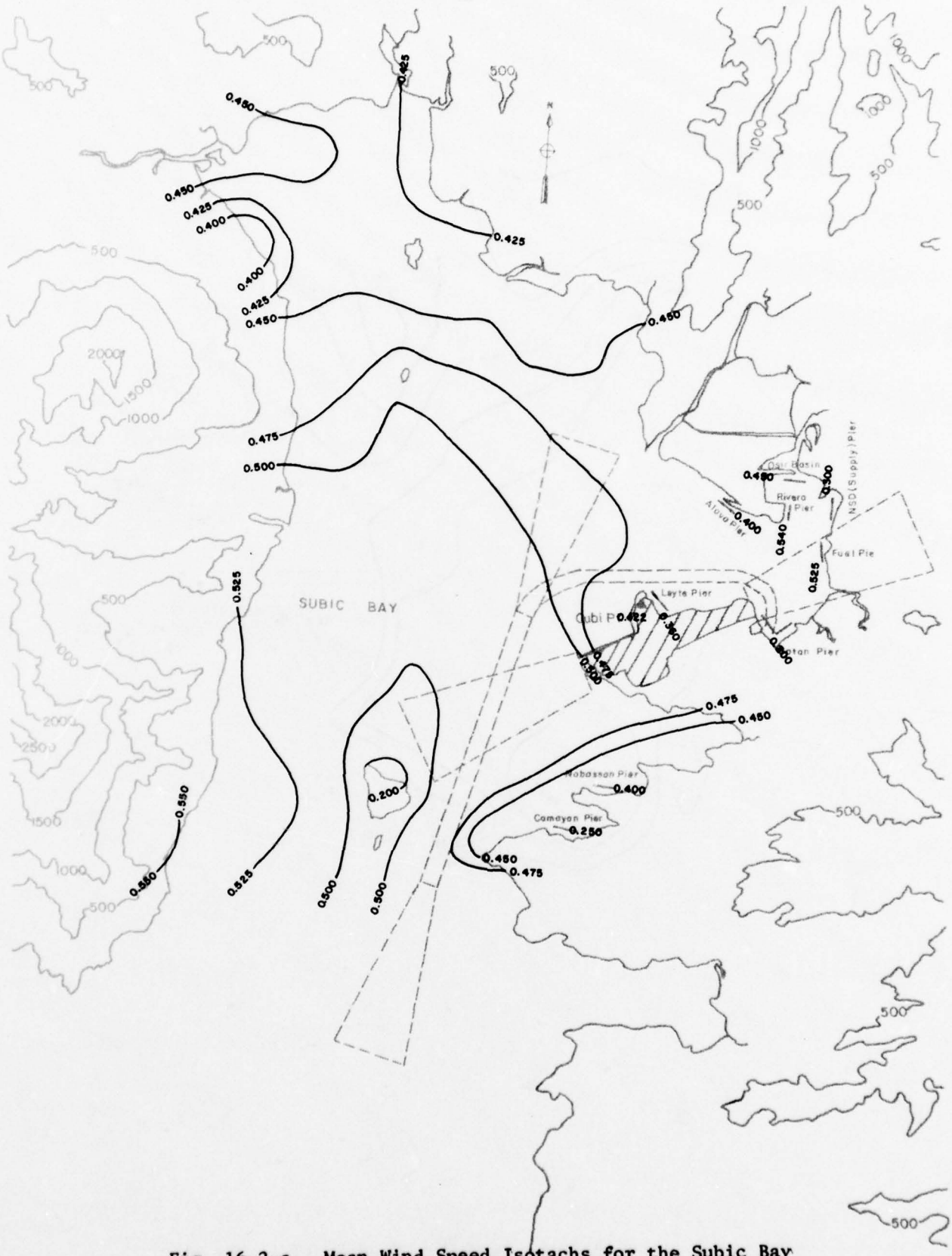

Fig. 16-2-a. Mean Wind Speed Isotachs for the Subic Bay Basin at 195°T, z = 150 ft (45.7 m)

Fig. 16-2-b. Turbulence Intensity Contour Lines for the Subic Bay Basin at 195°T, z = 150 ft (45.7 m)

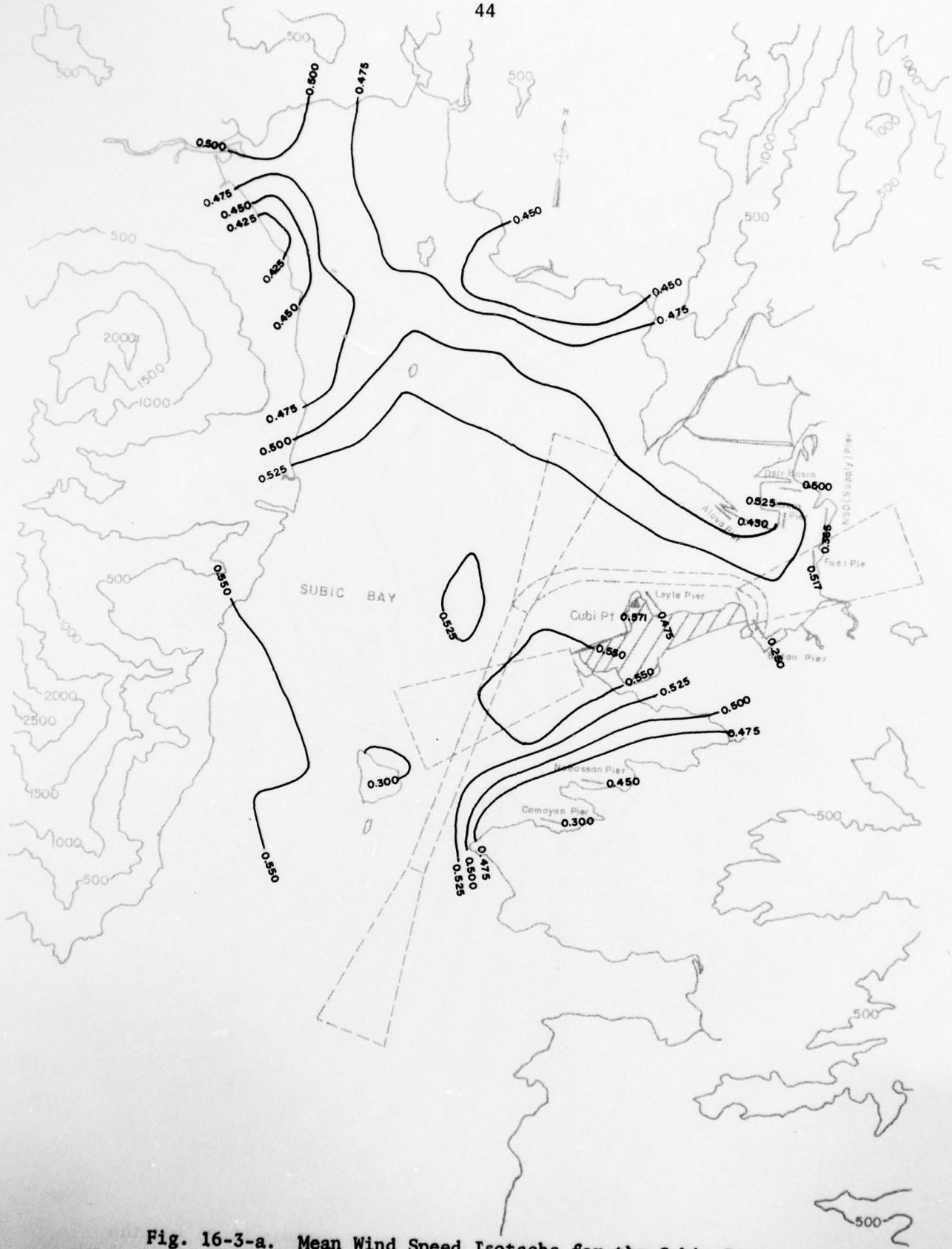

Fig. 16-3-a. Mean Wind Speed Isotachs for the Subic Bay Basin at 195°T, z = 195 ft (59.5 m)

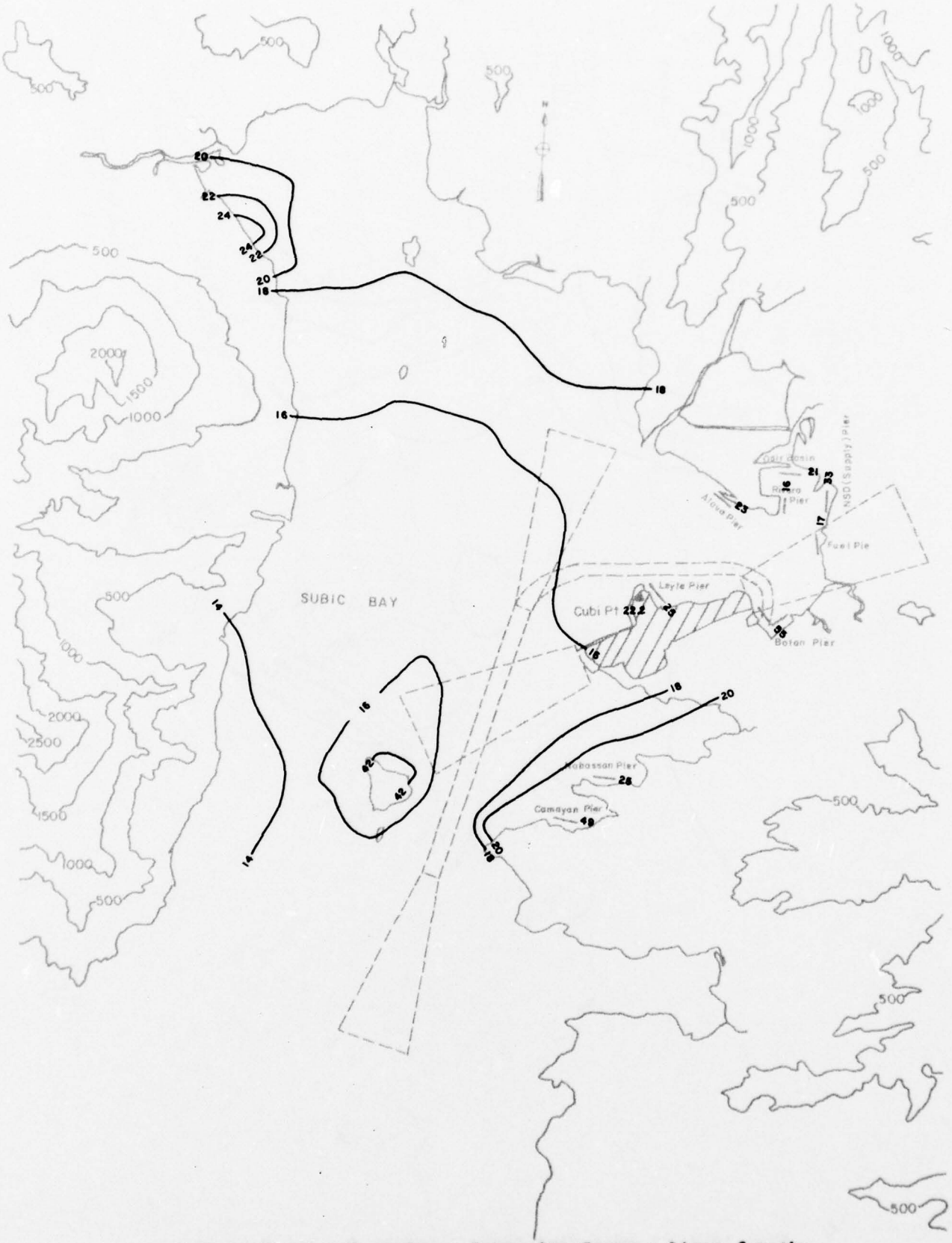

Fig. 16-3-b. Turbulence Intensity Contour Lines for the Subic Bay Basin at 195°T, z = 195 ft (59.5 m)

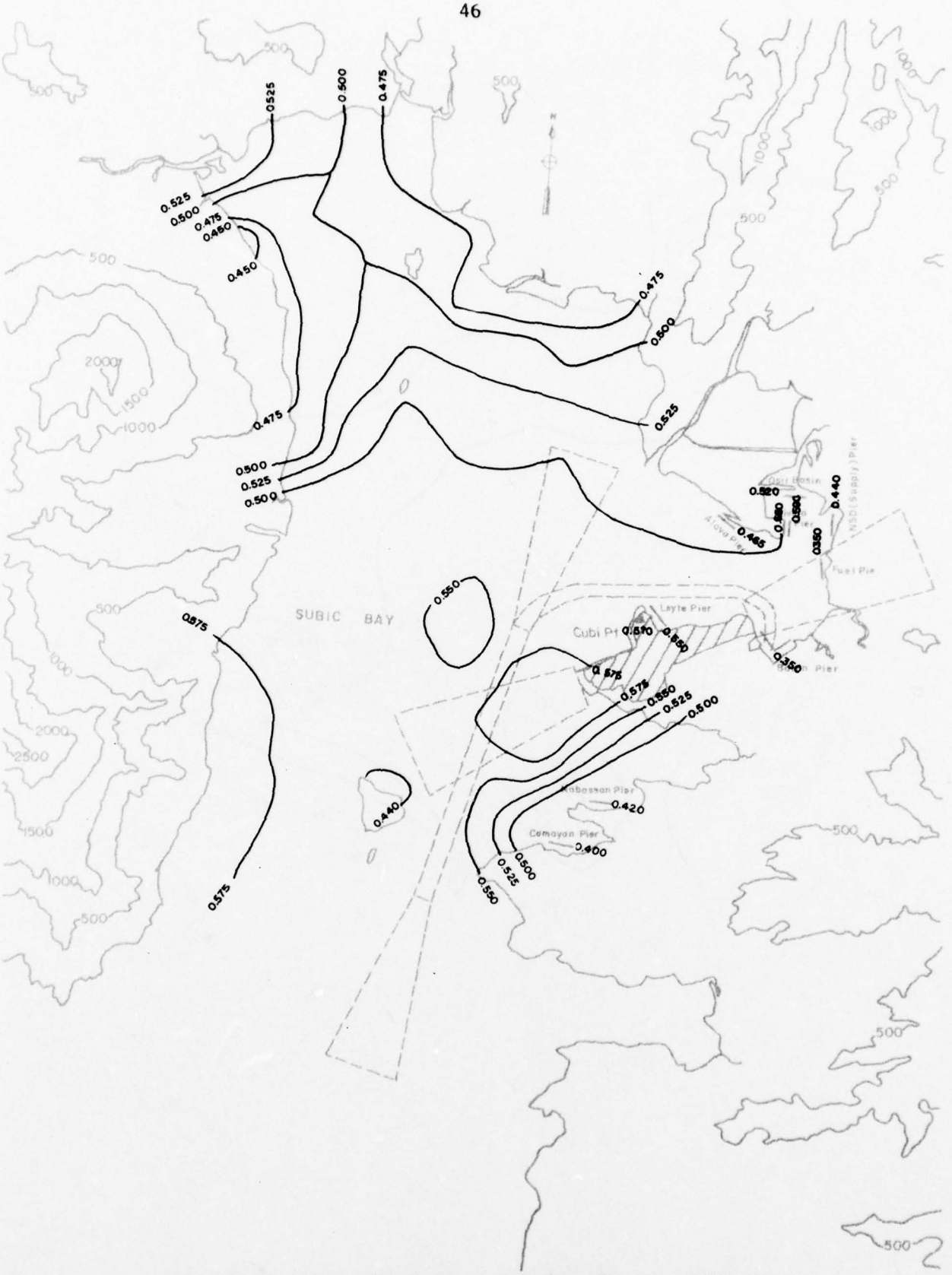

Fig. 16-4-a. Mean Wind Speed Isotachs for the Subic Bay Basin at 195°T, z = 275 ft (83.9 m)

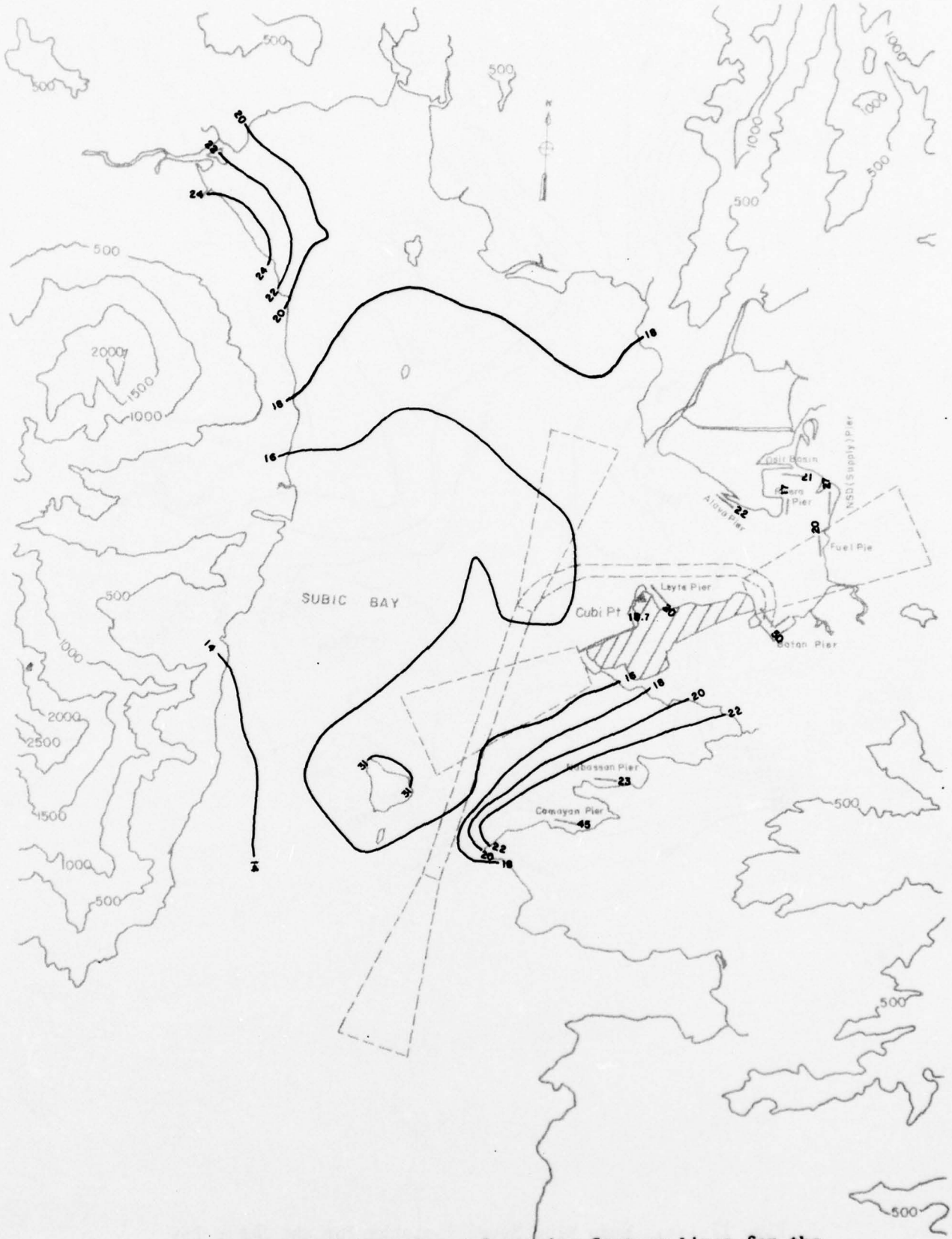

Fig. 16-4-b. Turbulence Intensity Contour Lines for the Subic Bay Basin at 195°T, z = 275 ft (83.9 m)

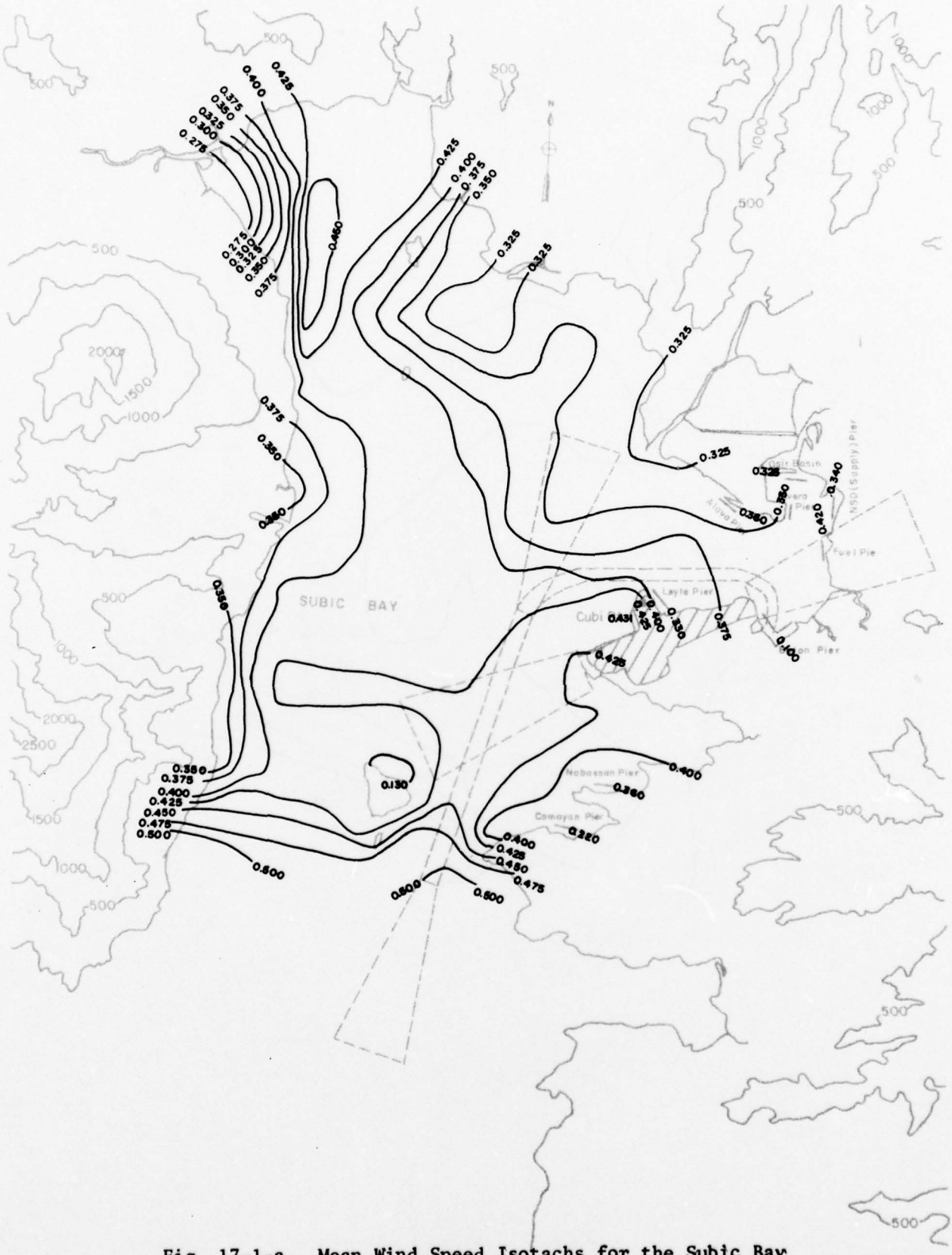

Fig. 17-1-a. Mean Wind Speed Isotachs for the Subic Bay Basin at 210°T, z = 70 ft (21.3 m)

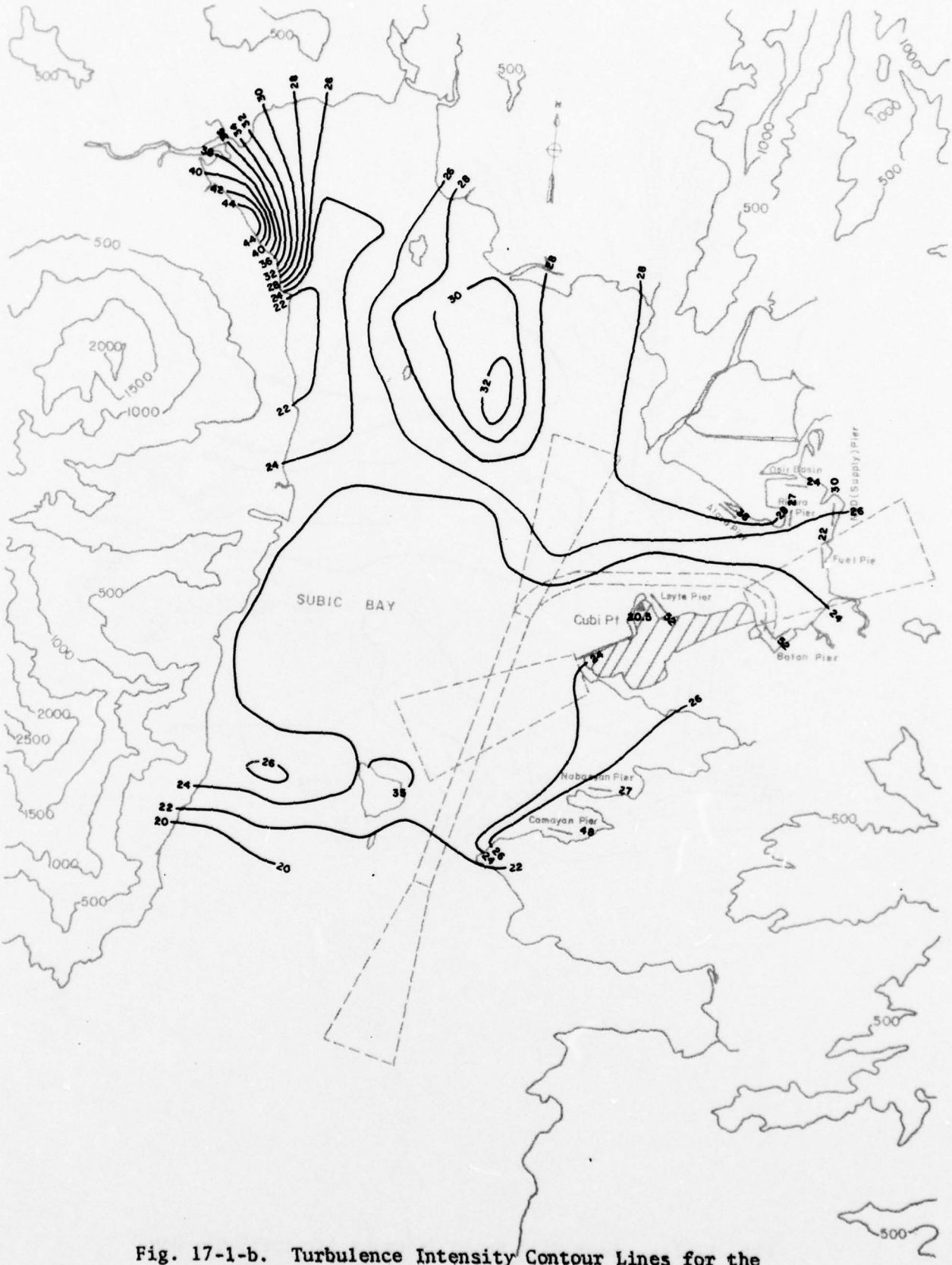

Fig. 17-1-b. Turbulence Intensity Contour Lines for the Subic Bay Basin at 210°T, z = 70 ft (21.3 m)

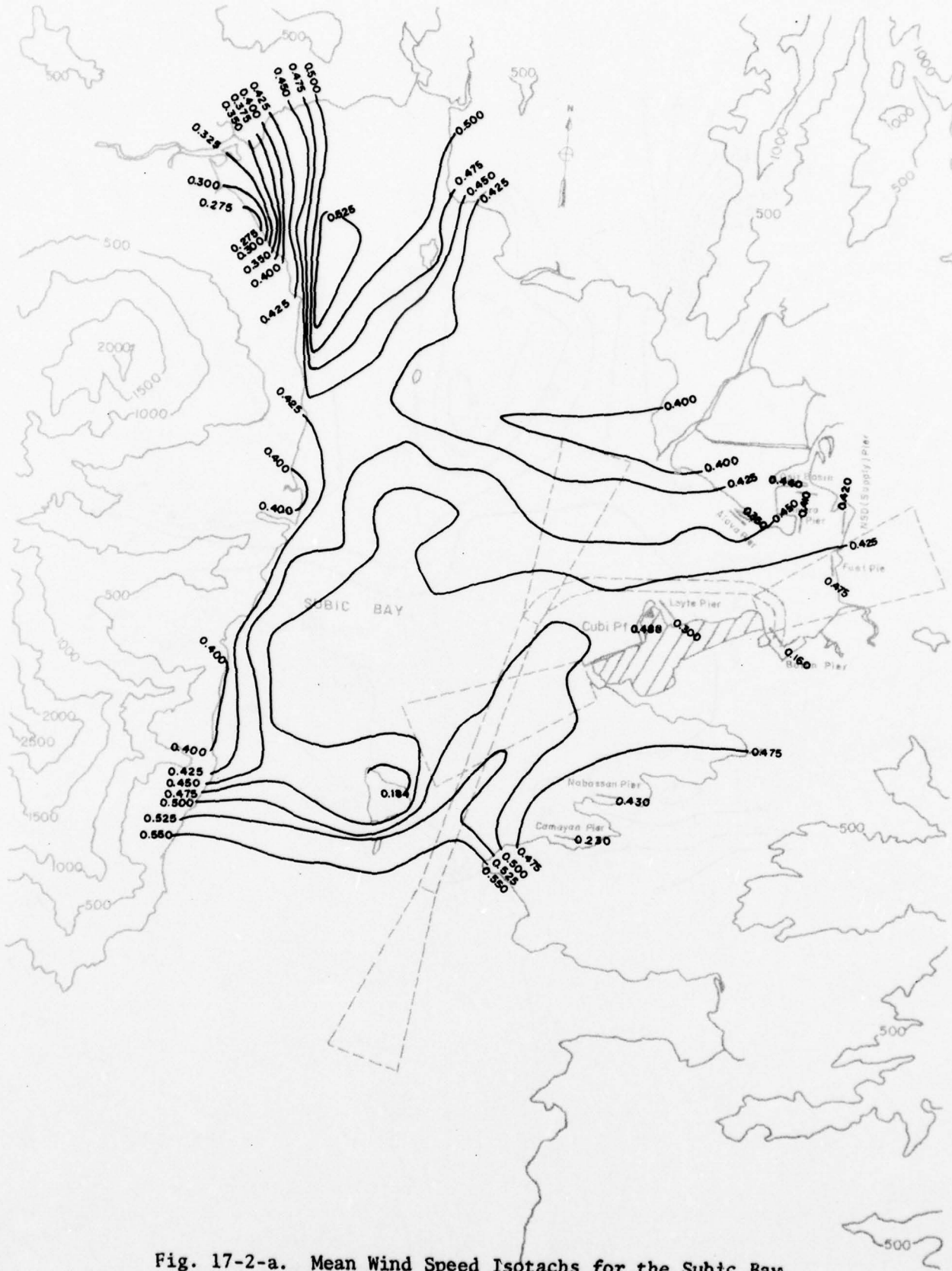

Fig. 17-2-a. Mean Wind Speed Isotachs for the Subic Bay Basin at 210°T, z = 150 ft (45.7 m)

Fig. 17-2-b. Turbulence Intensity Contour Lines for the Subic Bay Basin at 210°T, z = 150 ft (45.7 m)

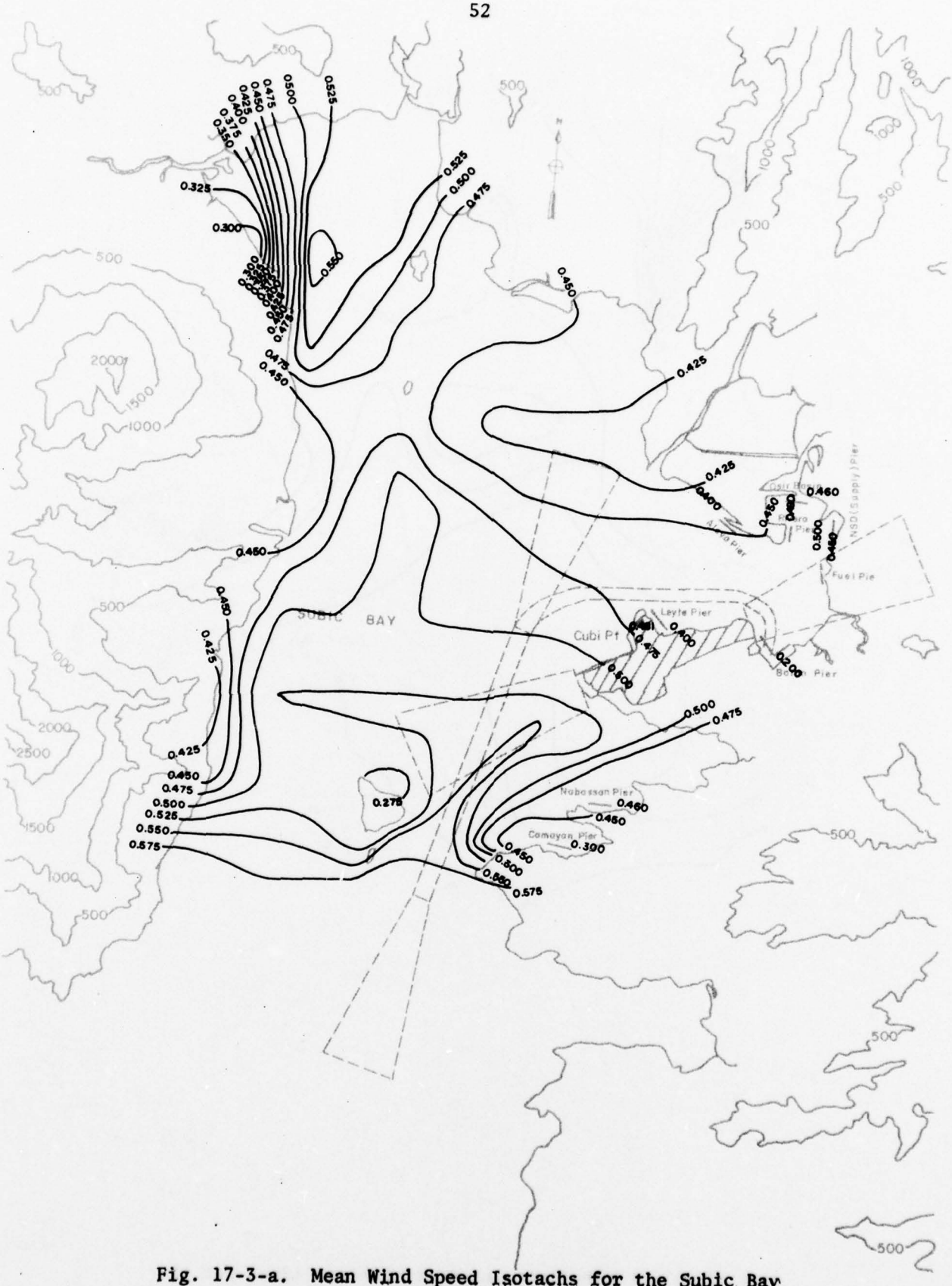

Fig. 17-3-a. Mean Wind Speed Isotachs for the Subic Bay Basin at 210°T, z = 195 ft (59.5 m)

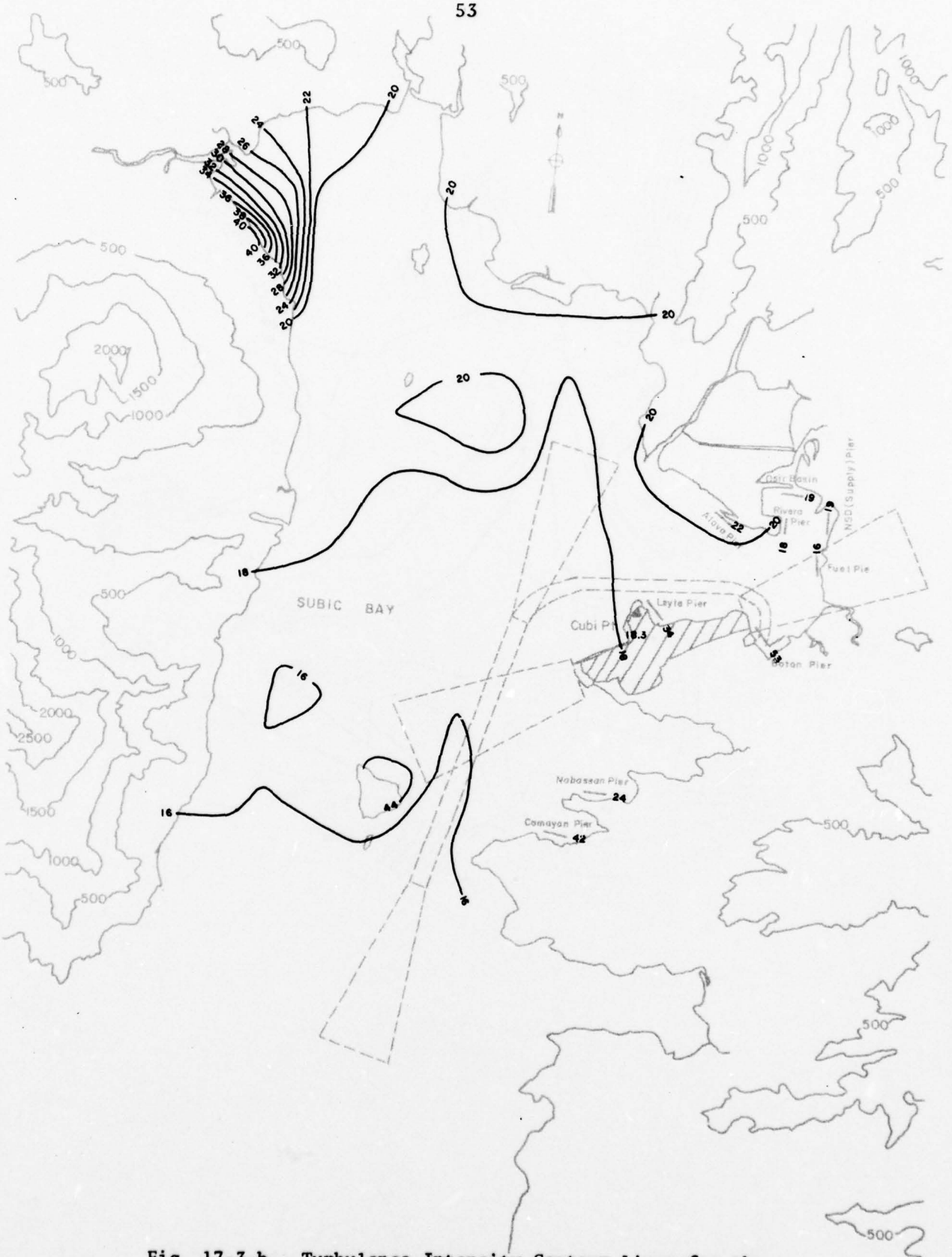

Fig. 17-3-b. Turbulence Intensity Contour Lines for the Subic Bay Basin at 210°T, z = 195 ft (59.5 m)

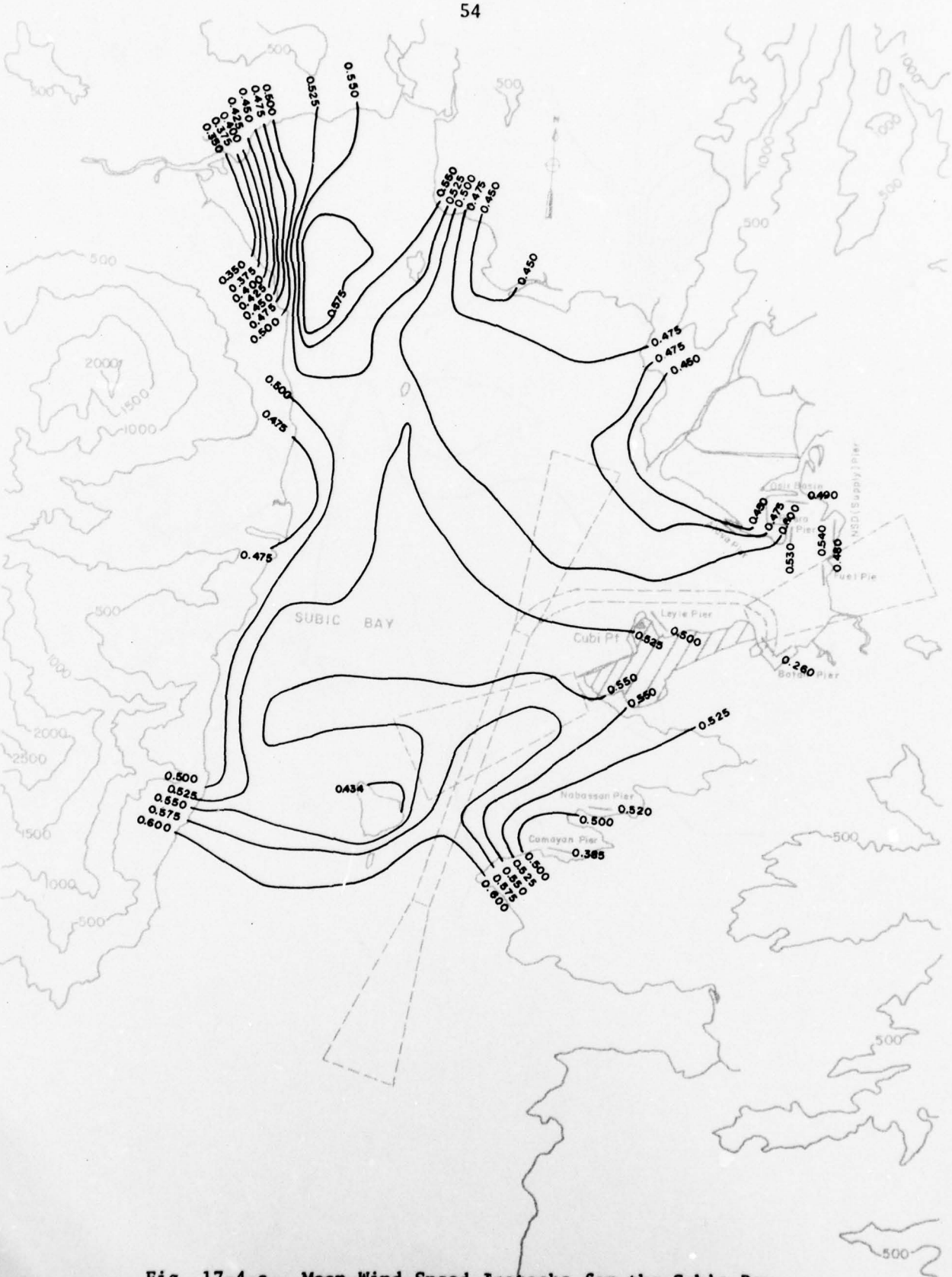

Fig. 17-4-a. Mean Wind Speed Isotachs for the Subic Bay Basin at 210°T, z = 275 ft (83.9 m)

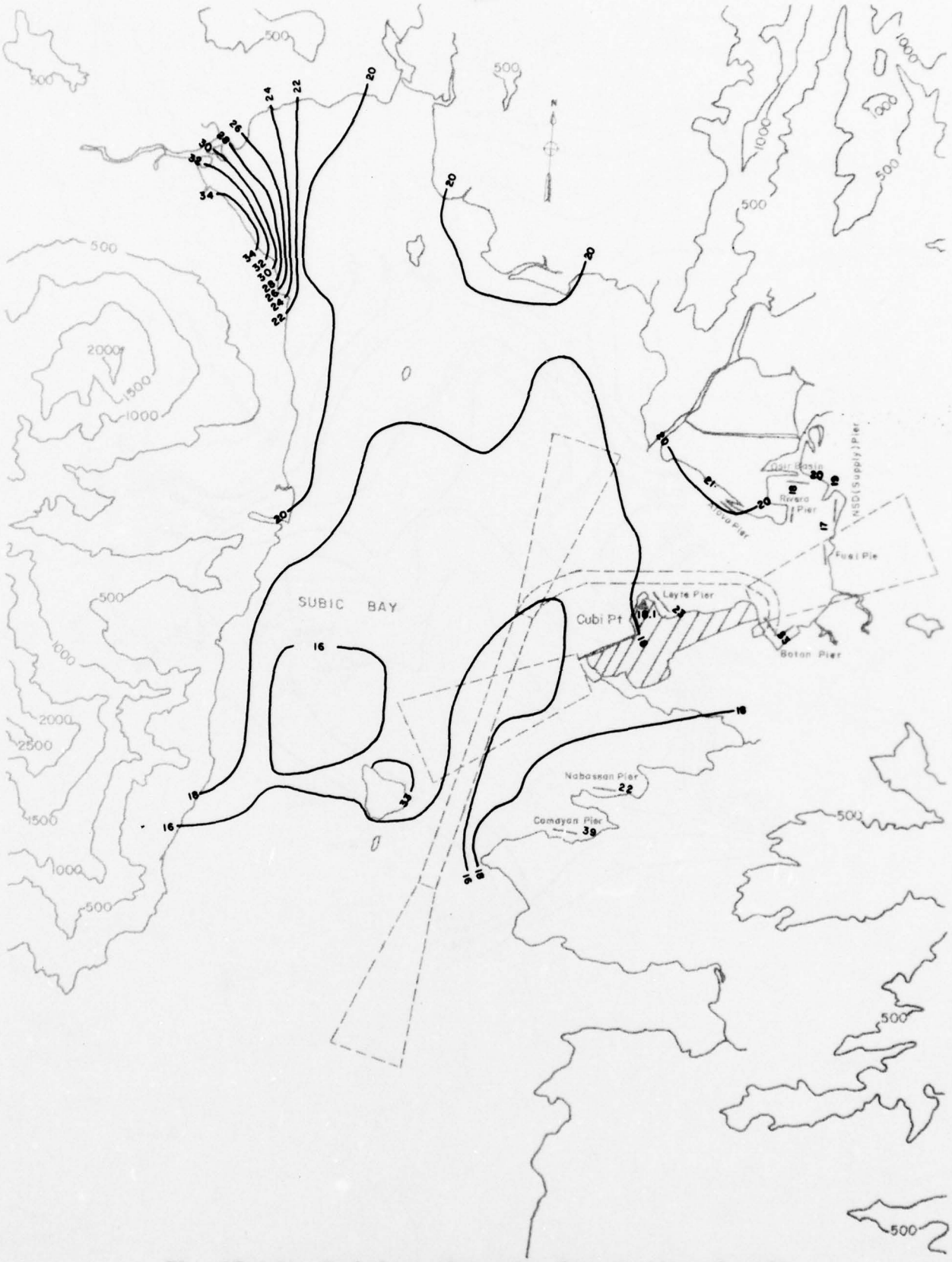

Fig. 17-4-b. Turbulence Intensity Contour Lines for the Subic Bay Basin at 210°T, z = 275 ft (83.9 m)

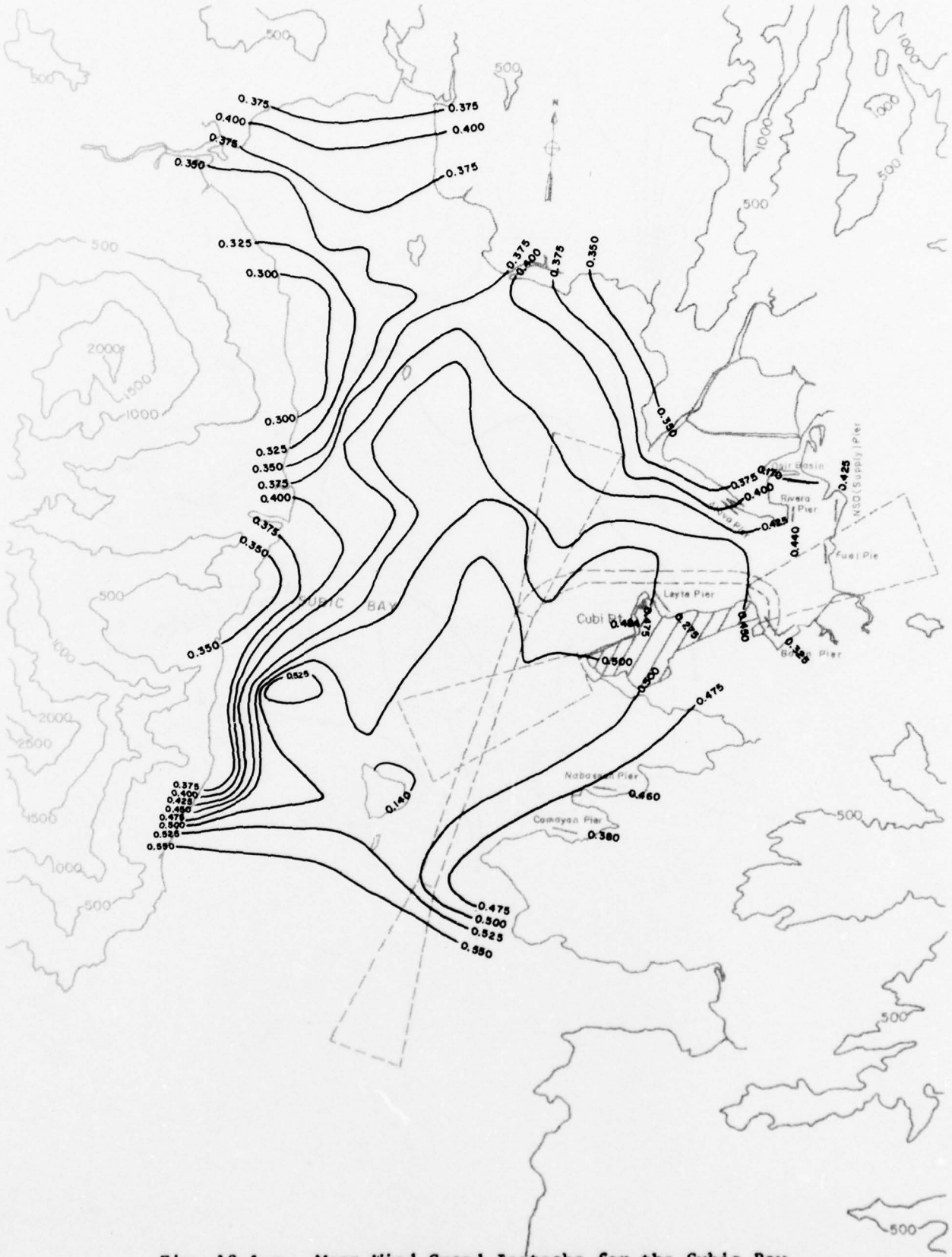

Fig. 18-1-a. Mean Wind Speed Isotachs for the Subic Bay Basin at 225°T, z = 70 ft (21.3 m)

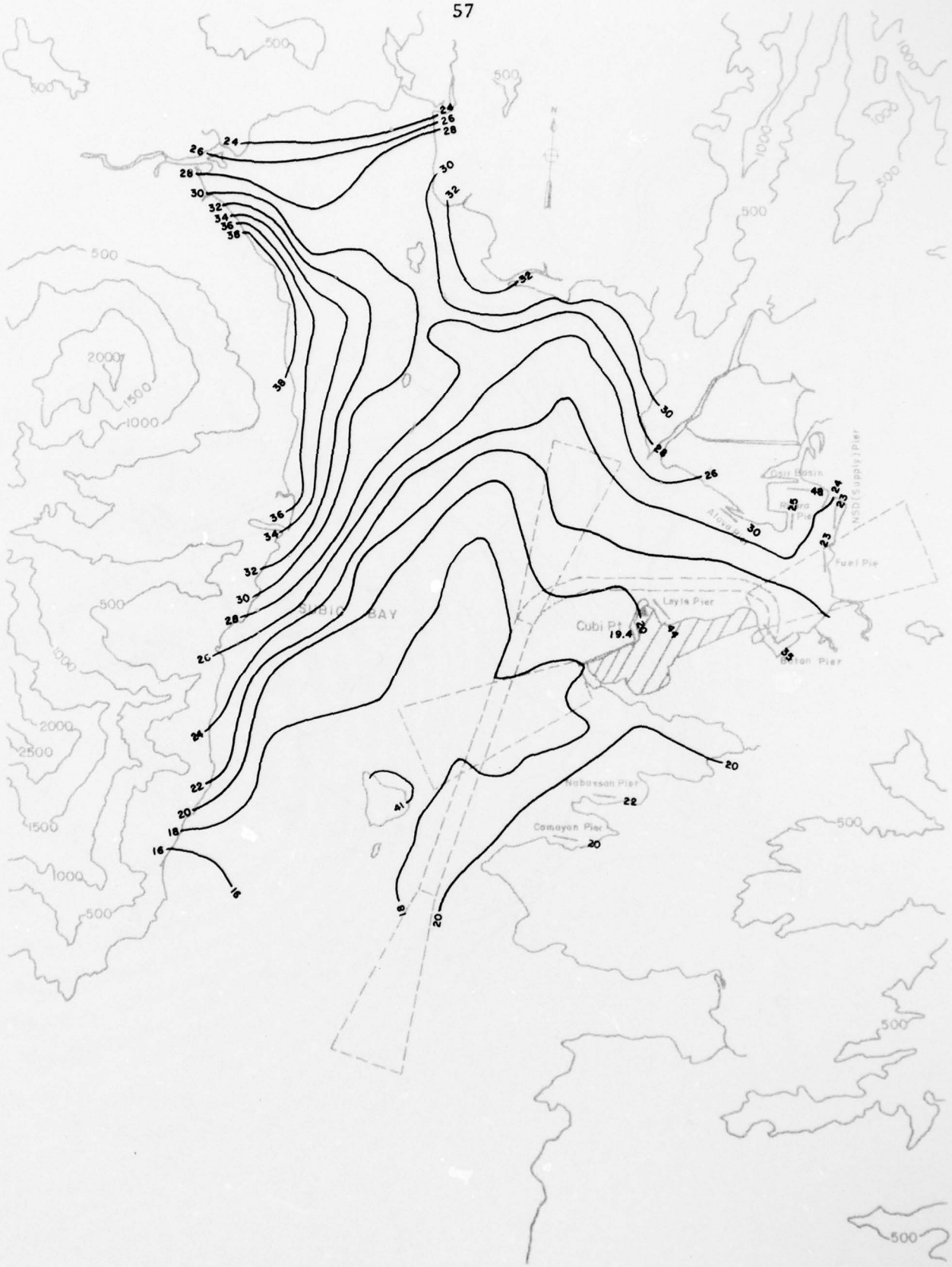

Fig. 18-1-b. Turbulence Intensity Contour Lines for the Subic Bay Basin at 225°T, z = 70 ft (21.3 m)

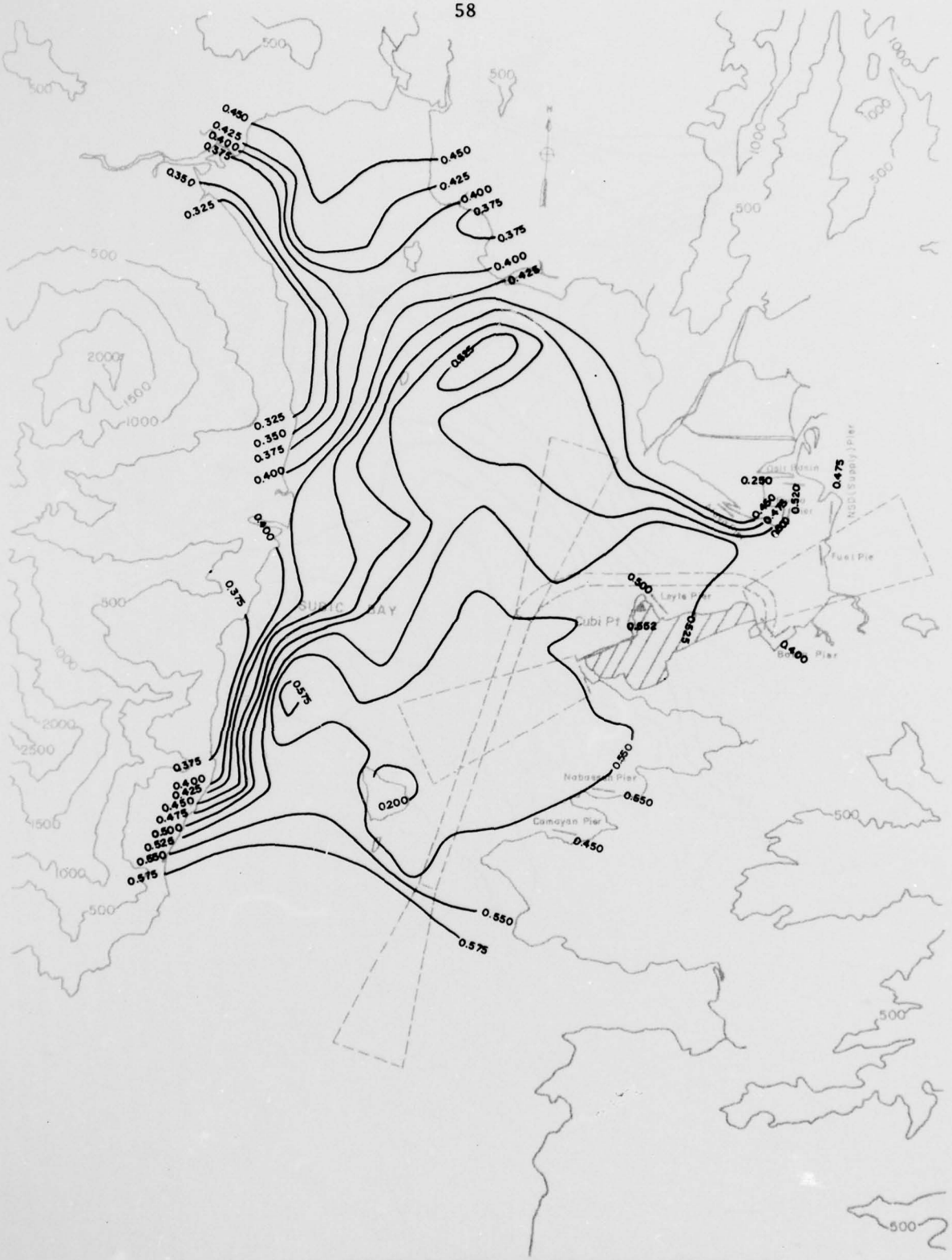

Fig. 18-2-a. Mean Wind Speed Isotachs for the Subic Bay Basin at 225°T, z = 150 ft (45.7 m)

Fig. 18-2-b. Turbulence Intensity Contour Lines for the Subic Bay Basin at 225°T, z = 150 ft (45.7 m)

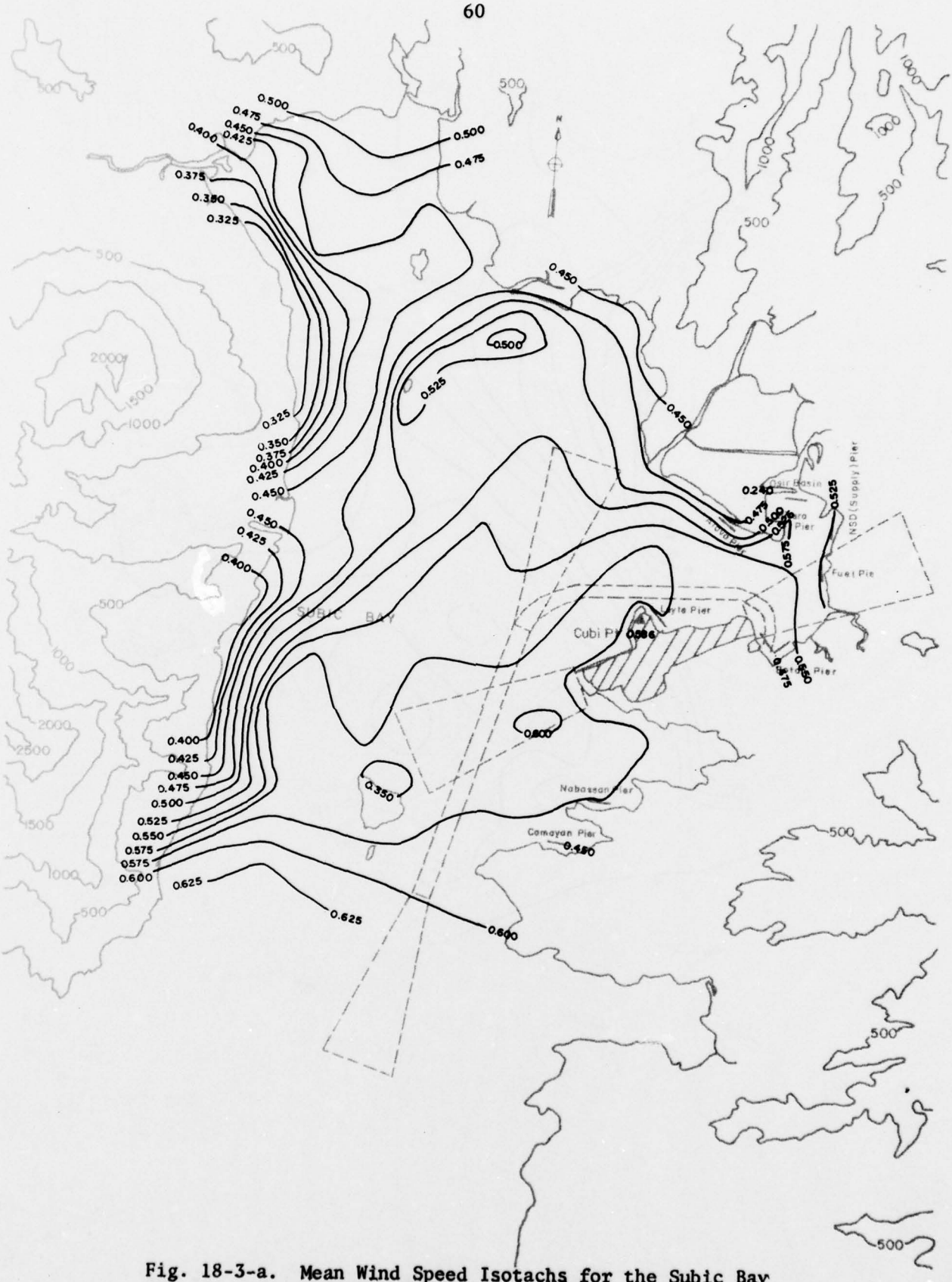

Fig. 18-3-a. Mean Wind Speed Isotachs for the Subic Bay Basin at 225°T, z = 195 ft (59.5 m)

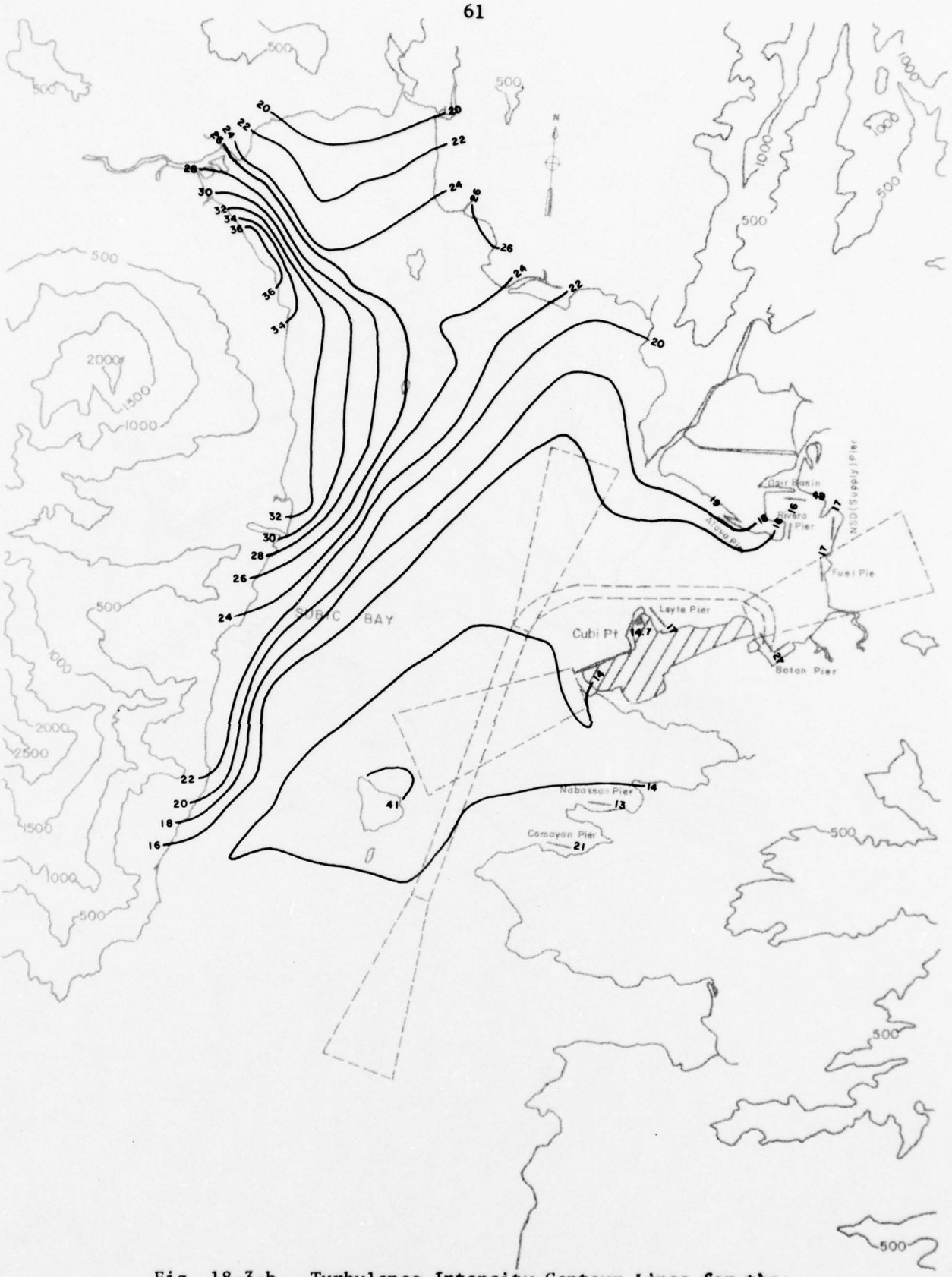

Fig. 18-3-b. Turbulence Intensity Contour Lines for the Subic Bay Basin at 225°T, z = 195 ft (59.5 m)

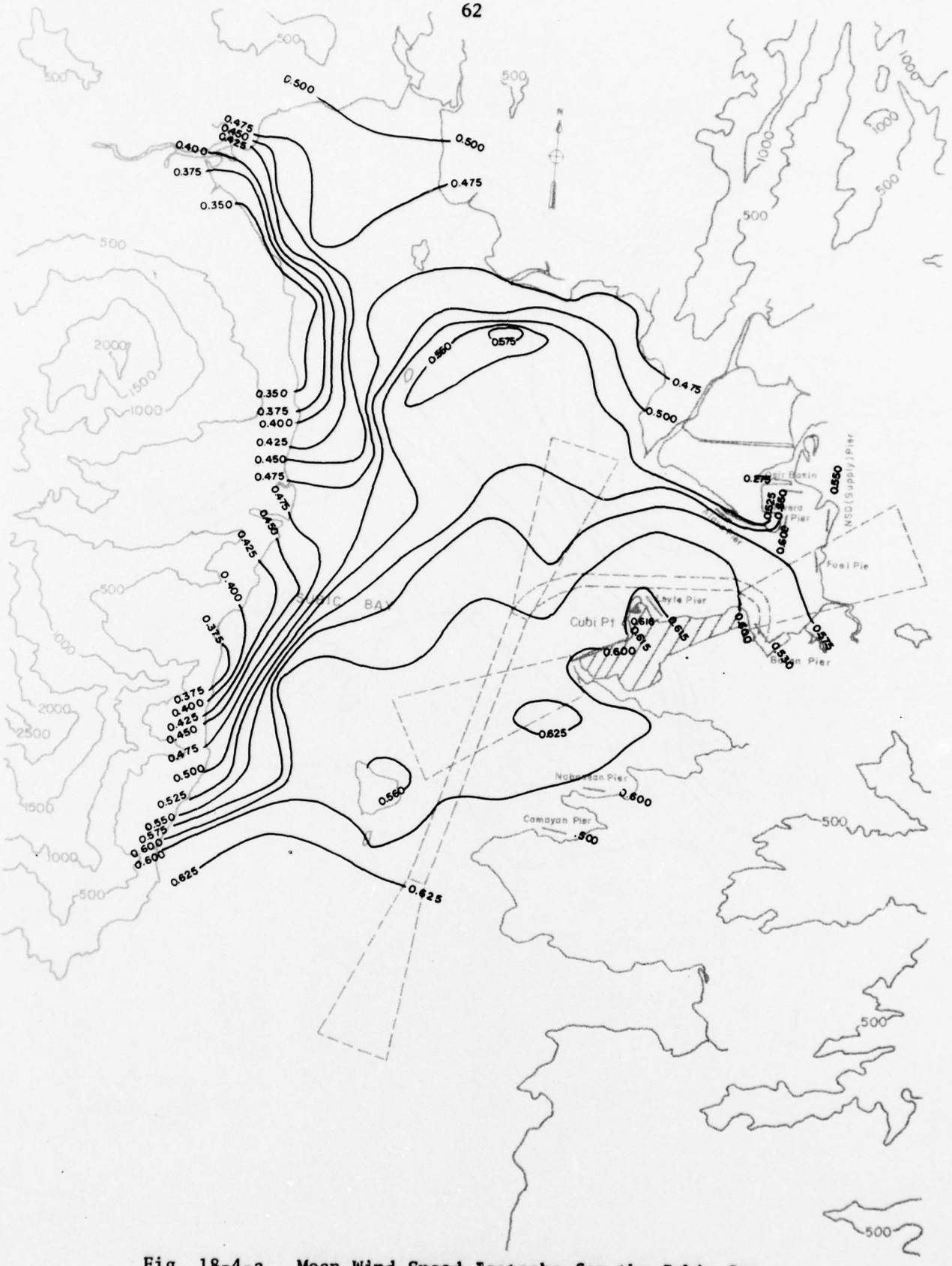

Fig. 18-4-a. Mean Wind Speed Isotachs for the Subic Bay Basin at 225°T, z = 275 ft (83.9 m)

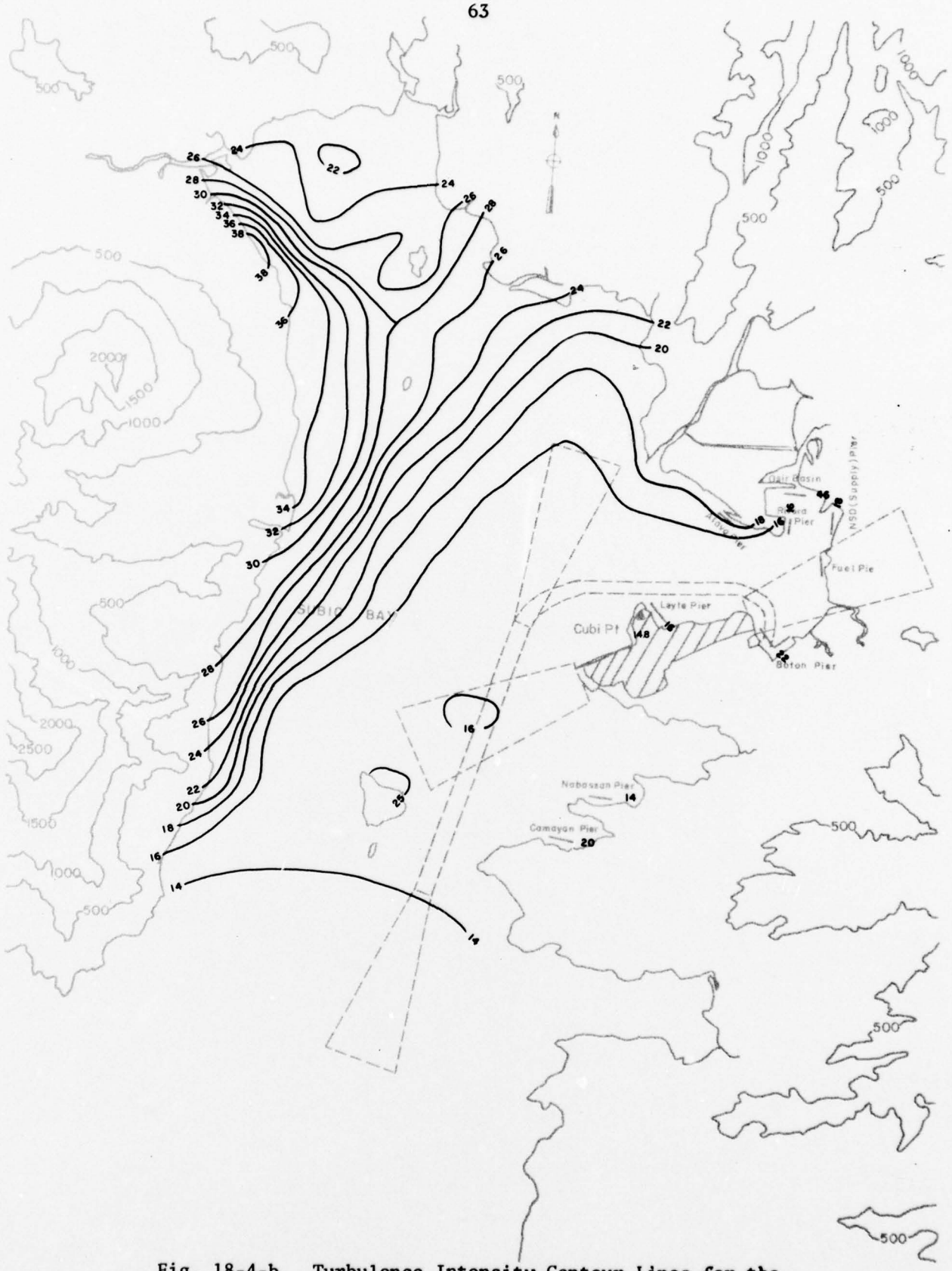

Fig. 18-4-b. Turbulence Intensity Contour Lines for the Subic Bay Basin at 225°T, z = 275 ft (83.9 m)

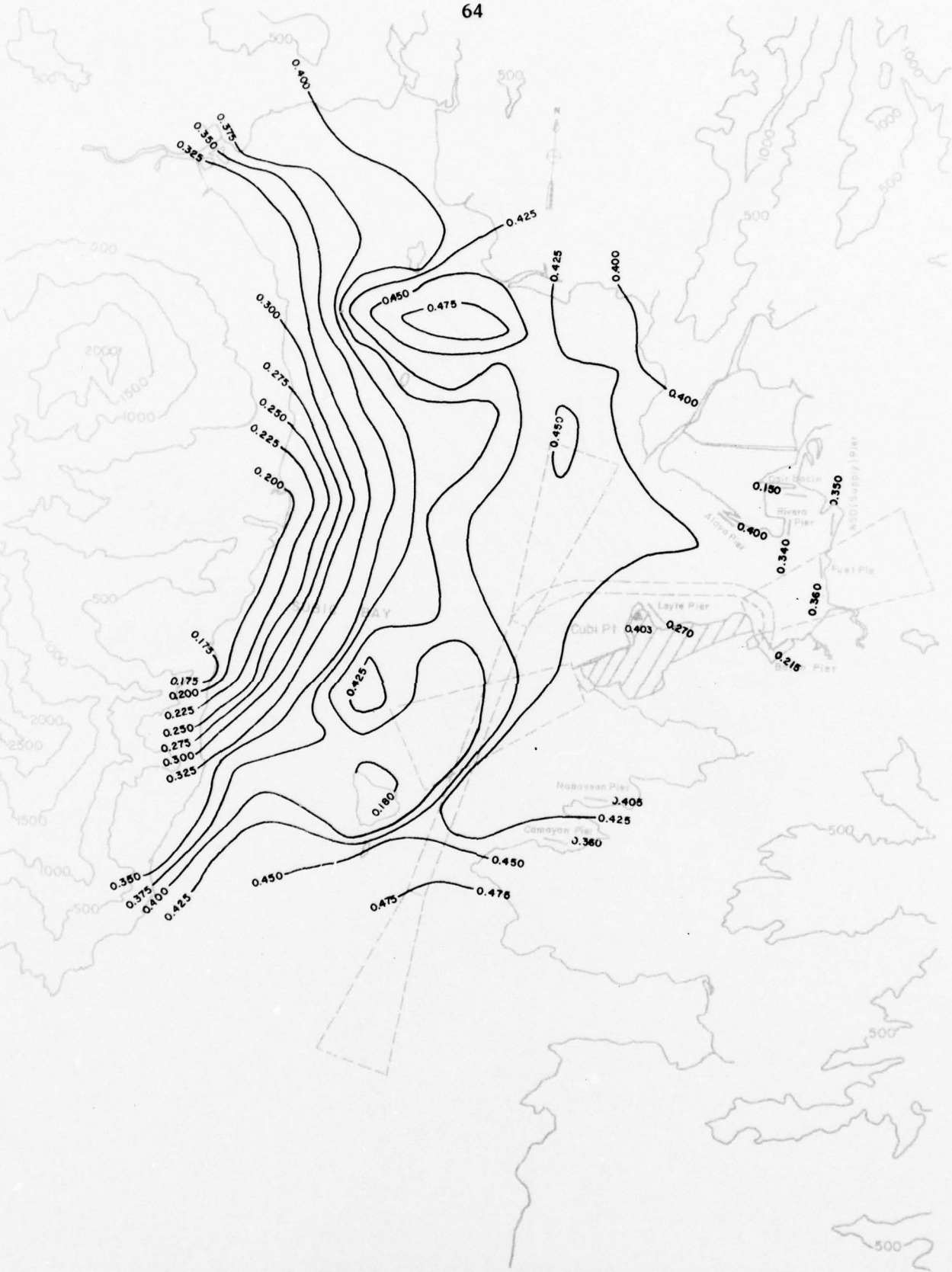

Fig. 19-1-a. Mean Wind Speed Isotachs for the Subic Bay Basin at 240°T, z = 70 ft (21.3 m)

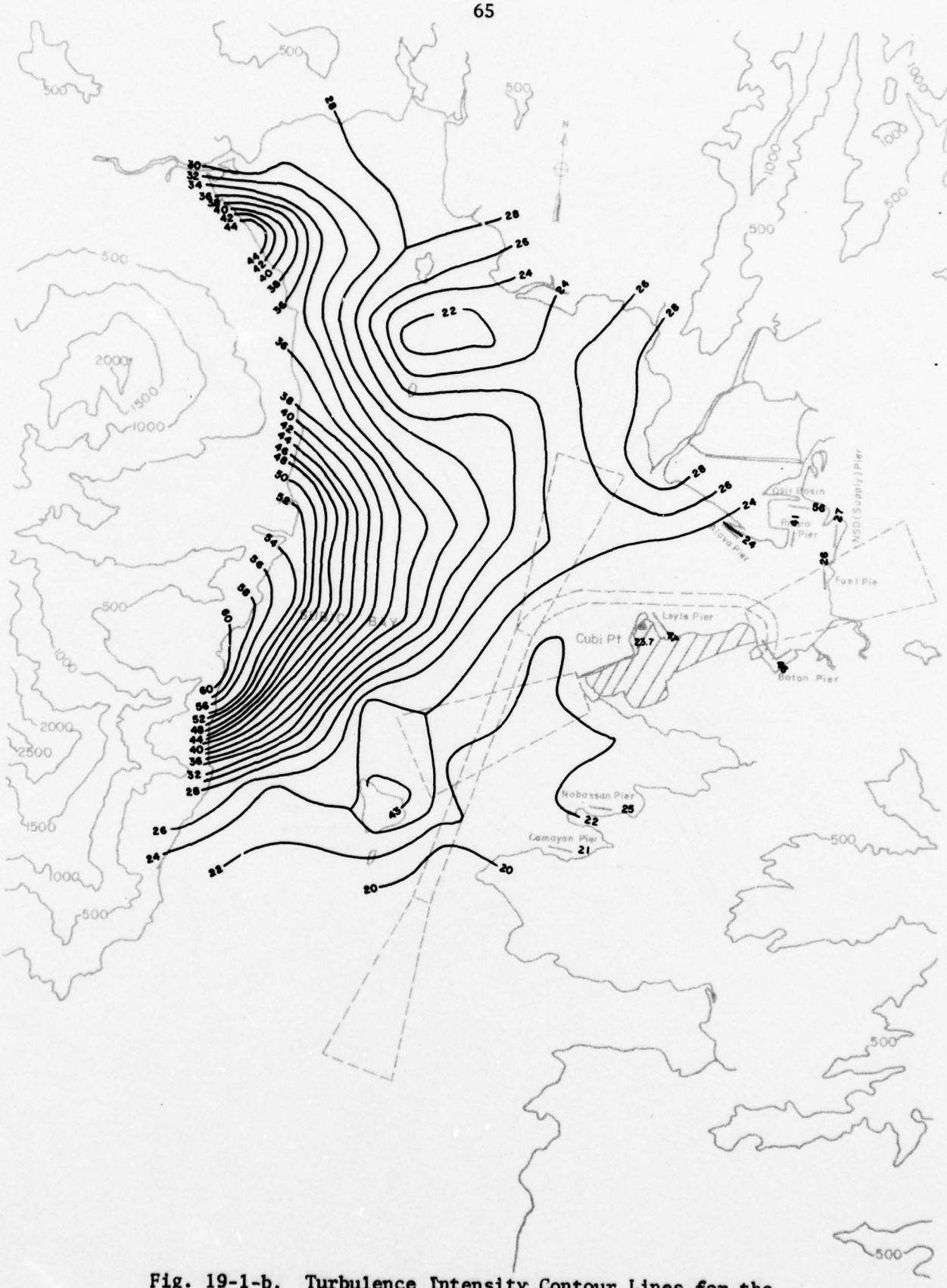

Fig. 19-1-b. Turbulence Intensity Contour Lines for the Subic Bay Basin at 240°T, z = 70 ft (21.3 m)

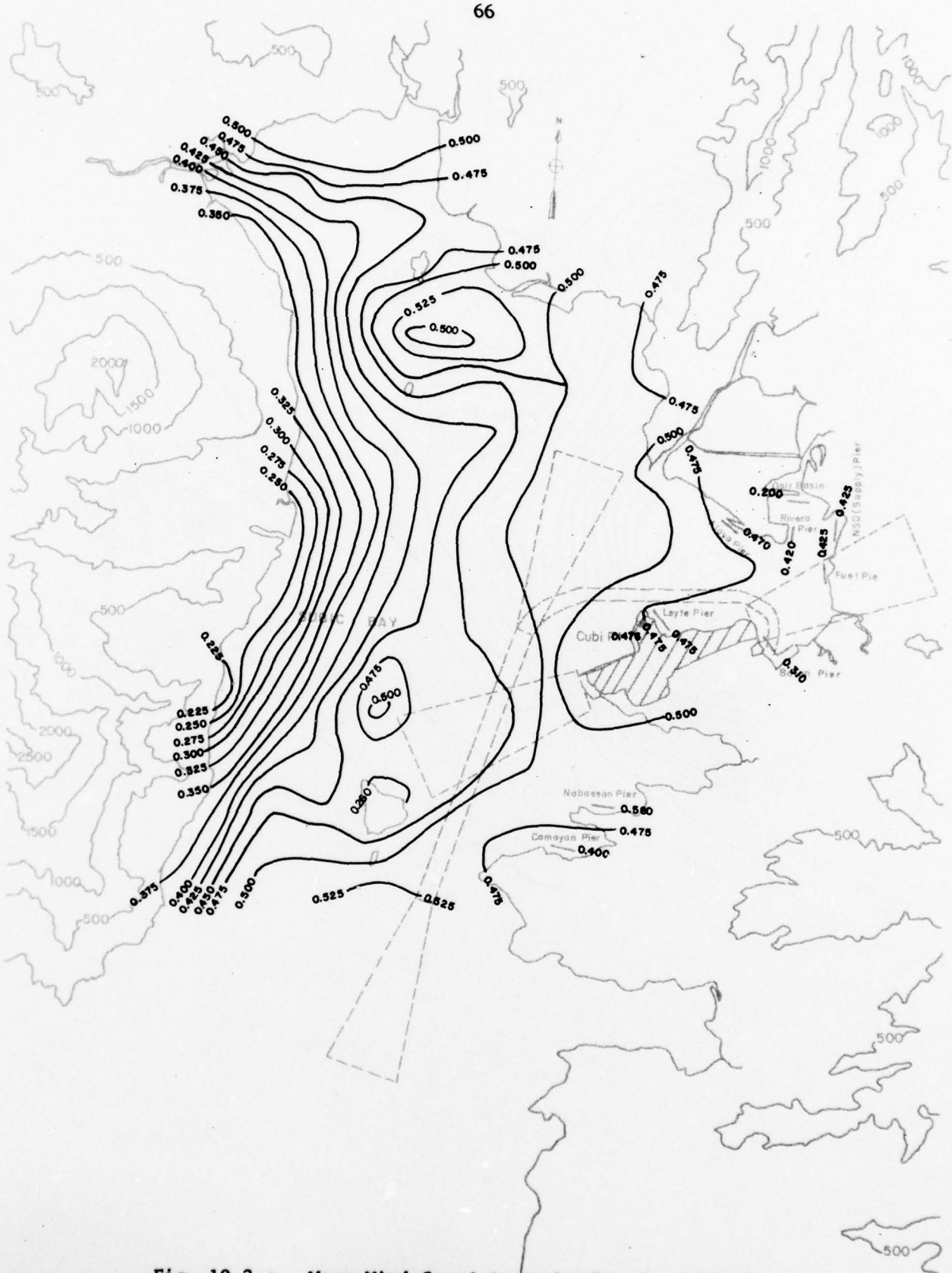

Fig. 19-2-a. Mean Wind Speed Isotachs for the Subic Bay Basin at 240°T, z = 150 ft (45.7 m)

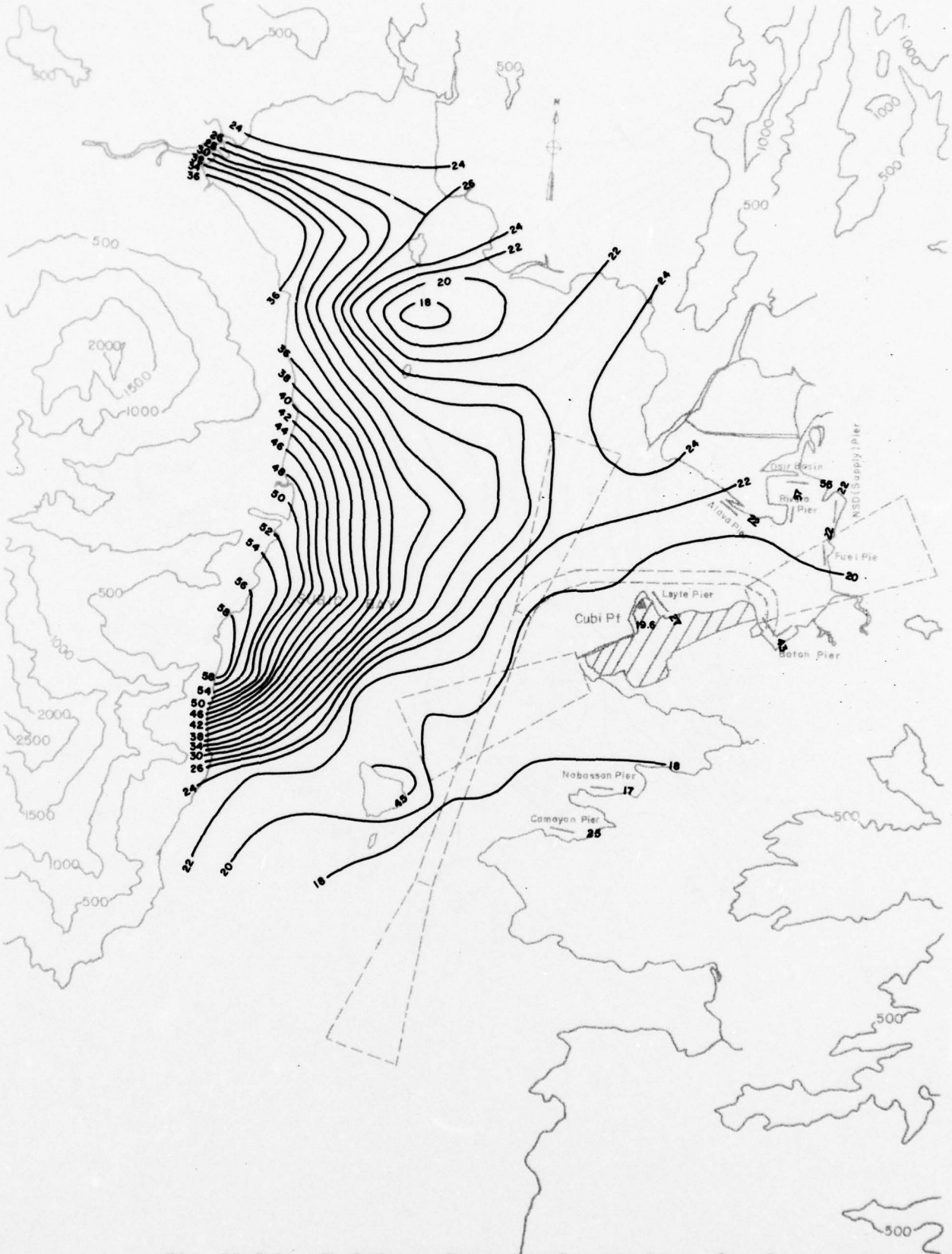

Fig. 19-2-b. Turbulence Intensity Contour Lines for the Subic Bay Basin at 240°T, z = 150 ft (45.7 m)

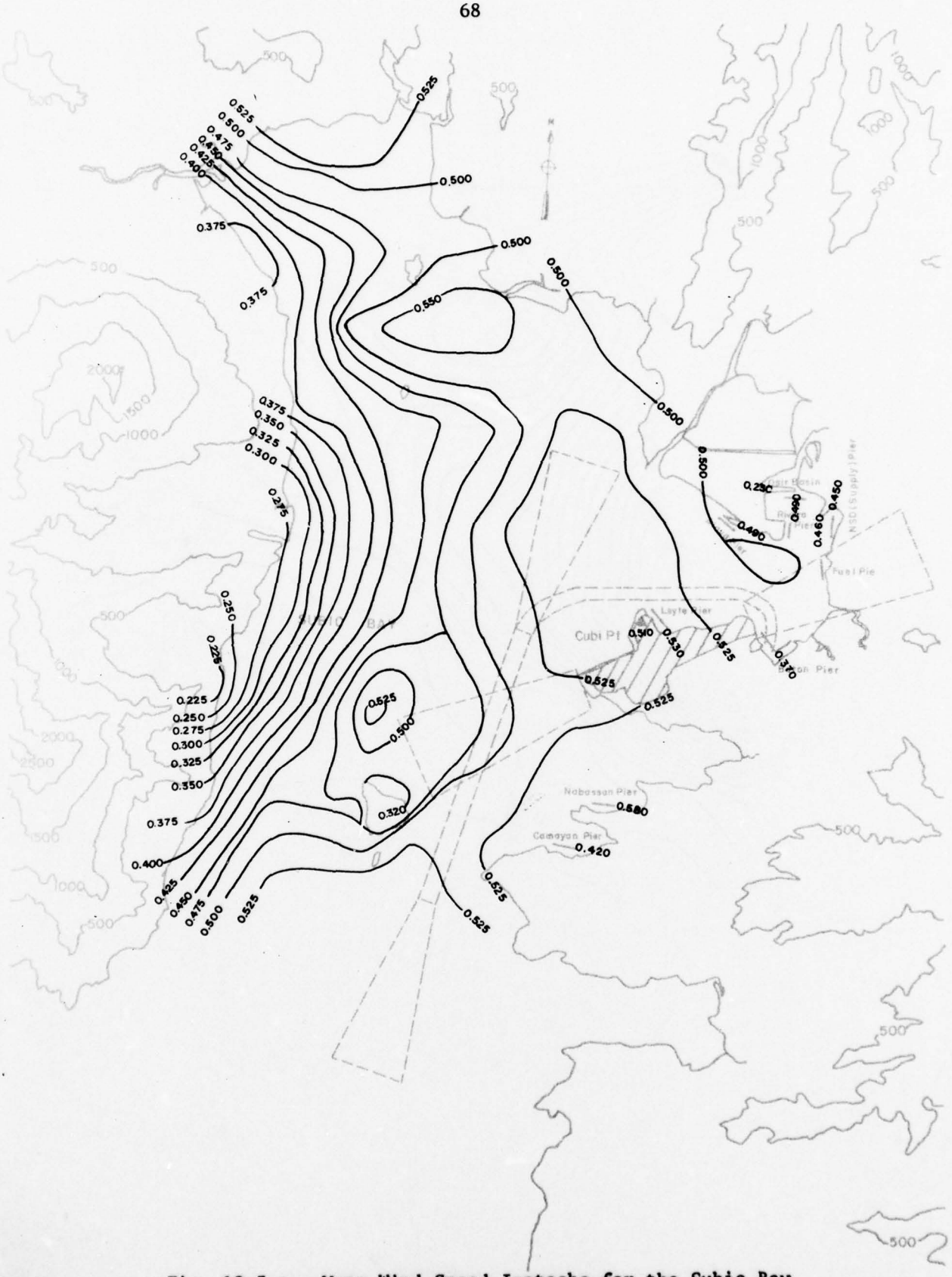

Fig. 19-3-a. Mean Wind Speed Isotachs for the Subic Bay Basin at 240°T, z = 195 ft (59.5 m)

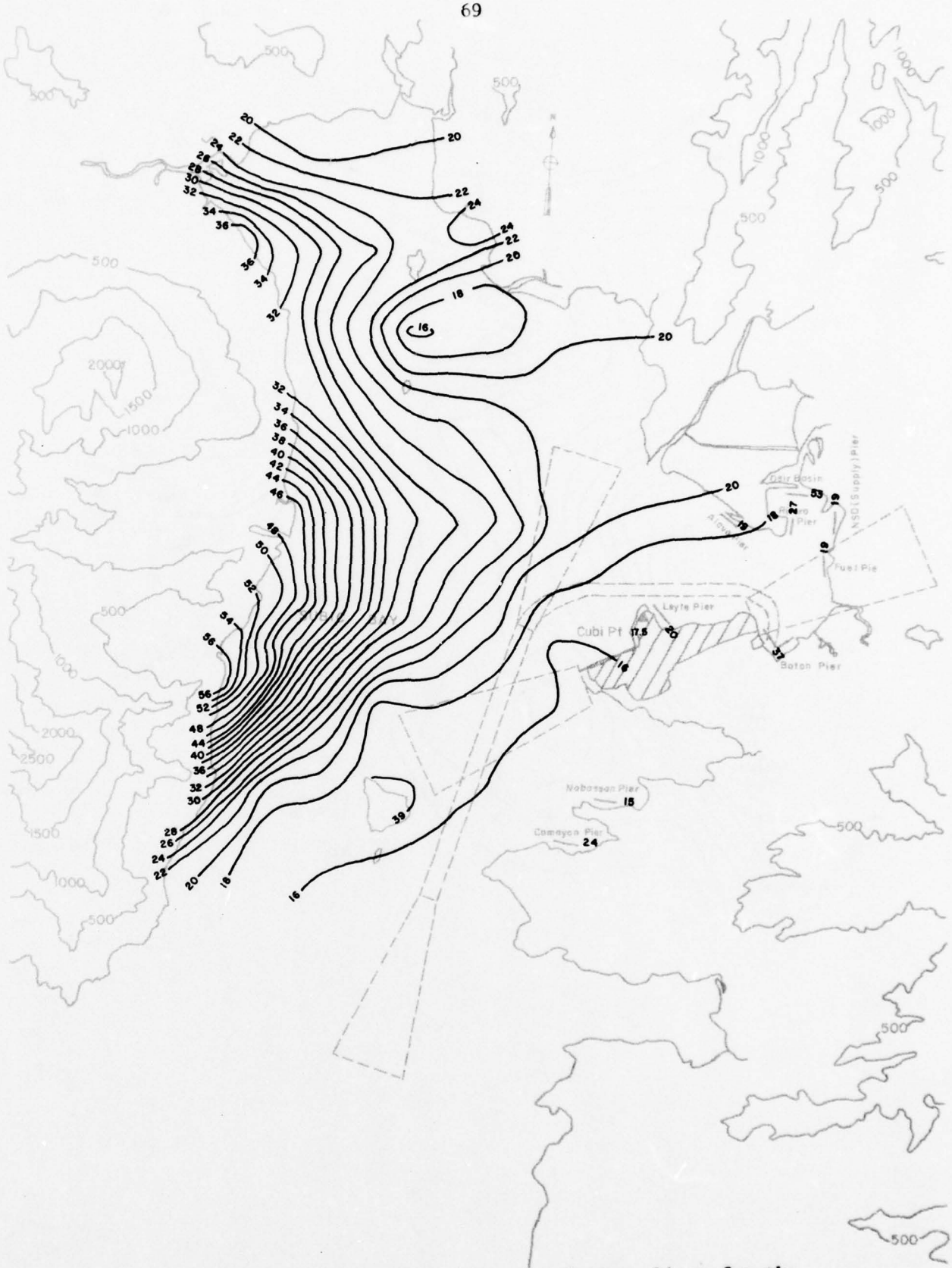

Fig. 19-3-b. Turbulence Intensity Contour Lines for the Subic Bay Basin at 240°T, z = 195 ft (59.5 m)

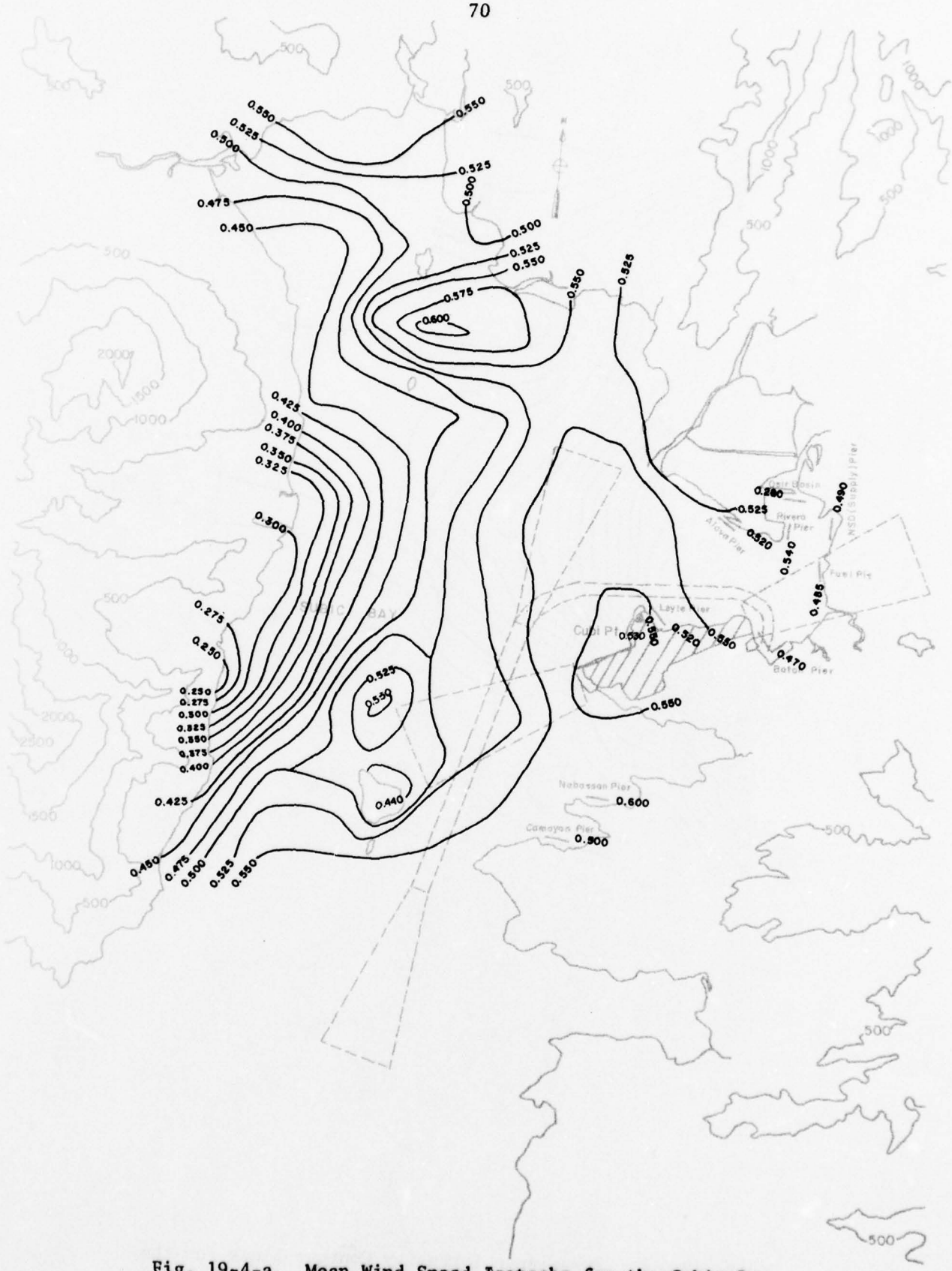

Fig. 19-4-a. Mean Wind Speed Isotachs for the Subic Bay Basin at 240°T, z = 275 ft (83.9 m)

Fig. 19-4-b. Turbulence Intensity Contour Lines for the Subic Bay Basin at 240°T, z = 275 ft (83.9 m)

Fig. 18-2-a. Mean Wind Speed Isotachs for the Subic Bay Basin at 225°T, z = 150 ft (45.7 m)

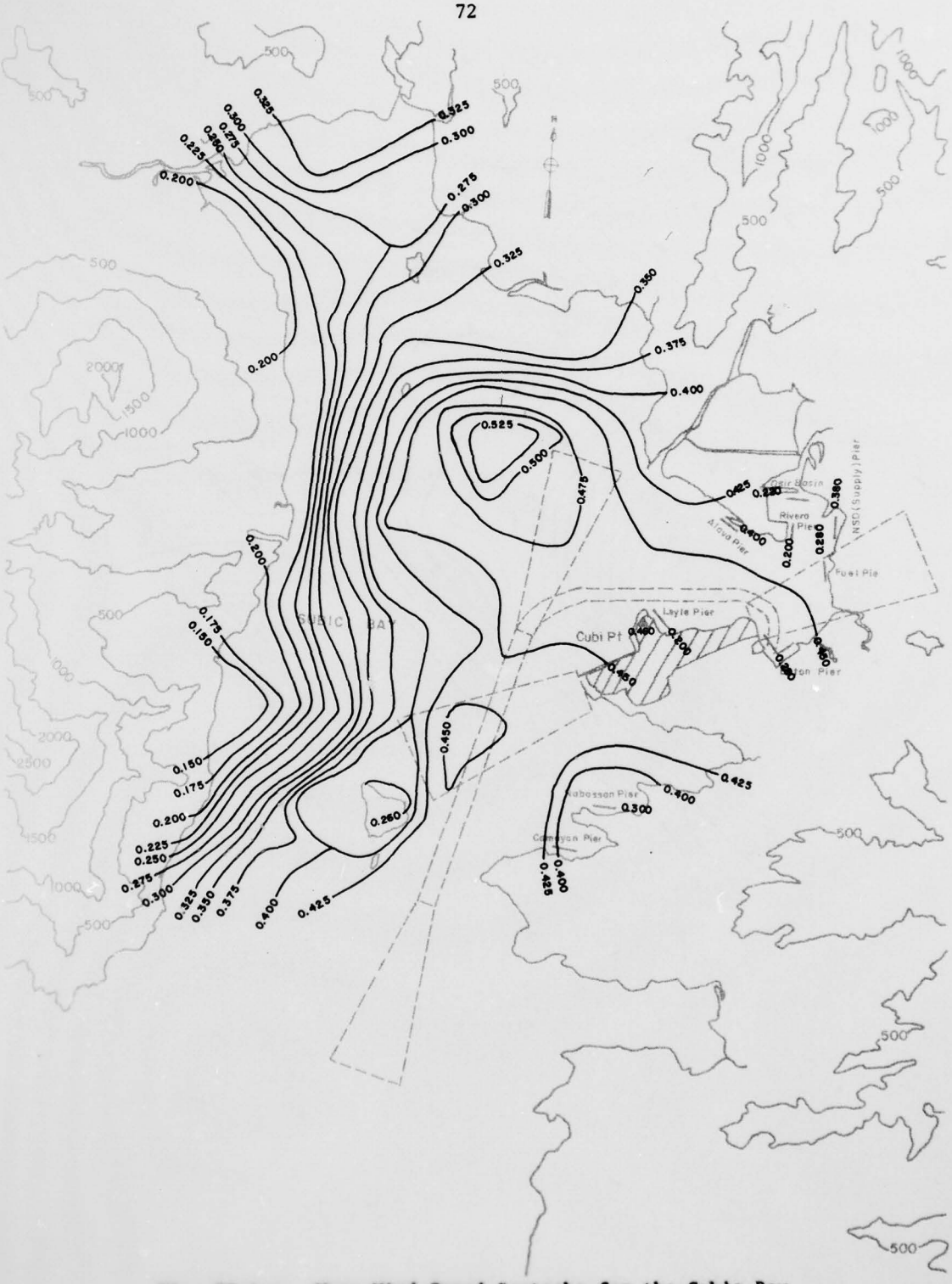

Fig. 20-1-a. Mean Wind Speed Isotachs for the Subic Bay Basin at 255°T, z = 70 ft (21.3 m)

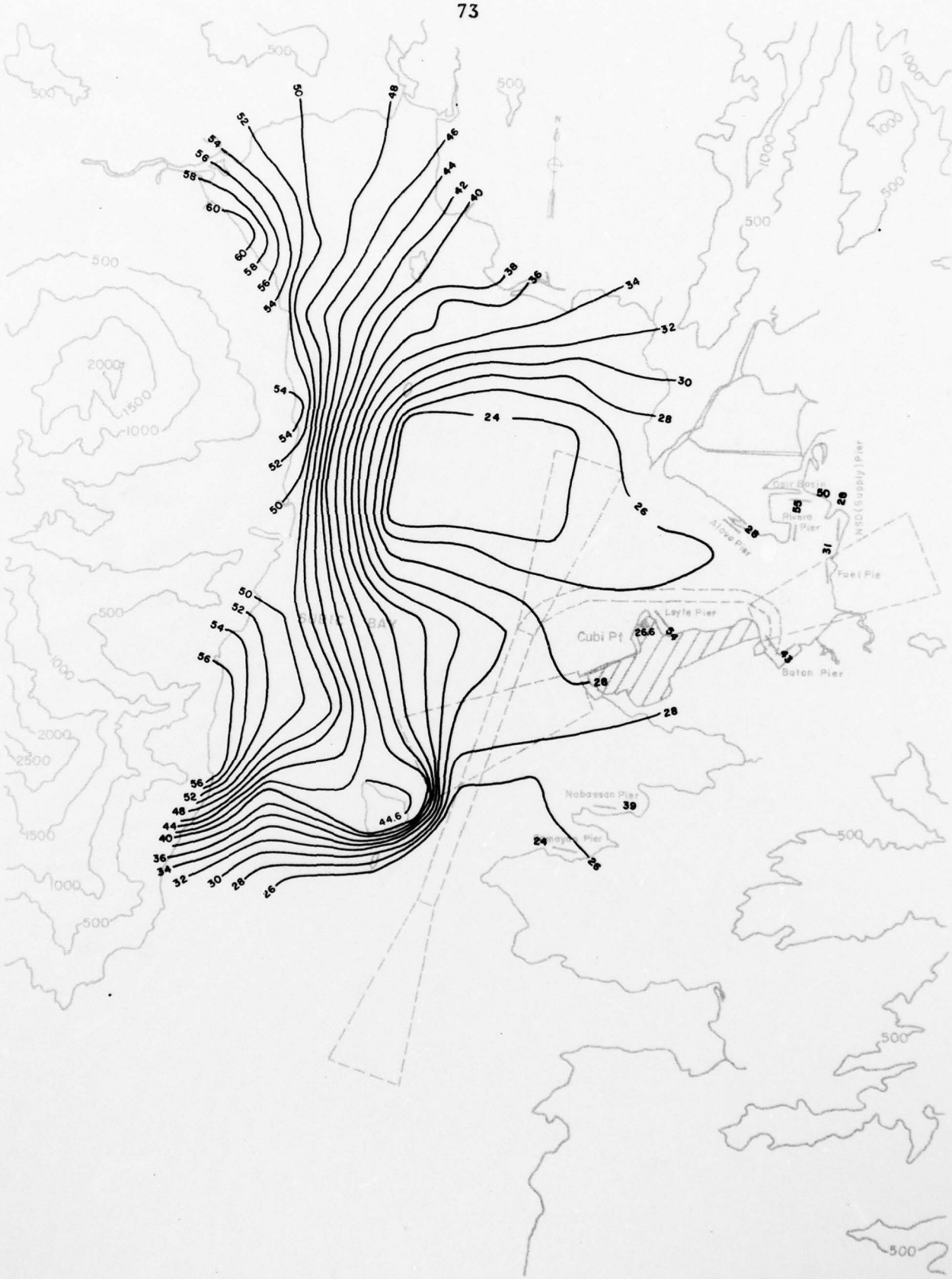

Fig. 20-1-b. Turbulence Intensity Contour Lines for the Subic Bay Basin at 255°T, z = 70 ft (21.3 m)

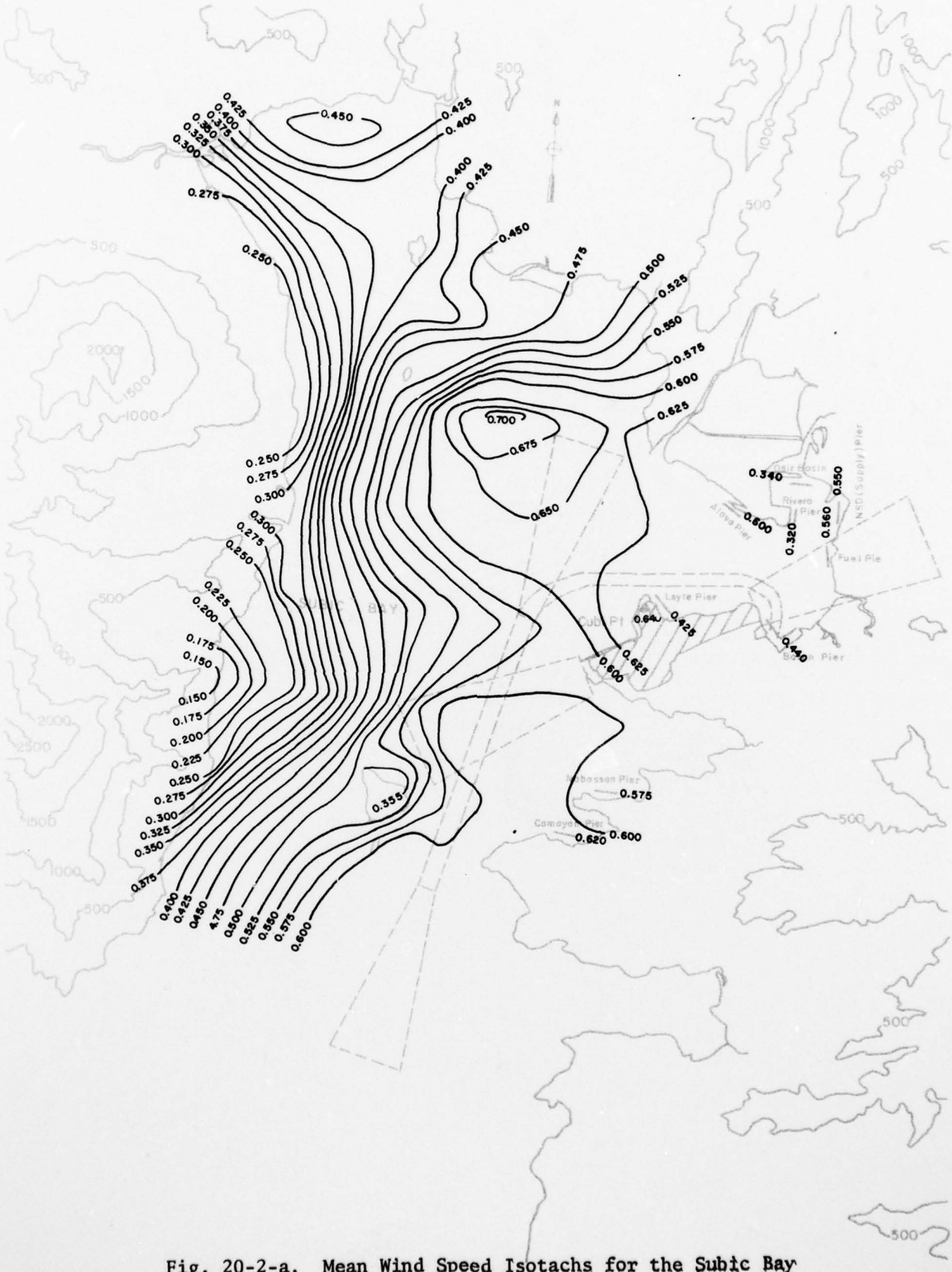

Fig. 20-2-a. Mean Wind Speed Isotachs for the Subic Bay Basin at 255°T, z = 150 ft (45.7 m)

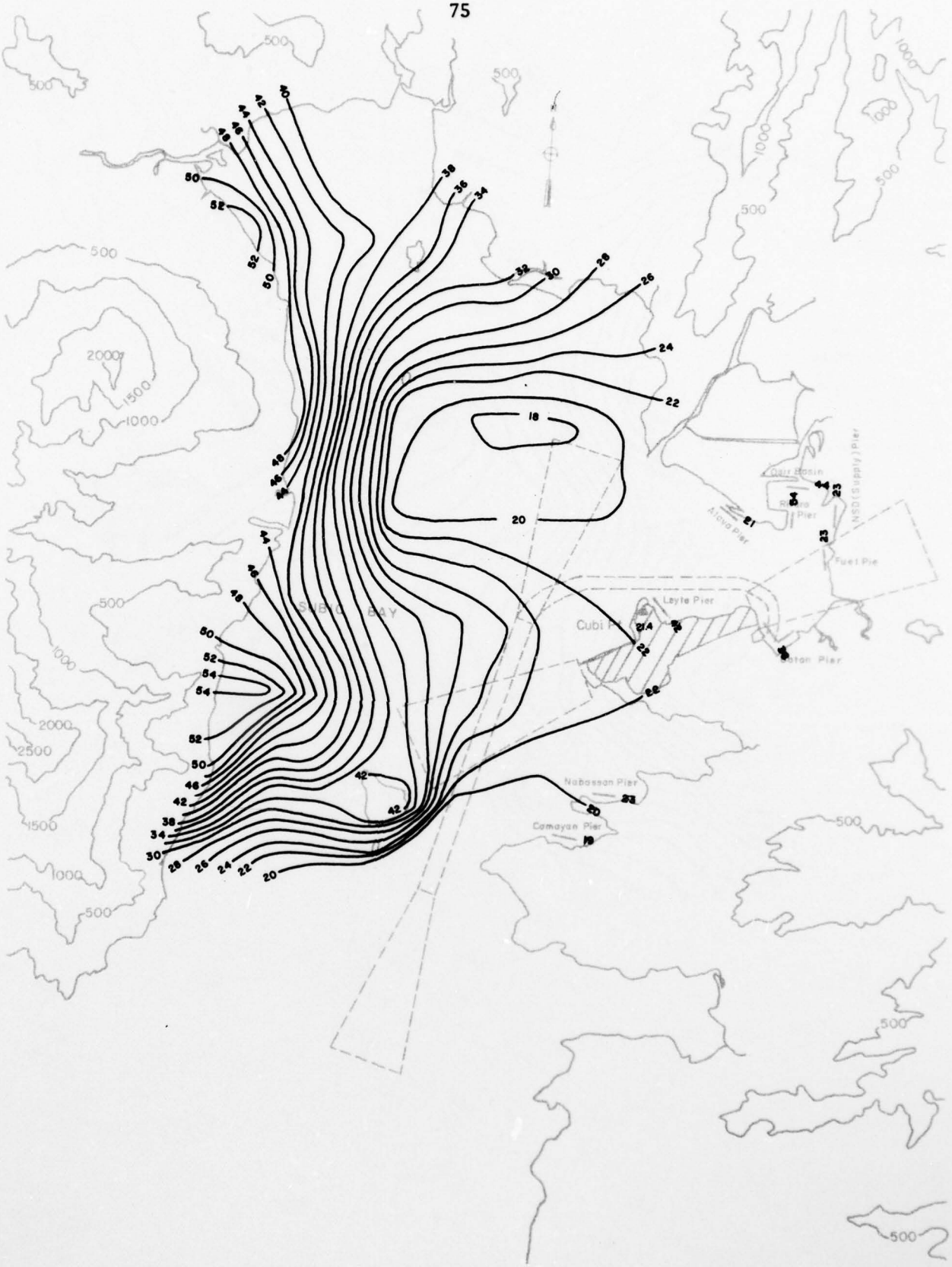

Fig. 20-2-b. Turbulence Intensity Contour Lines for the Subic Bay Basin at 255°T, z = 150 ft (45.7 m)

Fig. 20-3-a. Mean Wind Speed Isotachs for the Subic Bay Basin at 255°T, z = 195 ft (59.5 m)

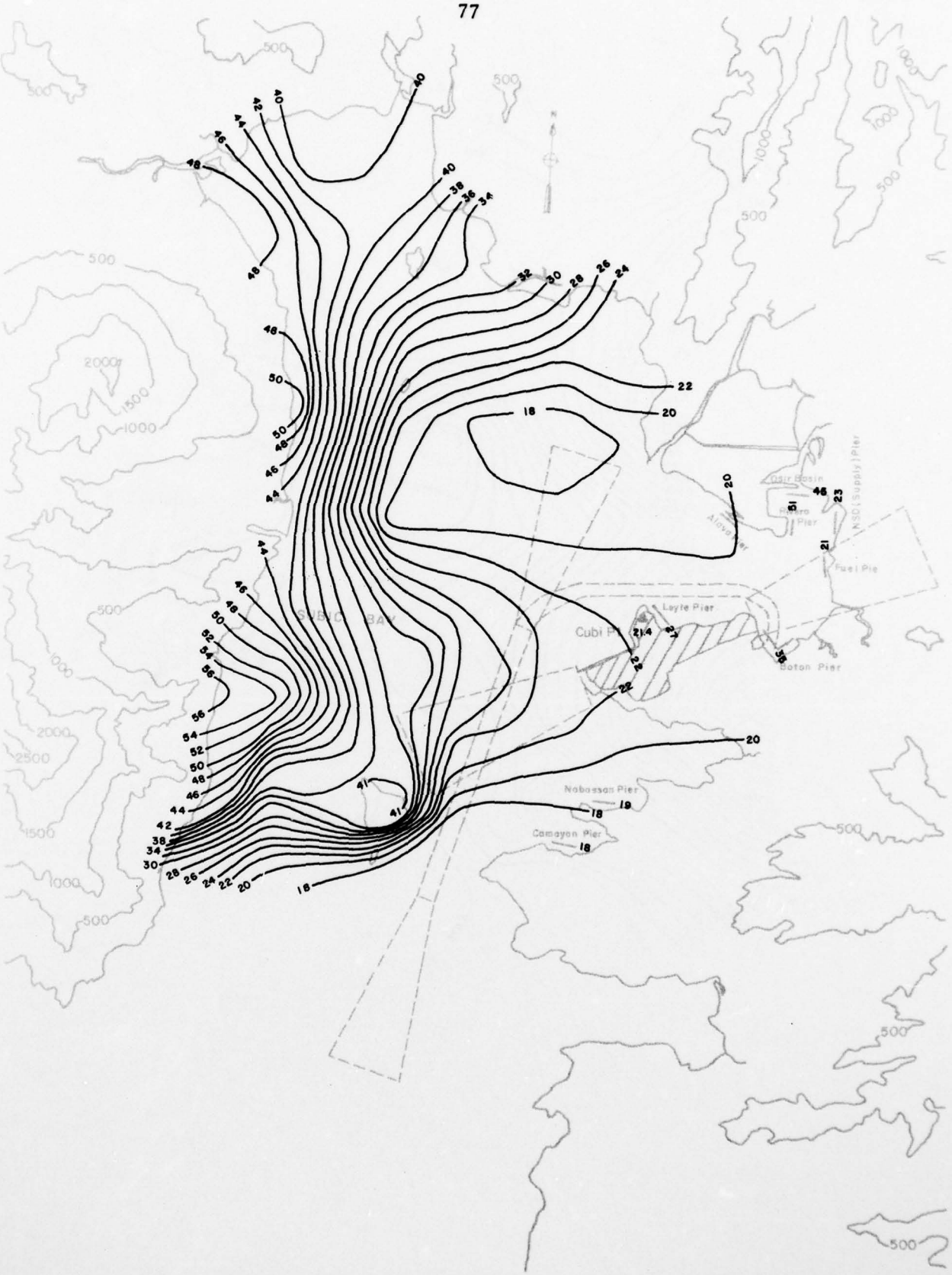

Fig. 20-3-b. Turbulence Intensity Contour Lines for the Subic Bay Basin at 255°T, z = 195 ft (59.5 m)

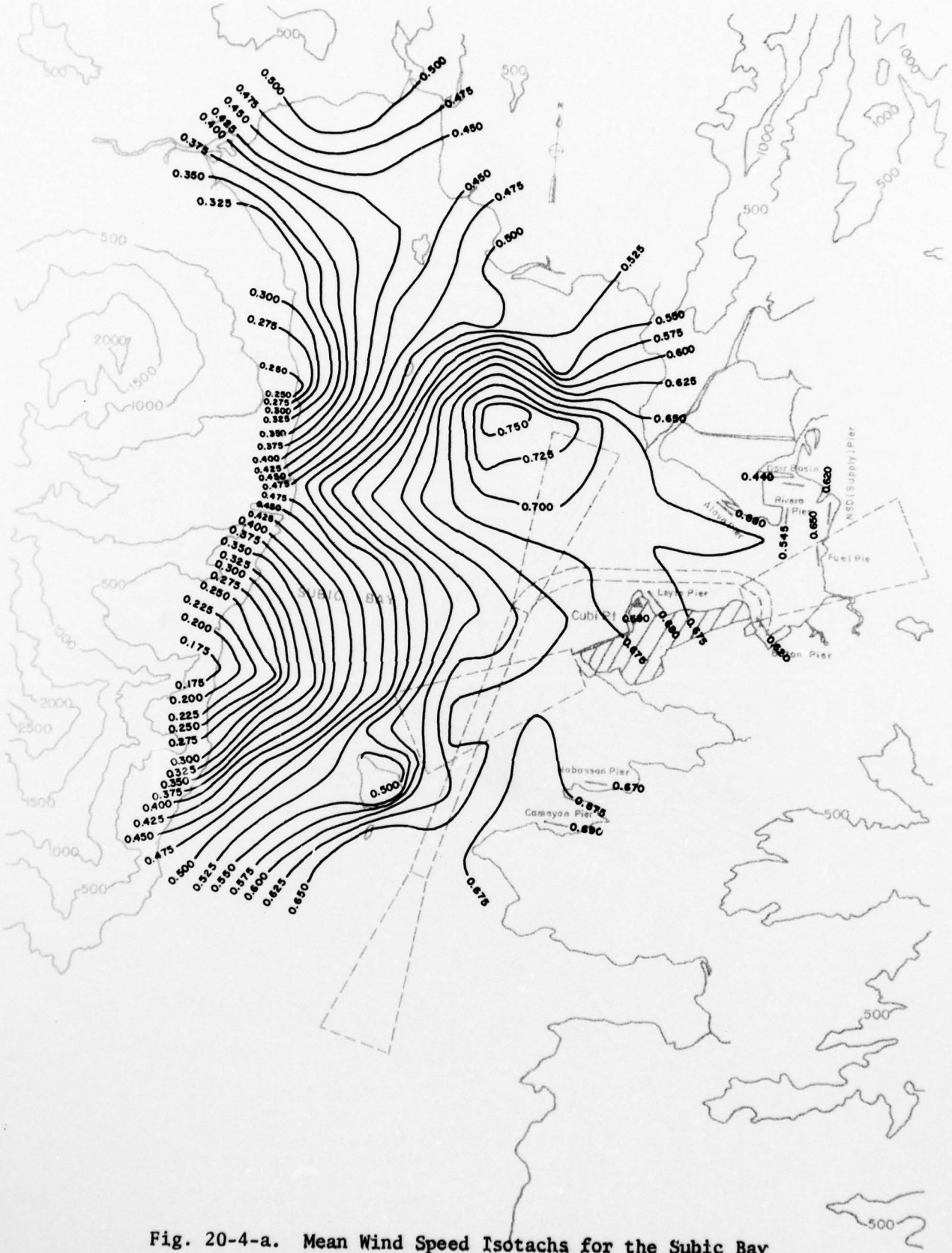

Fig. 20-4-a. Mean Wind Speed Isotachs for the Subic Bay Basin at 255°T, z = 275 ft (83.9 m)

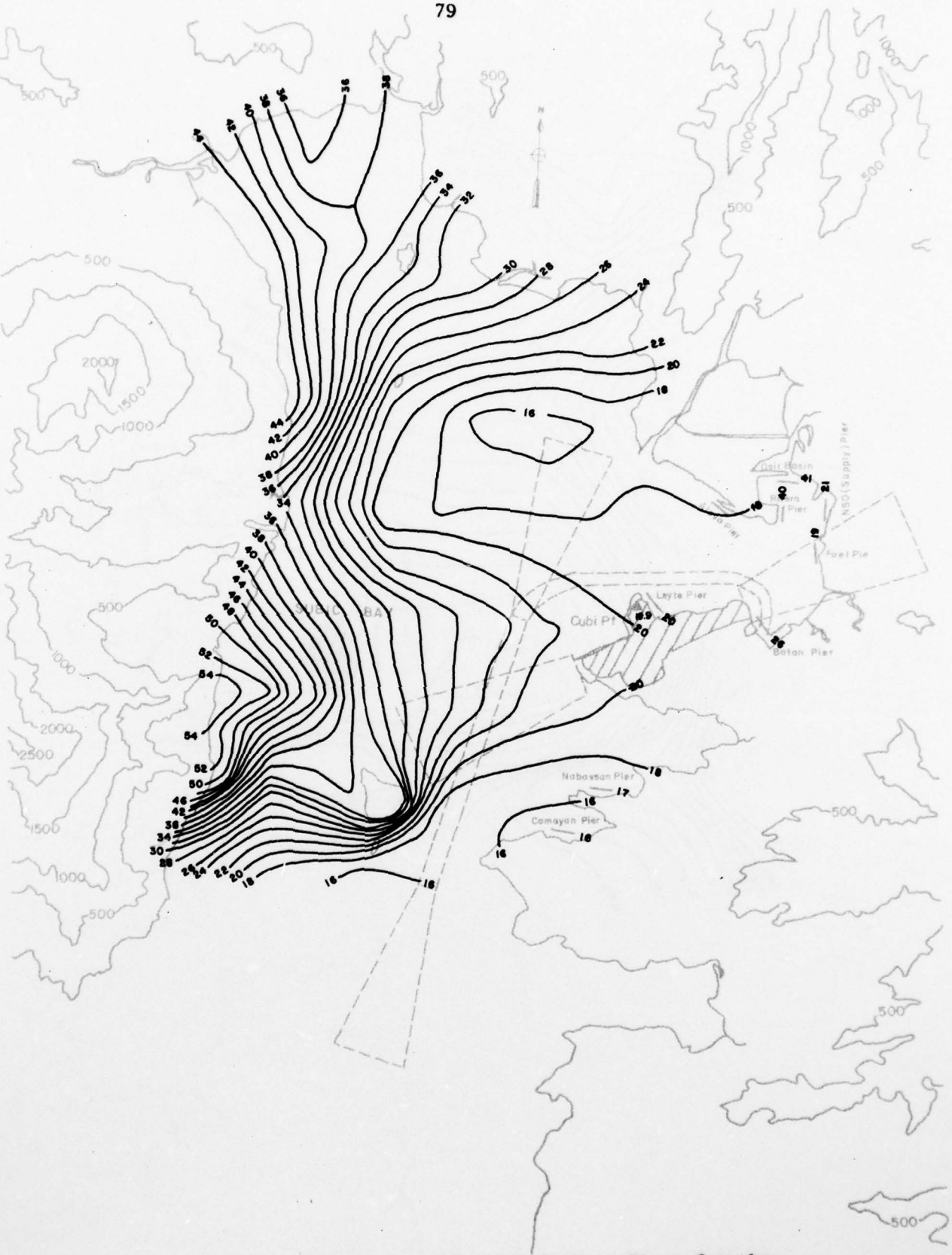

Fig. 20-4-b. Turbulence Intensity Contour Lines for the Subic Bay Basin at 255°T, z = 275 ft (83.9 m)

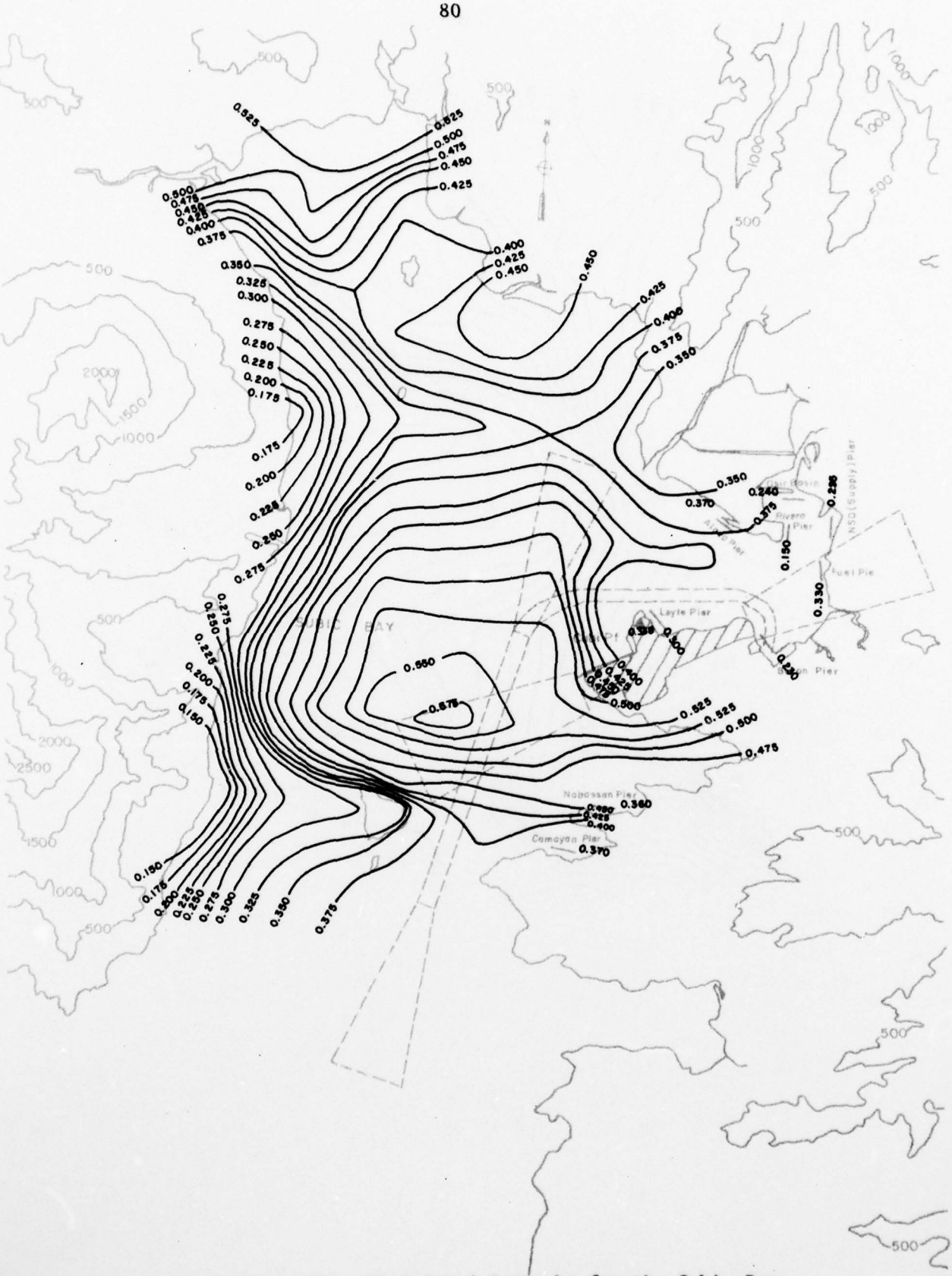

Fig. 21-1-a. Mean Wind Speed Isotachs for the Subic Bay Basin at 270°T, z = 70 ft (21.3 m)

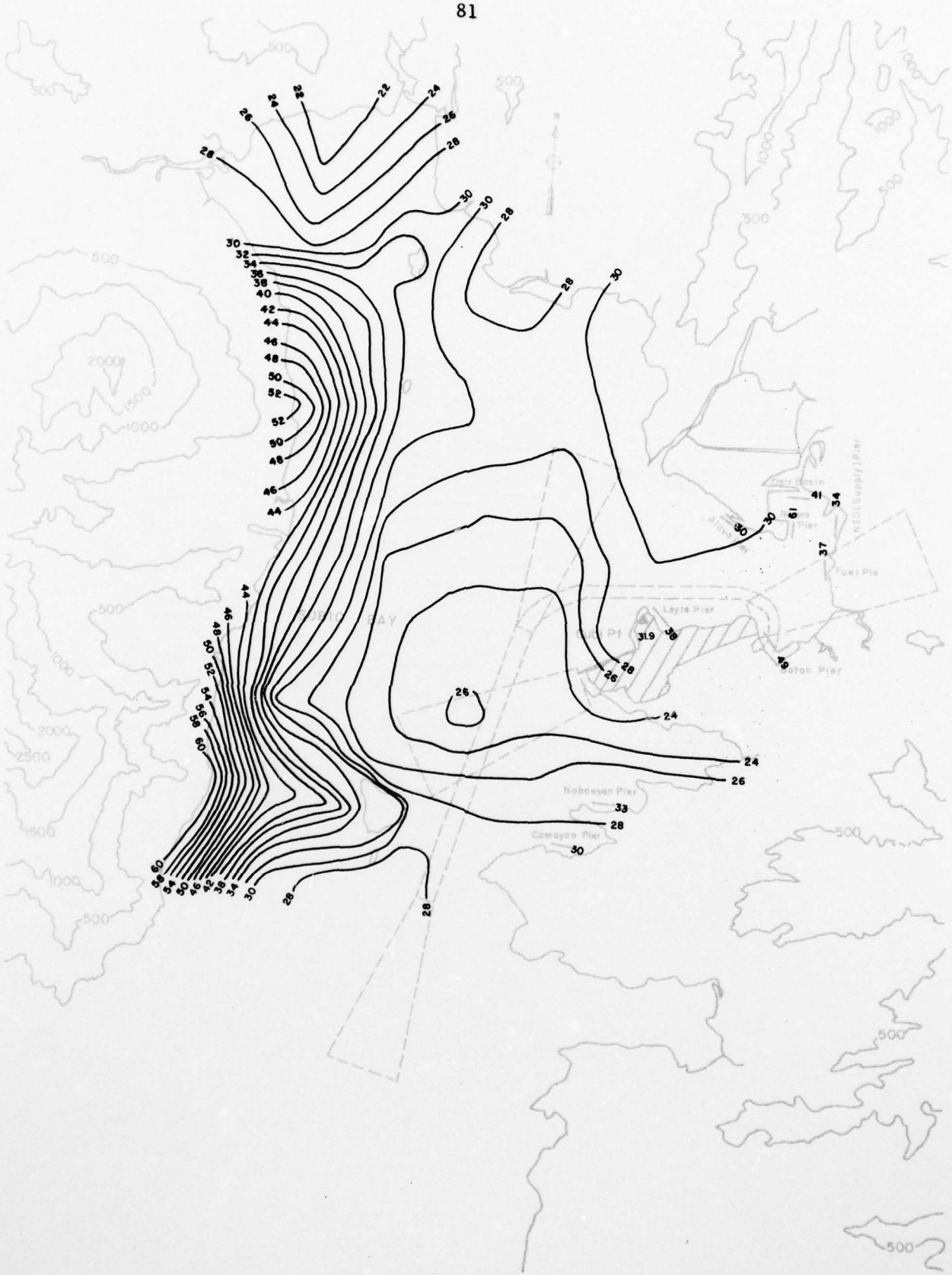

Fig. 21-1-b. Turbulence Intensity Contour Lines for the Subic Bay Basin at 270°T, z = 70 ft (21.3 m)

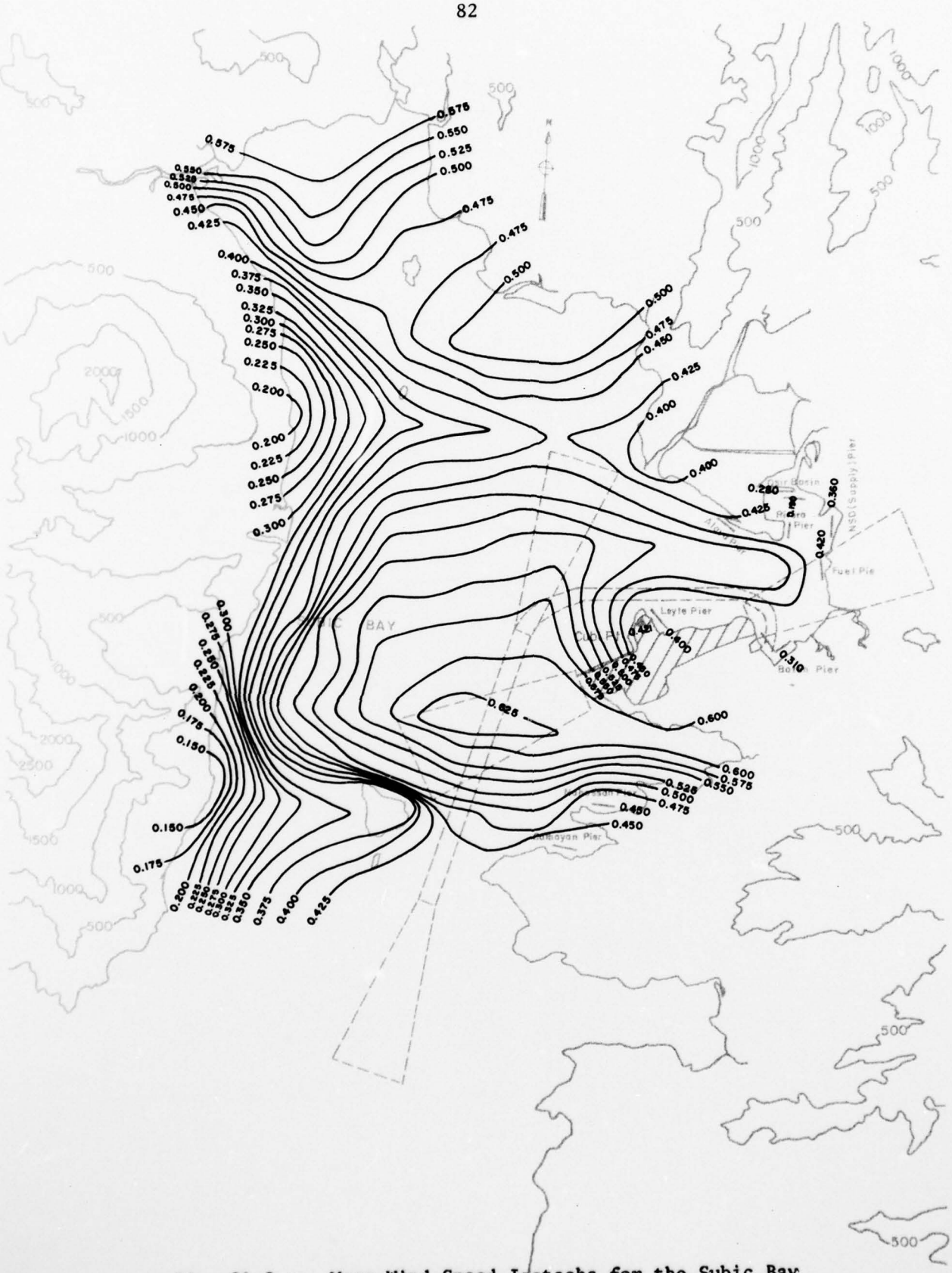

Fig. 21-2-a. Mean Wind Speed Isotachs for the Subic Bay Basin at 270°T, z = 150 ft (45.7 m)

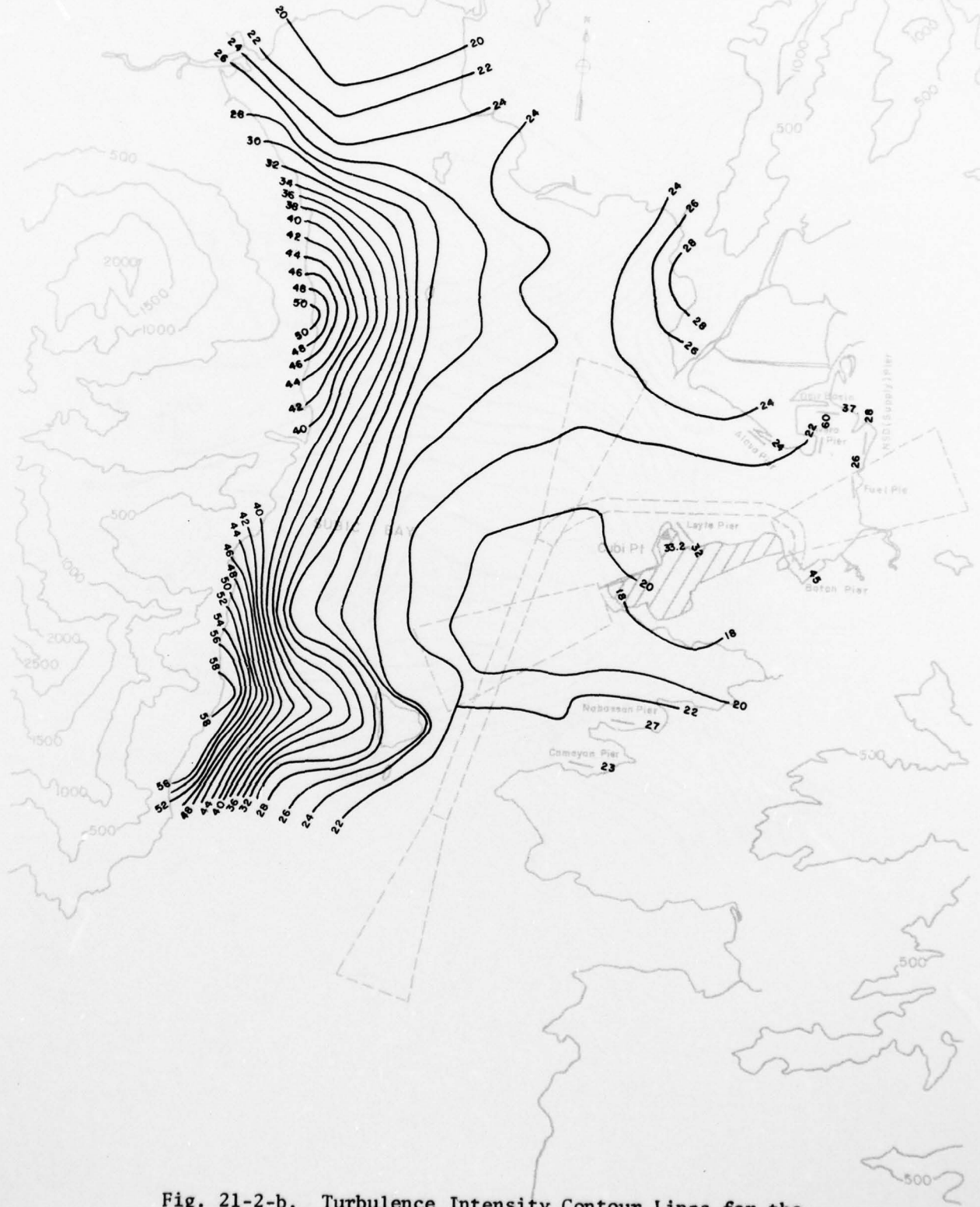

Fig. 21-2-b. Turbulence Intensity Contour Lines for the Subic Bay Basin at 270°T, z = 150 ft (45.7 m)

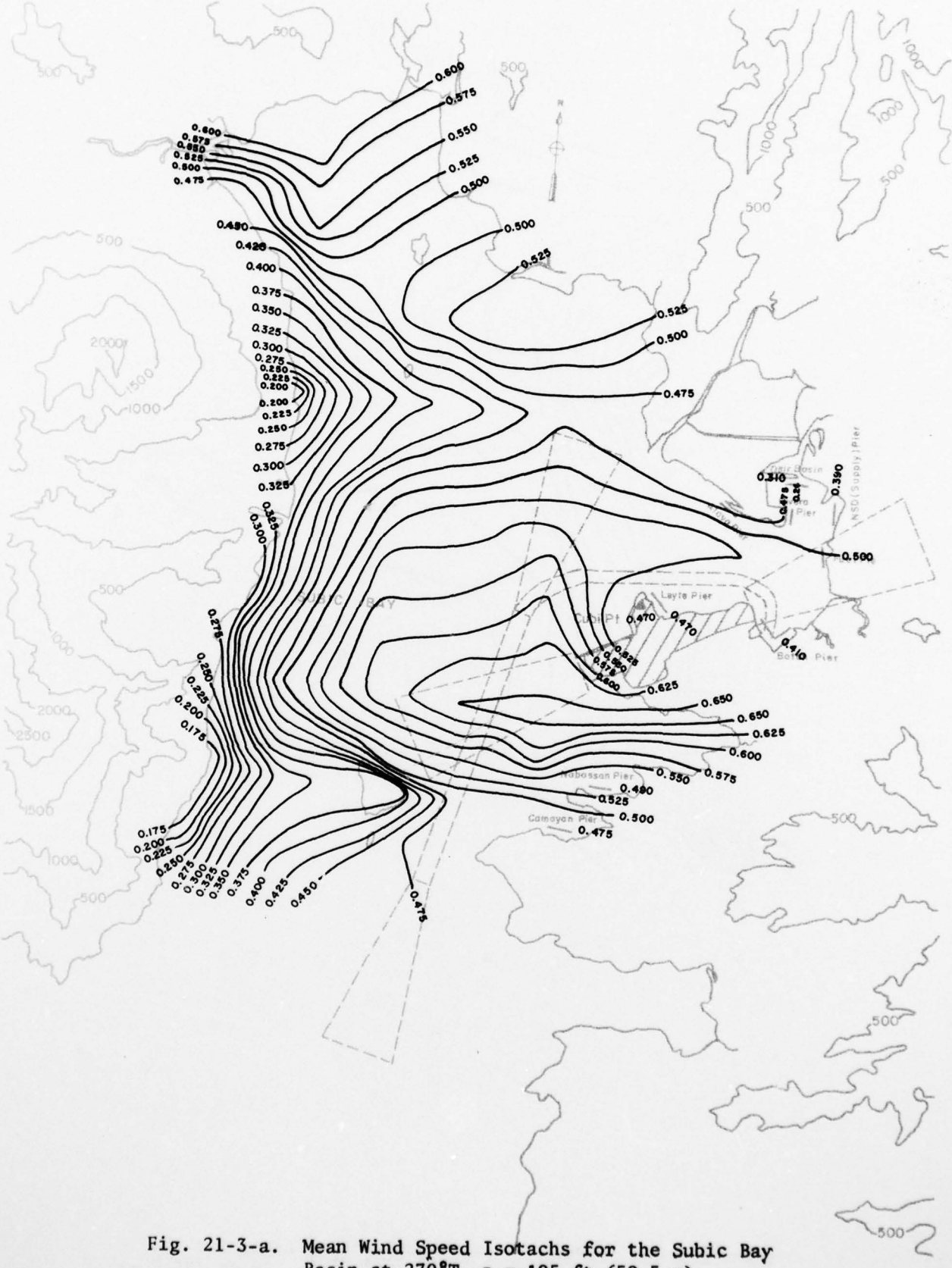

Fig. 21-3-a. Mean Wind Speed Isotachs for the Subic Bay Basin at 270°T, z = 195 ft (59.5 m)

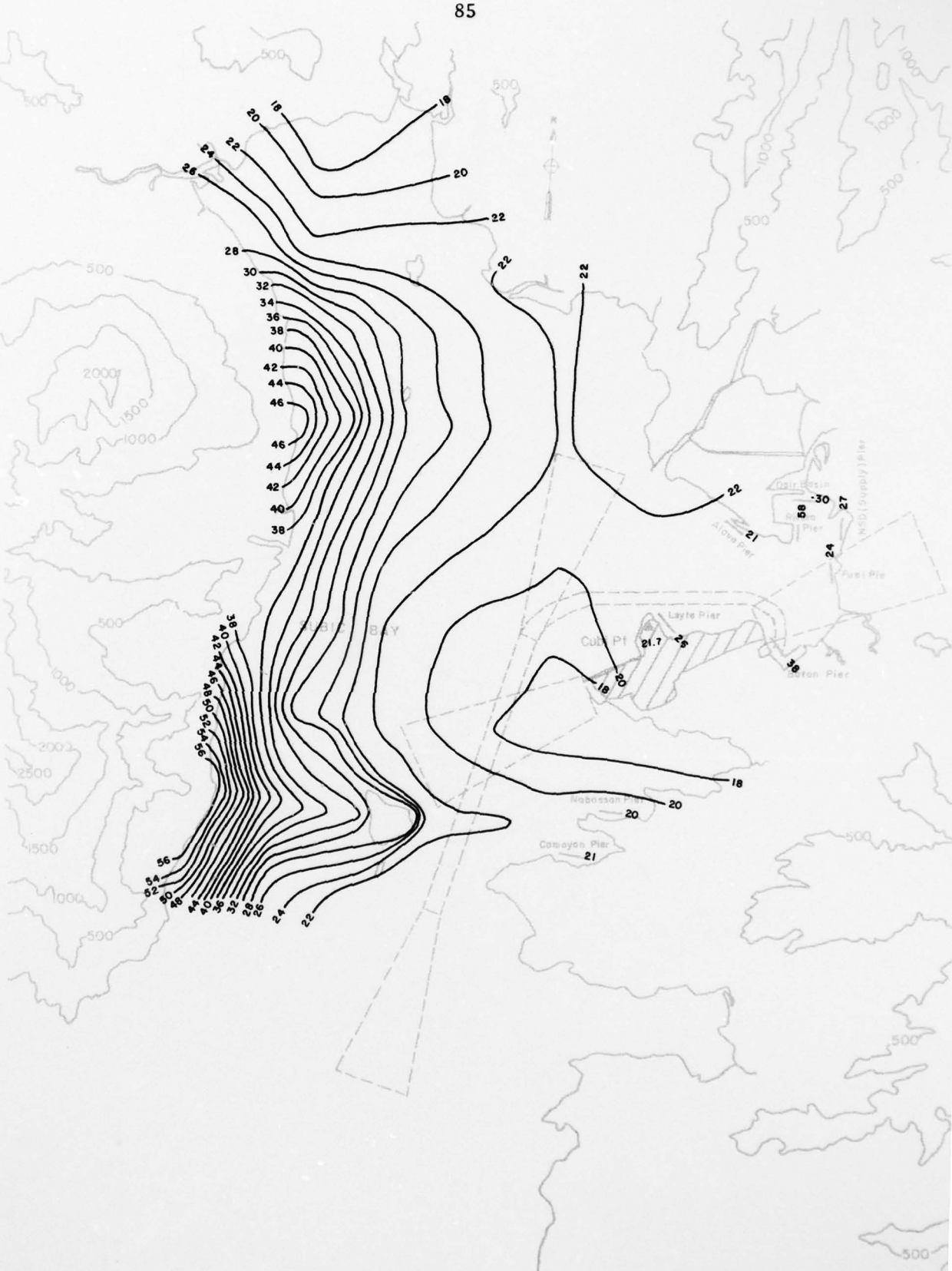

Fig. 21-3-b. Turbulence Intensity Contour Lines for the Subic Bay Basin at 270°T, z = 195 ft (59.5 m)

AD-A065 929 COLORADO STATE UNIV FORT COLLINS DEPT OF CIVIL ENGI--ETC F/G 4/2
WIND CHARACTERISTICS OVER SUBIC BAY, PHILIPPINE ISLANDS, DURING--ETC(U)
OCT 78 H B WOO, J E CERMAK, J J LOU N00228-77-C-3086
UNCLASSIFIED CSU-CER77-78HW-JEC-JJL-43 NEPRF-CR-78-02 NL

2 OF 2
AD
A065829

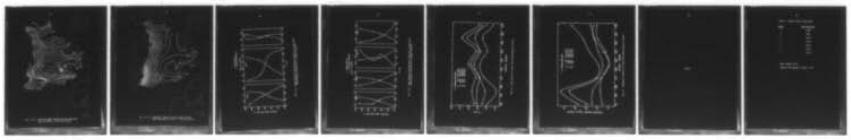

END
DATE
FILMED
5-79
DDC

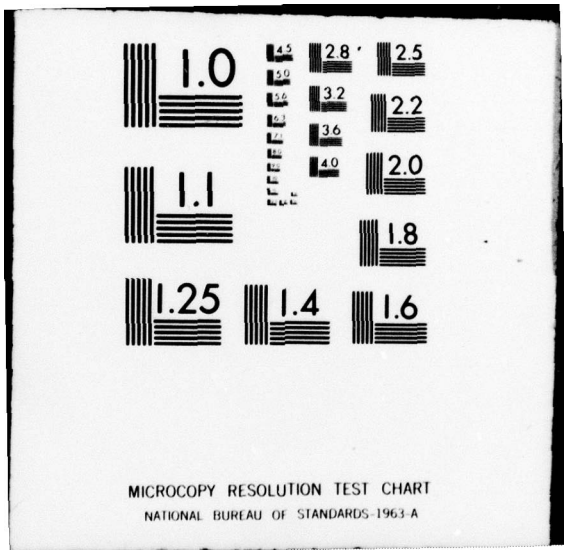
1.0
1.1
1.25
1.4
1.6
1.8
2.0
2.2
2.5
2.8
3.2
3.6
4.0
MICROCOPY RESOLUTION TEST CHART
NATIONAL BUREAU OF STANDARDS-1963-A

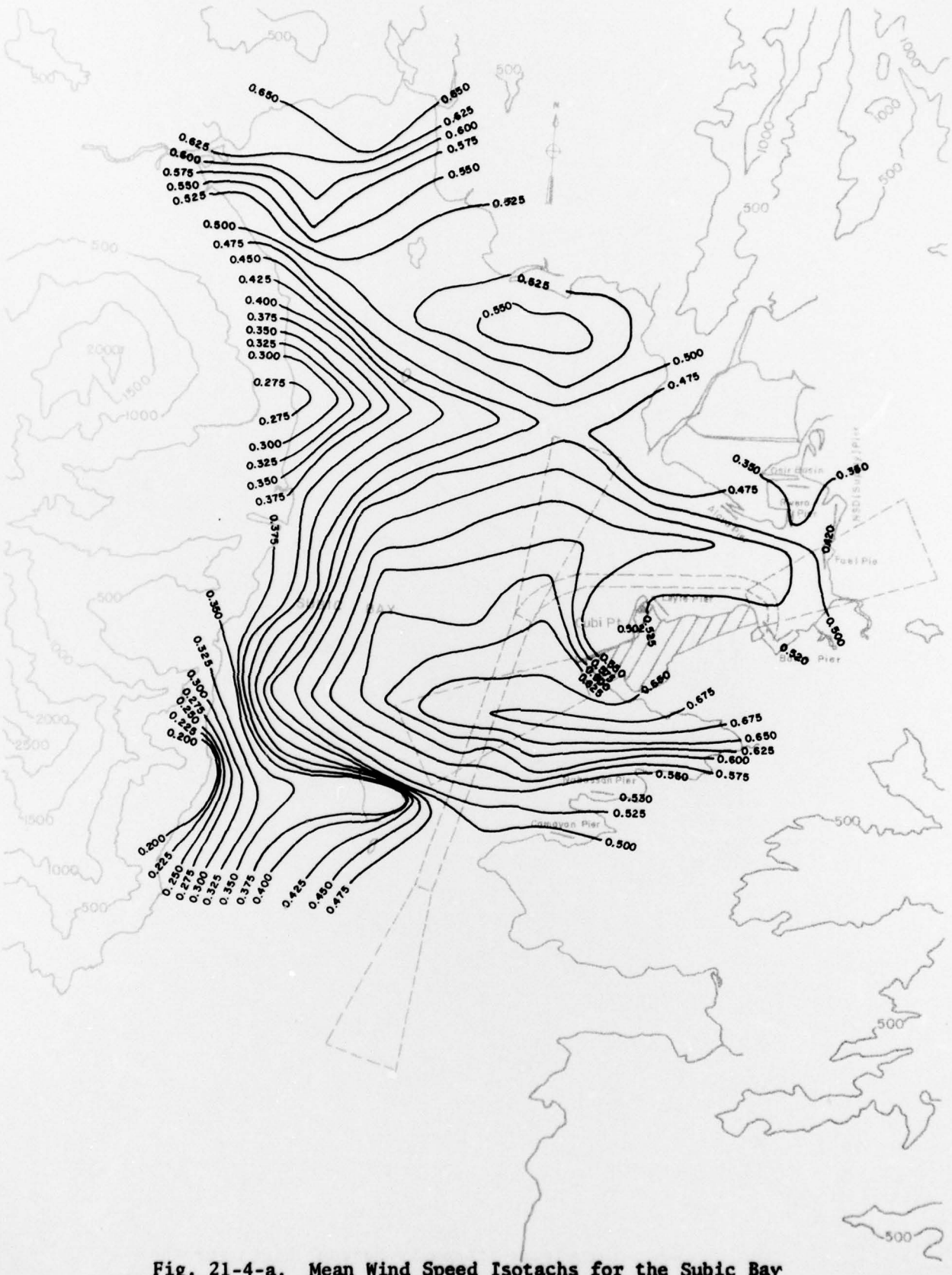

Fig. 21-4-a. Mean Wind Speed Isotachs for the Subic Bay Basin at 270°T, z = 275 ft (83.9 m)

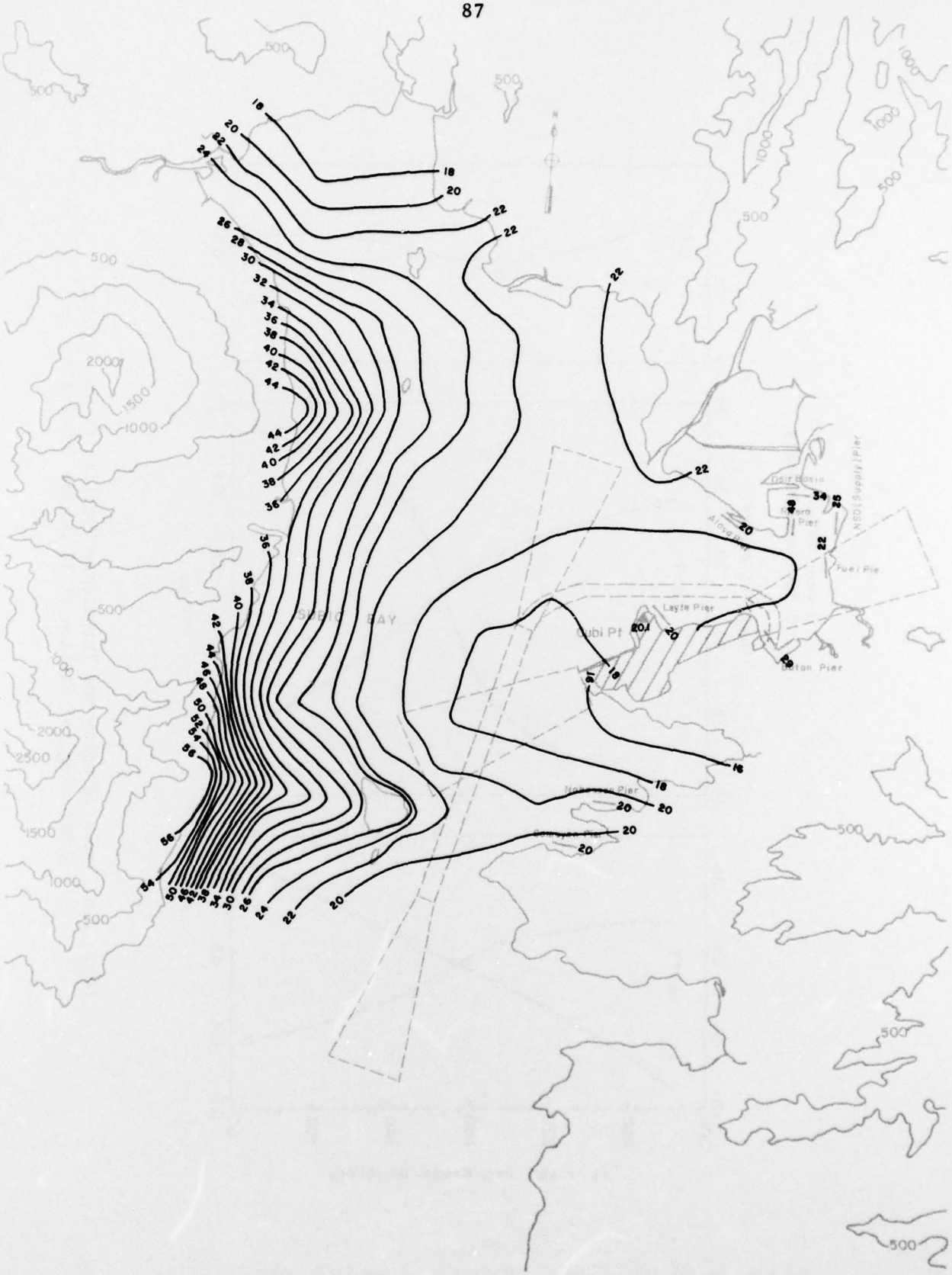

Fig. 21-4-b. Turbulence Intensity Contour Lines for the Subic Bay Basin at 270°T, z = 275 ft (83.9 m)

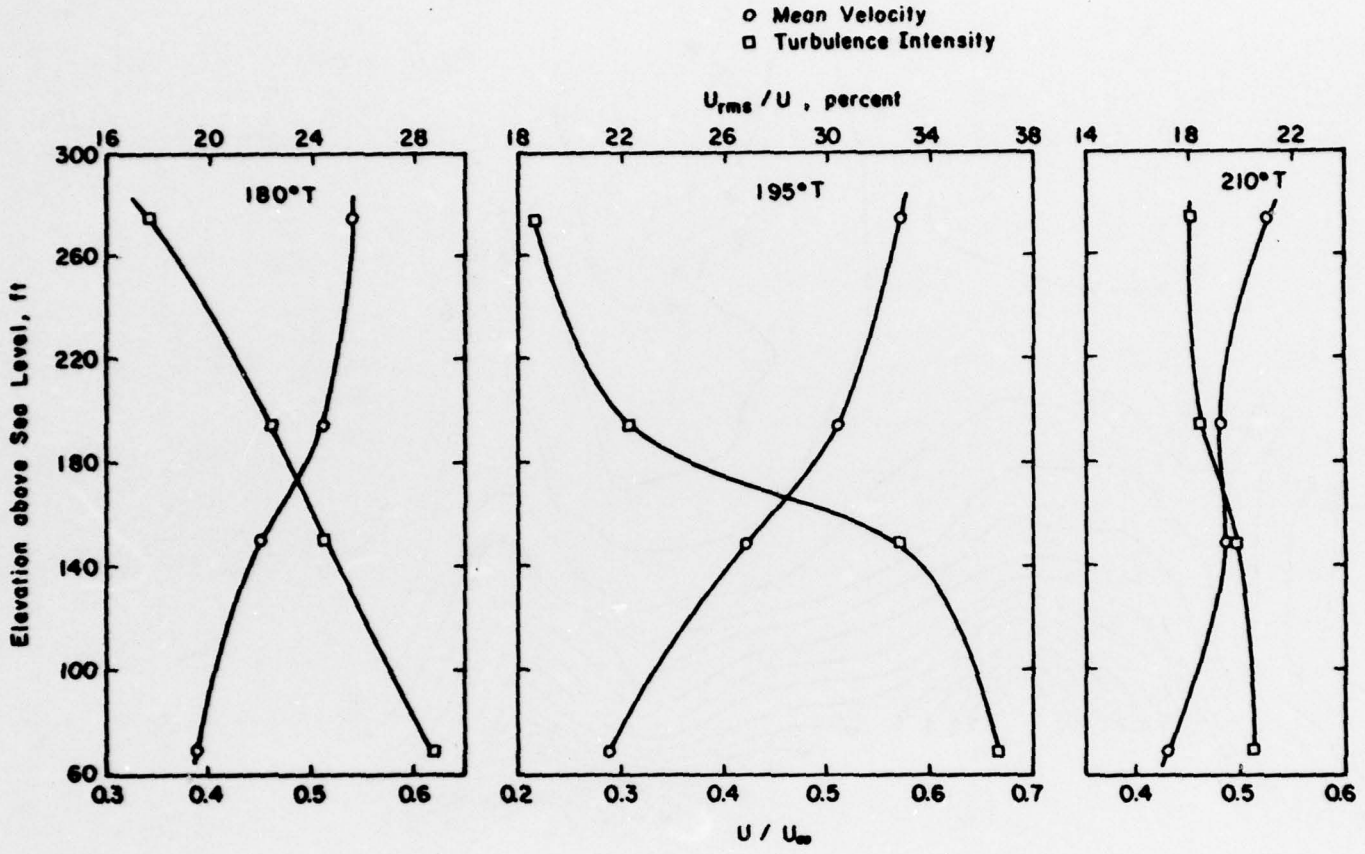

Fig. 22-a. Mean Velocity and Turbulence Profiles at Cubi Point Meteorological Station at 15 Degree Intervals

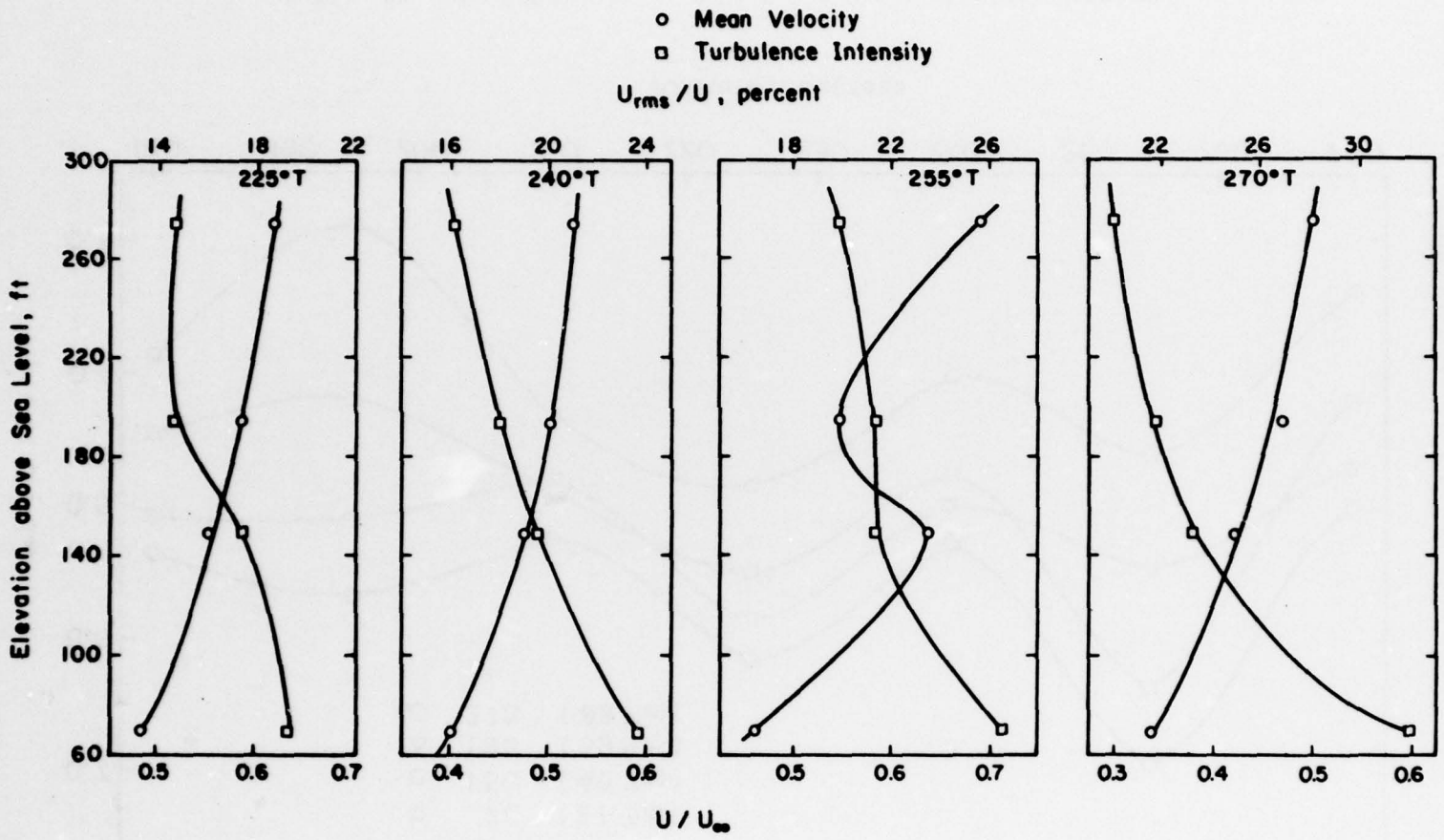

Fig. 22-b. Mean Velocity and Turbulence Profiles at Cubi Point Meteorological Station at 15 Degree Intervals

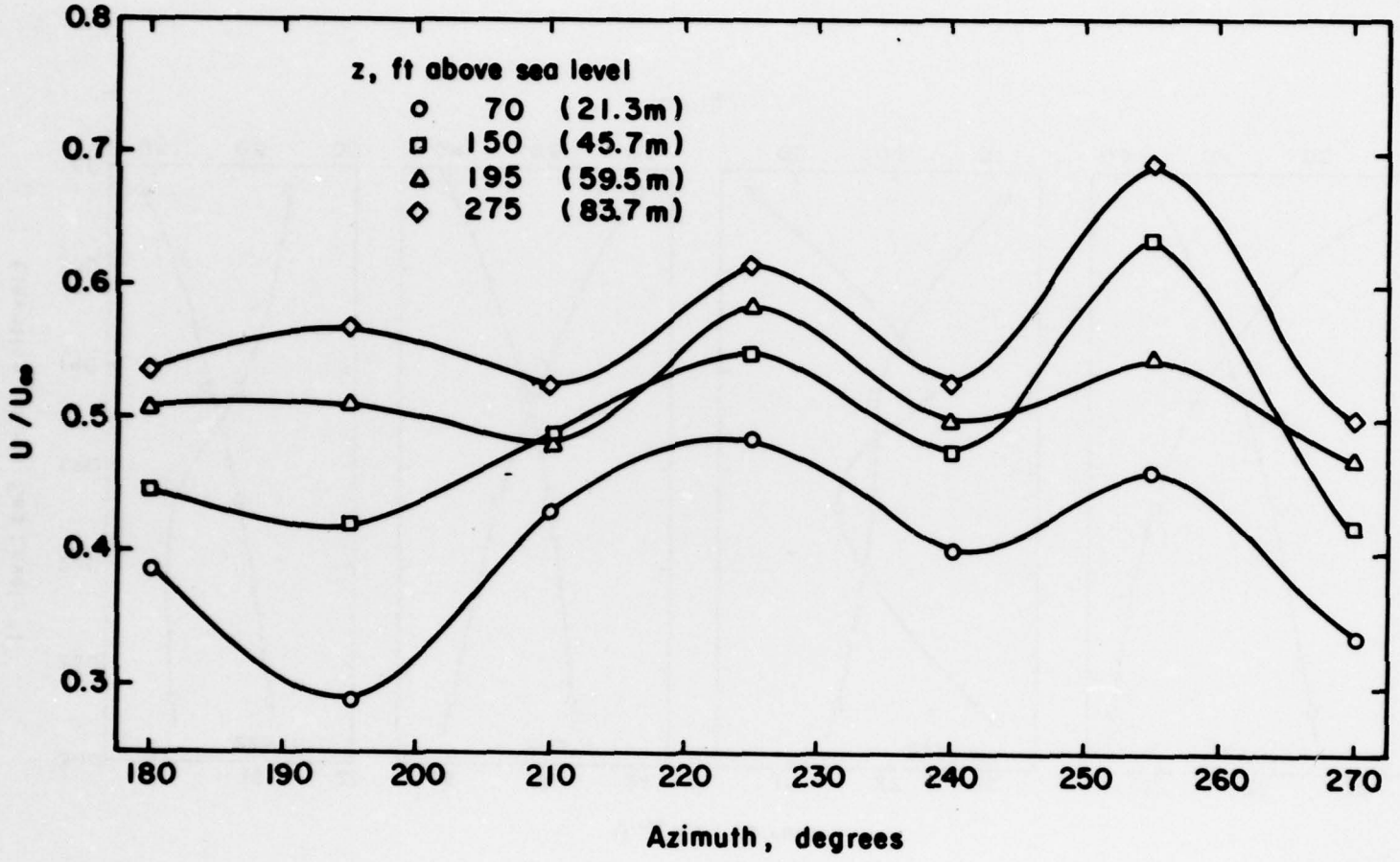

Fig. 23. Mean Velocity at Cubi Point Meteorological Station

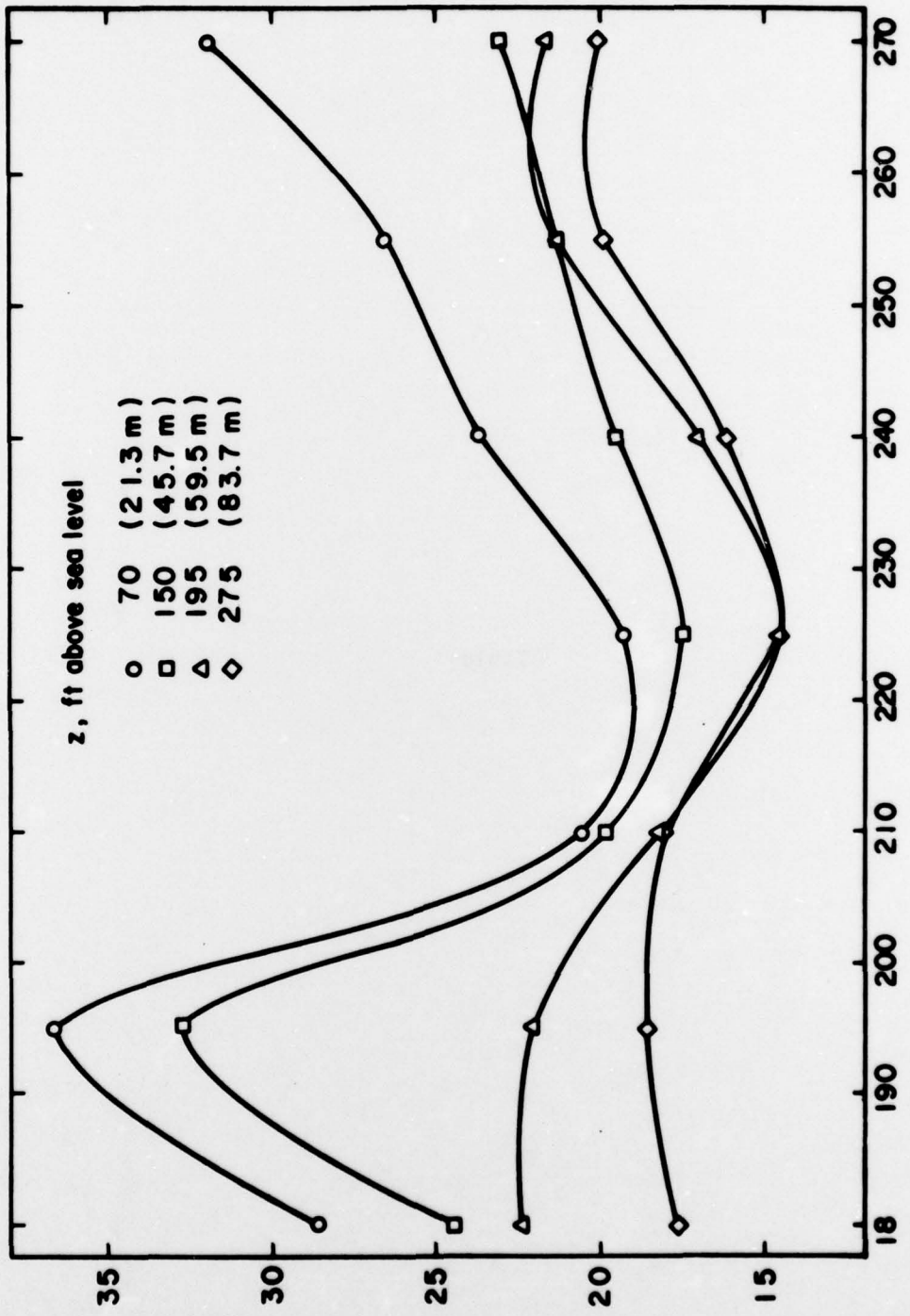

Fig. 24. Turbulence Intensity at Cubi Point Meteorological Station

Tables

Table 1. Motion picture scene guide.

Scene	Wind Direction
1	180°T
2	195°T
3	210°T
4	225°T
5	240°T
6	255°T
7	270°T

Movie length 743 ft.

Running time (approx.) 20 min. 5 sec.